

The valorization of volatiles released during torrefaction of various kinds of agricultural biomass

A study on the modelling and economics of torrefaction

by Joannes Jacobus de Koning

to obtain the degree of Master of Science at the Delft University of Technology,
to be defended publicly on Tuesday June 2, 2020 at 14:00 PM.

Student number: 4284038

Thesis committee:	Prof. dr. ir. W. de Jong,	TU Delft, supervisor
	Prof. dr. ir. A. de Haan,	TU Delft
	Prof. dr. D. J. E. M. Roekaerts,	TU Delft
	Dr. ir. L. Cutz,	TU Delft

Abstract

Pretreatment and densification processes such as torrefaction coupled with pelletization have proven to be valuable techniques to convert biomass to solid biofuels. Presently, waste streams from the torrefaction process in the form of volatiles are usually combusted to generate heat required for the torrefaction process. Nevertheless, the chemical characteristics of the torrefaction gas combined with recent technologies have opened new alternatives that could be used for further valorization of volatiles in other ways than combustion. The aim of this Thesis was to find alternative pathways other than straight up combustion of volatiles to valorize the volatiles released during torrefaction of biomass. Two types of biomass were investigated: corn stalk and sugarcane bagasse. Four different configurations for valorization were developed for their prospects of valorization: (1) valorization via straight up combustion, (2) chemical looping combustion, (3) chemical looping steam reforming and (4) a combination of chemical looping combustion and straight up combustion. A model based on experimental data was build in Aspen Plus to simulate the drying, torrefaction and valorization for a torrefaction plant with a capacity of 100 kton/year. The results were analysed in terms of process efficiency and economics. Results indicate that chemical looping combustion of all volatiles is the most attractive option of valorization, both in terms of efficiency and economics. The gross LHV efficiency for this option is 92 % for corn stalk and 84 % for sugarcane bagasse. The production costs in these scenarios are €208/ton for torrefied corn stalk pellets and €180/ton for torrefied sugarcane bagasse pellets. The capital investment required for the torrefaction plant for this configuration is €527/kW installed for corn stalk and €650/kW installed for sugarcane bagasse.

Acknowledgements

The last 9 months of my life revolved around writing this Thesis, which forms the culmination of my time as a student at TU Delft. Completing this Thesis wouldn't have been possible without the aid and support of several persons. First and foremost, I'd like to thank Luis Cutz. This research would have been impossible without his advice, guidance and contributions throughout the duration of the project. Furthermore, special thanks goes to Wiebren de Jong. I'm profoundly grateful for his supervision, insights on torrefaction and enthusiasm for the subject. I'd like to thank André de Haan and Dirk Roekaerts for being on my thesis committee. On a personal level, thank goes out to my girlfriend and roommates for keeping spirits high when things were looking down. Lastly, I'd like to express my deep gratitude to my parents, who've supported me throughout my time in Delft in every way possible.

Contents

1	Introduction	1
1.1	Aim of this study	3
1.2	Structure	4
2	Literature review	5
2.1	Biomass	5
2.1.1	Behaviour of biomass as a fuel	6
2.2	Dryer	8
2.2.1	Belt dryer	9
2.2.2	Rotary drum dryer	9
2.2.3	Indirect tubular steam dryer	10
2.2.4	Fluidized bed dryer	11
2.2.5	Dryer simulation	12
2.3	Torrefaction reactor	13
2.3.1	Moving bed reactor	14
2.3.2	Rotating drum reactor	14
2.3.3	Screw conveyor	15
2.3.4	Scale	15
2.3.5	Torrefaction modelling	16
2.3.6	Torrefaction in Aspen Plus	19
2.4	Volatiles valorization	19
2.4.1	Combustion	19
2.4.2	Chemical looping combustion	20
2.4.3	Chemical looping steam reforming	22
3	Methodology	25
3.1	Biomass selection	25
3.2	Aspen Plus modelling	26
3.2.1	Environmental conditions	26
3.2.2	Basic simulation model	27
3.3	Dryer	28

3.3.1	Drying kinetics	28
3.3.2	Torrefaction	38
3.3.3	Simulating the torrefaction reactor in Aspen Plus	49
3.3.4	Grinding & pelletization	53
3.4	Valorization unit: scenarios	53
3.4.1	Combustion of all volatiles	53
3.4.2	Chemical looping of all volatiles	55
3.4.3	Combustion of non-condensable volatiles and CLC of condensable volatiles	58
3.4.4	Chemical looping of all volatiles coupled with hydrogen production	60
3.4.5	Scale	63
3.5	Economic analysis	64
3.5.1	Capital expenditures	64
3.5.2	Operating expenditures	66
3.5.3	Net present value	69
3.5.4	End use	69
4	Results & Discussion	71
4.1	Equipment dimensioning	71
4.1.1	Dryer	71
4.1.2	Torrefaction unit	73
4.2	Operating conditions & production	75
4.2.1	Energy consumption	77
4.3	Economics	78
4.3.1	Capital expenditures	78
4.3.2	Operating expenditures	80
4.3.3	Overall economic results and & comparison with literature	83
4.3.4	Sensitivity analysis	85
4.3.5	Net present value	86
4.3.6	Comparison with other sources of energy	87
5	Conclusion	89
6	Recommendations	91
	Appendices	110
1.1	Coefficients V1 and V2	111
1.2	PFD configurations	112
1.3	Economics	116
1.4	Python code	119

1.4.1	Drying functions	119
1.4.2	Torrefaction functions	124
1.4.3	Corn Stalk code	139
1.5	Aspen calculator blocks	150
1.5.1	Dryer	150
1.5.2	Torrefaction reactor	151

List of Figures

2.1	Belt dryer	9
2.2	Rotary dryer	10
2.3	Indirect tubular steam dryer	11
2.4	Fluidized bed dryer	12
2.5	Moving bed reactor	14
2.6	Rotating drum reactor	15
2.7	Screw conveyor	15
2.8	Torrefaction mechanisms	17
2.9	Schematic overview of chemical looping	20
2.10	Schematic overview of chemical looping	22
2.11	Phase diagram of FeOx	23
3.1	Basic block scheme	28
3.2	Drying regimes	29
3.3	Drying data	30
3.4	Curves fitted to drying data (see Table 3.4 for input values)	31
3.5	Drying Coefficients A & k versus temperature	32
3.6	Equilibrium moisture content sugarcane bagasse	34
3.7	Black box model for the dryer	35
3.8	Drying time comparison (6 % final moisture, particle details in Table 3.4)	36
3.9a	Weight loss data torrefaction corn stalks	39
3.9b	Weight loss data torrefaction sugarcane bagasse	39
3.10a	Weight loss torrefaction CS fitted to a 2-step mechanism	42
3.10b	Weight loss torrefaction SCB fitted to a 2-step mechanism	42
3.11	Torrefaction coefficients versus temperature	43
3.12	Compositions of V1 and V2 versus time	46
3.13	HHV for corn stalk and sugarcane bagasse during torrefaction	47
3.14	Torrefaction plots corn stalks	49
3.15	Torrefaction plots sugarcane bagasse	49
3.16	Torrefaction reactor cross section	50
3.17	Combustion model	54

3.18	CLC model	56
3.19	NiO validation	58
3.20	CLC condensables and combustion non-condensables model	59
3.21	Volatiles separation model	59
3.22	CLC and hydrogen production model	60
3.23	Steam reactor	61
3.24	Fe_2O_3 validation	63
4.1	Energy consumption	77
4.2	Equipment costs	79
4.3	CAPEX	80
4.4	OPEX	81
4.5	Utility costs	82
4.6	IRR sensitivity CS_{clc} and SCB_{clc}	86
1	PFD configuration 1	112
2	PFD configuration 2	113
3	PFD configuration 3	113
4	PFD configuration 4	114
5	PFD configuration 5	114
6	PFD configuration 6	115
7	PFD configuration 7	115
8	PFD configuration 8	116

List of Tables

2.1	Proximate analysis	7
2.2	Ultimate analysis	8
2.3	Drying fitting comparison	13
3.1	Properties CS and SCB from literature	30
3.2	Curve fitting results corn stalk	31
3.3	Curve fitting results sugarcane bagasse	31
3.4	Standardized length parameters drying in Aspen Plus	34
3.5	Comparison of fitting methods for torrefaction	40
3.6	K relations for each type of biomass	44
3.7	Estimated coefficients for Boie correlation	47
3.8	Correlation NiO validation	58
3.9	Correlation Fe_2O_3 validation	63
3.10	Sources equipment prices	65
3.11	CAPEX factors	66
3.12	Prices catalysts	67
3.13	Utility prices	67
4.1	Configuration summary	71
4.2	Dryer results	72
4.3	Volatiles compositions	74
4.4	Torrefaction reactor results	74
4.5	Summary of operational conditions and production	76
4.6	Overall results	83
4.7	Sensitivity analysis	85
4.8	Cost comparison ($\eta_{th}=45\%$)	88
1	Coefficients V1 SCB	111
2	Coefficients V2 SCB	111
3	Coefficients V1 CS	111
4	Coefficients V2 CS	112
5	Equipment costs	116

6	CAPEX	117
7	OPEX	118
8	NPV	119

Nomenclature

Symbols

ΔH	Enthalpy of reaction (kJ/kg)
ΔT	Temperature difference ($^{\circ}C$)
ϵ	Fill grade (-)
η	Efficiency (-)
\dot{m}	Mass flow (kg/hr)
μ	Viscosity ($kg/(m \cdot \cdot \cdot)$)
ϕ	Porosity (-)
ρ	Density (kg/m^3)
τ	Time (min)
A	Area (m^2)
A	Pre-exponential factor (-)
a_i	Boie coefficient (-)
C	Employees present at each time (-)
c_P	Heat capacity ($kJ/(kg \cdot K)$)
D	Diameter (m)
D	Diffusion coefficient (m^2/s)
d_P	Characteristic particle length (m)
E	Energy (J)

h	Heat transfer coefficient (W/m^2)
k	Exponential factor (-)
k_i	Rate of reaction (s^{-1})
L	Length (m)
m	exponential scale factor (-)
Pr	Prandtl Number (-)
Q	Heat loss (W)
R	Gas constant ($J/(mol \cdot K)$)
R	Oxygen carrier to C molar ratio (-)
r	Internal rate of return (-)
R^2	Coefficient of determination (-)
Re	Reynolds Number (-)
SC	Steam to C molar ratio (-)
Sc	Schmidt Number (-)
Sh	Sherwood Number (-)
T	Temperature ($^{\circ}C$ or K)
V_i	Volume (m^3)
W	Mass (kg)
X	Moisture content (kg water/kg dry biomass)
X	Plant capacity (ton/day)
X^2	Chi squared test (-)
X_{i,V_i}	Fraction in volatiles (-)
Y	Man-hours per processing step (hr/step)
Y	Weight fraction (-)

Abbreviations

AR	Air Reactor
c	Condensable
CAPEX	Capital Expenditures
CCS	Carbon Capture and Storage
CLC	Chemical Looping Combustion
CS	Corn Stalk
CS _{clc}	Corn stalk chemical looping combustion
CS _{comb+clc}	Corn stalk combustion + chemical looping combustion
CS _{comb}	Corn stalk combustion
CS _{H₂}	Corn stalk hydrogen production
db	Dry basis
FR	Fuel Reactor
HFL	Higher Flammability Limit
HHV	Higher Heating Value
HMF	Hydroxymethylfurfural
IRR	Internal Rate of Return
L	Length
LFL	Lower Flammability Limit
LH	Latent Heat
LHV	Lower Heating Value
MeO	Metal Oxide
MR	Moisture Ratio
nc	Non-condensable

NDR	Normalized Drying Rate
NMC	Normalized Moisture Content
NPV	Net Present Value
OC	Oxygen Carrier
OPEX	Operational Expenditures
PFD	Process Flow Diagram
RMSE	Root Mean Square Error
SCB	Sugarcane Bagasse
SCB _{clc}	Sugarcane bagasse chemical looping combustion
SCB _{comb+clc}	Sugarcane bagasse combustion + chemical looping combustion
SCB _{comb}	Sugarcane bagasse combustion
SCB _{H₂}	Sugarcane bagasse hydrogen production
SR	Steam Reactor
UK	United Kingdom
US	United States
V1	Volatiles 1
V2	Volatiles 2

Chapter 1

Introduction

The invention of fire has been one of the great achievements of mankind. Biomass was used as the source of fuel. Ever since the start of the industrial revolution, which was marked by the invention of steam-powered machinery, fossil fuels have replaced biomass as the primary source of fuel. Their higher energy content and higher density made them more attractive than biomass. The reign of fossil fuels has lasted for the last 250 years, but new concerns have risen over their influence on global climate through the emissions of green house gasses. In the search for new sources of energy, biomass can contribute significantly to the world's energy mix. As of 2017, 70 % of the renewable energy produced worldwide was attributed to bioenergy [1]. It leaves no doubt that biomass will provide a significant share of the world's energy demand during the energy transition from fossil fuels to renewables.

Biomass as a fuel provides a wide range of benefits. For starters, combustion of biomass is CO_2 neutral, as long as the carbon released during burning is sequestered by plants [2]. When the biomass is burned to produce energy, the CO_2 is released into the atmosphere again, completing the cycle. Currently, over 85 % of the heat and electricity produced by biomass is contributed to forestry products, for example wood chips and fuel wood [1]. An advantage of the use of forestry biofuel on a small scale (i.e. individual fuel usage) is its availability and cheap production costs [3]. A disadvantage on a larger scale (i.e. nationwide) is deforestation [4]. Agricultural biomass only makes up 10 % of the bioenergy mix as of today, offering an opportunity for growth [1]. A critique on the use of agricultural biomass in the production of energy is the misuse of food crops. First-generation types of biomass, like corn and sugarcane starch, reduce food availability thereby creating an ethical dilemma where one has to choose between food and energy [5]. Second generation biomass circumvent this dilemma by using feedstock not associated with food production, but rather energy crops, for example elephant grass and poplar wood, or agricultural residue, for example corn stalk and sugarcane

bagasse [1]. Up to 50 % of agricultural residues are currently left on the fields, providing enormous opportunities if these residues were used [1]. It is estimated that agricultural residues can provide 10-20 % of the world's energy supply [6].

However, there are some downsides to using agricultural biomass as a fuel source. Moisture in biomass lowers its calorific content and hampers combustion. This also applies to wet crops residues. As they are harvested, crops can have a moisture content of up to 40 % [7], and up to 50 % for processed residues [8]. In order to be suitable for energy conversion, these kinds of biomass first have to be dried. Drying results in decreased moisture content and thus increased calorific content. Another drawback is difficulty in transportation. As of now, fossil fuels are shipped around the world to provide energy to regions where energy is scarce. Fossil fuels have a high calorific value in terms of J/m^3 . Biomass is severely limited in this respect, because of its lower energy density (J/kg) and lower bulk density (kg/m^3). This makes transportation of biomass many times more expensive than fossil fuels [9]. Pretreatment and densification are required to convert raw biomass into a suitable fuel.

Pretreatment and densification processes regarding biomass produce either solid or liquid biofuels [10]. Liquid biofuels in the form of ethanol and biodiesel have been produced on an industrial scale since the oil crises of the 1970's to reduce the world's dependence on oil for gasoline [11]. The production of solid biofuels in the form of wood pellets started in the same period, especially in forest-rich areas like North-America and northern Europe [12]. Liquid biofuels are particularly useful as replacement for gasoline, whereas solid biofuels are more suitable for heat and electricity production [10]. As heat and electricity generation by coal is planned to be phased out to reduce carbon emissions [13], solid biofuels provide an opportunity to fill the gap left behind [1]. Among the potential pretreatment methods to produce solid biofuels out of agricultural residues is torrefaction, a thermal pretreatment method [10].

Torrefaction is a thermal process in which biomass undergoes mild-pyrolysis, usually conducted at temperatures between 200 °C to 300 °C [14]. During this process, the structure of the biomass itself changes. A part of the biomass devolatilizes into several different volatile compounds such as acetic acid, water, CO_2 and CO . As a result, the solid shrinks, increasing its calorific value, bulk density and grindability [10]. Torrefaction is usually preceded by drying [15], [16], [17]. During the drying process, biomass is dried to a standard moisture content, which ranges from 6 % to 15 % [18]. Doing this increases the calorific content of the biomass. Increased energy density results in more straightforward transportation of the same amount of energy later on. Furthermore, it is also important to standardize the composition of the biomass as much as possible in this part of the process. Biomass arrives from different farmers and places, and its composition is

slightly different, depending on local weather, soil type and sunlight. Drying to a standard moisture content ensures homogenization of the biomass.

The torrefaction process results in two different streams: a stream containing the torrefied biomass, and a stream of volatiles produced during torrefaction. The torrefied biomass is sent to a pelletizer where small pellets are formed out of the torrefied biomass. This makes the torrefied biomass better suitable for transportation, as these pellets are more robust than raw biomass, have a high calorific value, high density and are hydrophobic [9]. The pellets can either be used directly in a power plant or converted for the production of chemicals. The volatiles produced during torrefaction are usually combusted to generate the heat required for drying and torrefaction [17]. A lot of work has been done on the design and simulation of torrefaction processes [17],[19],[20],[21] while no work is known regarding the process design and simulation of torrefaction in combination with different methods of valorization of the volatiles other than combustion.

1.1 Aim of this study

The aim of this study is to valorize the volatiles produced during torrefaction through the design and evaluation of novel process configurations for a torrefaction plant. Valorization is the process of adding value to compounds by converting them to energy or other valuable compounds. Volatiles from torrefaction are composed of two different kinds of volatiles: condensables and non-condensables. The condensables volatiles are liquids at standard conditions, like water (H_2O), acetic acid (CH_3COOH) or formic acid (CH_2O_2), while the non-condensables remain in their gaseous form when cooled down after torrefaction, like CO_2 , H_2 and CO [22]. Volatiles can be valorized in different ways. This report will focus on four promising techniques:

1. Combustion
2. Chemical looping combustion
3. Chemical looping hydrogen combustion
4. A combination of combustion and chemical looping combustion

The process configurations will be analysed in terms of energy efficiency, CAPEX, OPEX and price per MWh. Aspen Plus was used as the modeling software to model all process configurations.

1.2 Structure

This report is divided in four chapters: Literature Review, Methodology, Results & Discussion and Conclusion. The first chapter, Literature Review, focuses on different biomass feedstocks, theory and simulation of drying and torrefaction as found in literature and theory and simulations approaches on volatiles valorization.

The second chapter, Methodology, focuses on the process simulation of biomass torrefaction and volatiles valorization in Aspen Plus, along with the method of economic analysis. The drying and torrefaction data gathered in literature are used to model the dryer and torrefaction reactor. The different process configurations considered for the valorization of volatiles and how they have been implemented in Aspen Plus are discussed. Lastly, the methods applied for the economic analysis are discussed. In the third chapter, Results & Discussion, all results from the models developed in Aspen are presented and discussed in terms of operational conditions and performance. Furthermore, this chapter includes the results of the economic analysis of all process configurations, along with a financial comparison with other sources of energy like wind, solar and fossil. The last chapter, conclusion, presents the main conclusions from this project and provides recommendations for further research about the valorization of volatiles from torrefaction.

Chapter 2

Literature review

This chapter provides the theoretical background necessary to develop the different process simulation models considered in this Thesis. First, this chapter provides a discussion on the types of biomass considered in this study and the proximate and ultimate composition of the biomass. Secondly, the drying and torrefaction kinetics of the biomass are discussed along with a literature review on drying and torrefaction equipment plus a literature review on drying and torrefaction simulation in Aspen Plus. Thirdly, the theory behind the valorization via combustion or chemical looping combustion is discussed, in combination with a literature review on valorization modelling in Aspen Plus. The outcomes of the literature reviews were used for process modelling in Aspen Plus.

2.1 Biomass

Biomass is an organic, wide-spread, abundant and renewable source of energy [23]. Biomass has a wide array of different appearances, from plants and trees to agricultural residues and processing residues [24]. It can be used for the production of (liquid or solid) biofuels, sugar, syngas, paper and many other products [25]. This study focuses on the use of agricultural residue and side-products generated by agricultural crop processing for the production of solid biofuel in the form of pellets. Different types of biomass were considered for evaluation as feedstock. These included sugarcane bagasse, corn stalk, corn cob, rape stalk, sunflower stalk, sunflower seed shells and sugar beet pulp. All of these types of biomass are widely available [26],[27],[28],[29],[30]. The behaviour of biomass as a fuel differs between different forms of biomass [24].

2.1.1 Behaviour of biomass as a fuel

The way biomass behaves as a fuel is influenced by its structure [24]. Biomass fuel is commonly characterized by three concepts: the proximate analysis, ultimate analysis and its calorific value [24].

The proximate analysis of biomass consists of four categories: volatile matter (VM), fixed carbon (FC), moisture (M) and ash (A). The VM fraction represents the part of the fuel which devolatilizes during heating [31]. The influence of the VM on the calorific content of biomass can differ. The creation of combustible volatiles, such as H_2 and CO increases the calorific content, while the generation of incombustible volatiles, such as CO_2 and H_2O decreases it [32]. The FC content represents the part of the fuel which burns in the solid state [31]. The FC has a positive impact on the calorific value of the biomass because of its burning characteristics [32]. The ash content is the inorganic material left after complete combustion [31]. Ash reduces the calorific content of biomass as it requires energy to be heated and due to the formation of inorganic compounds during heating [32]. The moisture content reduces the calorific content as it requires energy to vaporize the moisture in the biomass [24].

Table 2.1 presents the proximate analysis of the various types of feedstock researched, along with the standard deviation between the different sources. The VM, FC and A fraction are on a dry basis (db), while the M fraction is on a wet basis (wb). From Table 2.1 it was found that sunflower stalk has the highest VM content by weight (wt.) % at 86.25 %. Corn stalk had sunflower seed shells had the lowest amount of VM with 75.64 wt. %. The standard deviation for VM is the largest for corn cobs at 10.5 %. The FC content varies between 8.08 % for sunflower stalk and 21.71 % for sunflower seed shells. The standard deviation is low for sugarcane bagasse, rape stalk and sugar beet pulp, all showing a maximum standard deviation below 2 %. The ash content differs between 2.61 % for sugarcane bagasse and 5.67 % for sunflower stalk, with a small standard deviation of maximum 5.15 % for sunflower stalk and a minimum of 0.31 % for sunflower seed shells. The moisture content is very low for all (below 10 %) except for sugarcane bagasse. This is because all sources, besides the one used for sugarcane bagasse, used air-dried material for their tests, which yields a low moisture content. The sugarcane bagasse was not air dried in any of the sources, resulting in a moisture content of 48 % . The standard deviation for the moisture content is less than 5 % for all types of biomass. Fresh crops have a moisture content between 30 % and 60 % [15].

Table 2.1: Proximate analysis

Feedstock	VM (wt. % db)	FC (wt. % db)	A (wt. % db)	M (wt. % wb)	Sources
Corn stalk	75.64±5.59	14.91±4.55	3.63±1.26	5.82±2.54	[7] [33] [34][35]
Corn cobs	79.78±10.5	16.4±9.06	3.82±3.17	8.95±2.52	[7] [36] [37] [38]
Sugarcane bagasse	80.93±3.09	16.47±1.51	2.61±0.6	48.25±2.63	[8] [39] [40] [41]
Rape stalk	78.62±3.03	17.43±1.83	3.95±1.15	8.92±2.4	[42] [43] [44] [45]
Sunflower stalk	86.25±5.4	8.08±10.57	5.67±5.15	5.37±4.32	[46] [47] [48]
Sunflower seed shells	75.64±5.36	21.71±3.67	2.65±0.31	9.94±1.44	[49] [50] [51]
Sugar beet pulp	77.87±1.88	18.14±0.43	3.99±1.85	7.31±1.8	[52] [53] [54]

Table 2.2 presents the ultimate analysis in terms of weight percentage of all crops considered in this study, along with the standard deviation. The ultimate analysis represents the elemental composition of a fuel [55]. Carbon (C) and hydrogen (H) have a positive impact on the calorific value of biomass, while oxygen (O), sulfur (S) and nitrogen (N) have a negative impact [36]. All crops are fairly similar in the elemental composition, with each having large fraction of carbon, between 41.71 % for corn stalk and 48.17 % for sunflower seed shells, and oxygen, between 43.75 % for sunflower seed shells and 51.20 % for corn stalk. Each type of feedstock has a small fraction hydrogen (between 5.59 % for sunflower stalk and 6.63 % for corn stalk), nitrogen (between 0.30 % for corn cobs and 2.06 % for sugar beet pulp) and sulfur (between 0.02 % for sugarcane bagasse and 0.20 % for sugar beet pulp). The standard deviation in the ultimate analysis is below 6 % for all elements and types of feedstock. The last column of Table 2.2 presents the higher heating value (HHV) of the crops on a dry basis. The HHV is between 16.5 MJ/kg and 18 MJ/kg for all types of biomass, except for sunflower stalks, which have a much lower HHV of 14 MJ/kg. On a wet basis the HHV can drop to 8 to 9 MJ/kg [56]. The higher heating value of the most used coal, sub-bituminous coal, is 24 MJ/kg [57]. If biomass wants to be competitive with coal, it should have a higher heating value which approaches that of coal. Pretreatment of the biomass is necessary to achieve this.

Table 2.2: Ultimate analysis

Crop	C (wt. %)	H (wt. %)	O (wt. %)	N (wt. %)	S (wt. %)	HHV (MJ/kg)	Sources
Corn stalk	41.71±5.37	6.63±0.88	51.2±5.1	0.42±0.45	0.06±0.08	17.98±1.1	[7] [33] [34] [35]
Corn cobs	45.96±3.56	5.88±0.35	47.57±3.42	0.3±0.22	0.14±0.23	17.11±0.92	[7] [36] [37] [38]
Sugarcane bagasse	46.71±4.24	5.94±0.32	46.24±4.5	0.31±0.11	0.02±0.04	17.83±0.7	[8] [39] [40] [41]
Rape stalk	47±3.14	6.38±0.82	45.06±1.51	0.38±0.31	0.19±0.06	17.2±1.74	[42] [43] [44] [45]
Sunflower stalk	44.53±5.51	5.59±0.19	48.73±5.96	1.06±0.71	0.09±0.14	13.93±0	[46] [47] [48]
Sunflower seed shells	48.17±4.98	6.41±0.8	43.75±6.88	0.53±0.51	0.08±0.07	17.74±0.35	[49] [50] [51]
Sugar beet pulp	45.95±4.42	6.43±0.23	45.35±5.8	2.06±1.15	0.2±0	16.56±0.64	[52] [53] [54]

2.2 Dryer

Drying is a pretreatment step before torrefaction. The first main purpose of drying is to reduce the moisture content in biomass and homogenise the differences in moisture content. Different types of biomass hold different amounts of moisture. To ensure a standard product after torrefaction, it is necessary to average out differences before torrefaction. Varying moisture contents in the biomass would result in varying amounts of energy required in the torrefaction reactor, as a varying amount of energy would be needed for vaporization of the moisture. A standard moisture content of the biomass before it enters the torrefaction reactor would simplify the design of this reactor considerably. Thus, by homogenising the differences in moisture it is ensured the torrefaction plant works as efficiently as possible [17]. The second main purpose of drying is to prevent wet torrefaction [15],[17]. Volatiles, produced by the torrefaction process, with a high moisture content have unfavourable conditions for combustion as the moisture narrows the flammability limits and lowers the adiabatic flame temperature [17]. The wet biomass enters the reactor with a moisture content between 30 % and 60 % [15]. The moisture content of biomass before torrefaction should be between 10 % and 6% [17],[58]. Dryers are divided in two categories:

1. directly heated
2. indirectly heated

The directly heated dryers use a hot stream to heat the biomass directly, while the indirectly heated dryers heat the outside of the dryer to heat up the biomass. Possible sources of heat are flue gasses, hot air and high pressure steam [15]. Of these, only flue gasses and hot air have potential to be used in a directly heated

dryer, as long as these drying contain a low amount of moisture, enabling the absorption of moisture from the biomass [15]. The following types of dryers can be used for biomass drying before torrefaction.

2.2.1 Belt dryer

A schematic overview of a belt dryer is presented in Figure 2.1. A belt dryer blows a drying agent, entering as Air in in Figure 2.1, over a thin layer of biomass, entering as wet material in Figure 2.1. The biomass is moving over a belt while the drying agent evaporates moisture out of the biomass. Apart from air, hot flue gas can be used as drying agent [15]. An advantage of the belt dryer is the simplicity of design and a uniform moisture content after drying. Due to the lack of good mass and heat transfer, belt dryers are often very large [15].

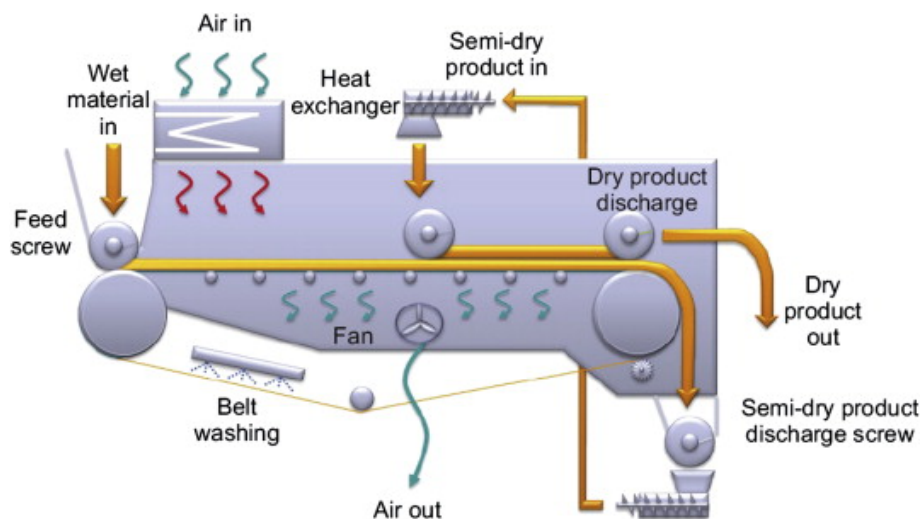


Figure 2.1: Belt dryer

Source: [15]

2.2.2 Rotary drum dryer

The rotary drum dryer, of which an overview is presented in Figure 2.2, is a directly heated dryer which uses hot air or flue gasses as a drying agent. The drying agent enters the dryer at the same side as the biomass at a temperature between 250 °C and 400 °C to prevent burning of the biomass [15]. The dryer rotates to move the biomass around the dryer to improve heat and mass transfer [15]. The dried product is separated from the drying agent, after which the drying agent is sent through a number of cyclones to remove any fines entrained in it [15]. The rotary

drum dryer is the most used dryer in the industry for bio-energy plants because of the relative simplicity of design and its improved heat and mass transfer as opposed to the belt dryer [15].

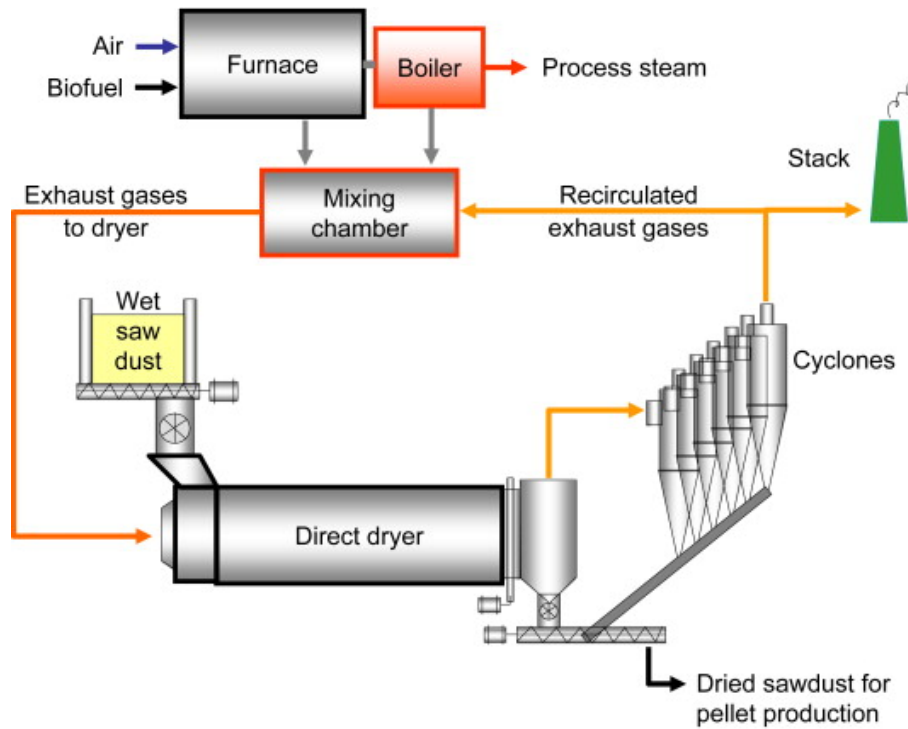


Figure 2.2: Rotary dryer

Source: [15]

2.2.3 Indirect tubular steam dryer

Figure 2.3 presents an overview of an indirect tubular steam dryer, which uses saturated steam to heat the biomass in the dryer and evaporate moisture. The steam flows through pipes attached to the dryer in which steam is supplied at a pressure between 0.6 and 1.0 MPa [58]. An advantage of the indirect tubular steam dryer is its compactness and improved heat and mass transfer characteristics over a belt dryer. A disadvantage of an indirect tubular steam dryer is the difficulty of design and the large amount of steam required [15].

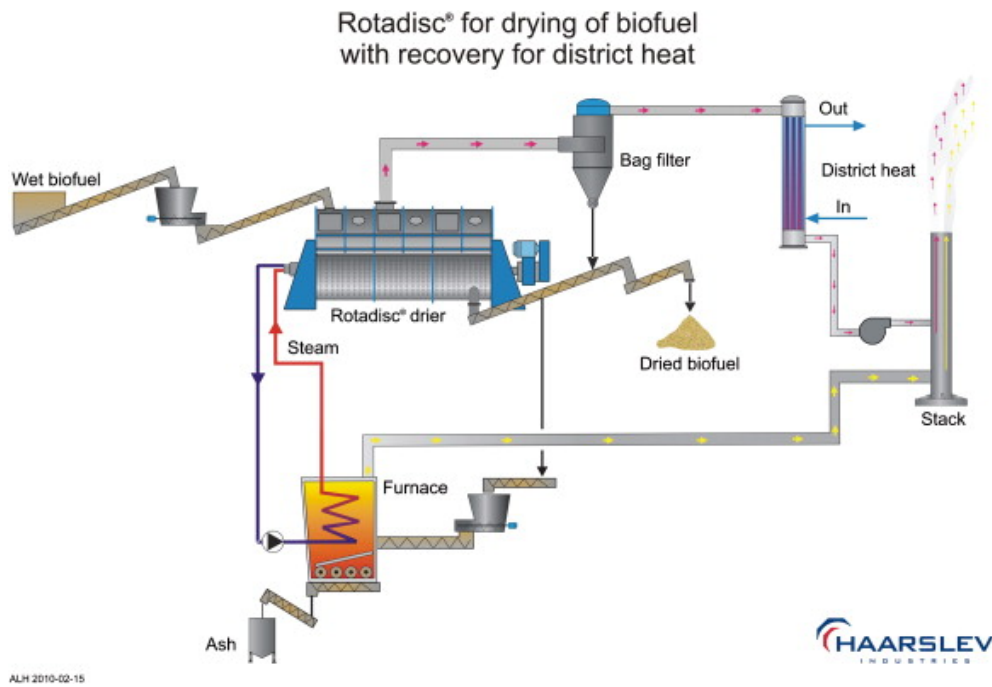


Figure 2.3: Indirect tubular steam dryer

Source: [15]

2.2.4 Fluidized bed dryer

Figure 2.4 presents a schematic overview of a fluidized bed dryer. A fluidized bed dryer uses the fast heat and mass transfer characteristics of a fluidized bed to dry biomass faster than the other options stated above [15]. Hot air, flue gasses or superheated steam enter the biomass layer from the bottom, fluidizing this layer [15]. The fast mass and heat transfer result in a fast drying process, reducing the size of the dryer [15]. A disadvantage to such a dryer is the small particle size (0.5-5mm) required for fluidization [15].

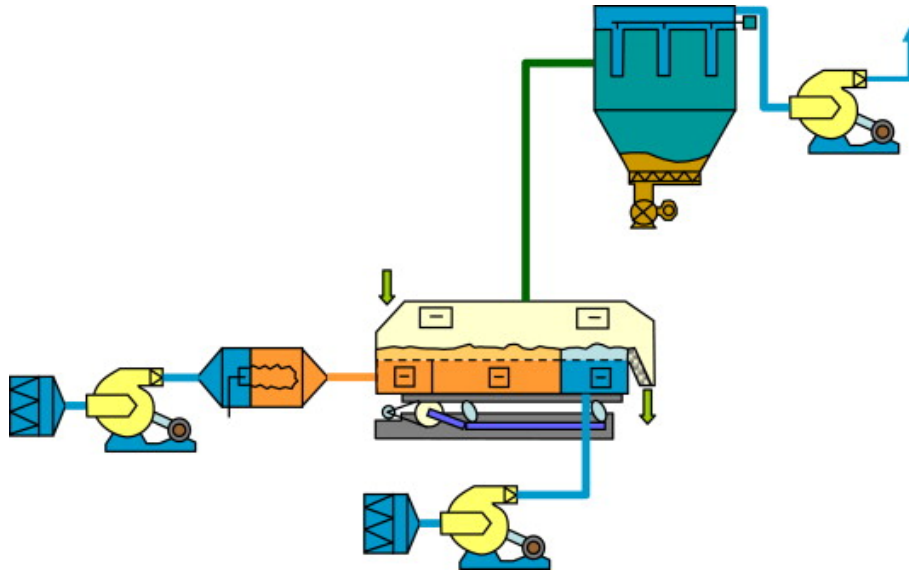


Figure 2.4: Fluidized bed dryer

Source: [15]

2.2.5 Dryer simulation

As stated in the introduction, Aspen Plus was used to simulate the process of drying, torrefaction and volatile valorization. Various different methods have been used by others to simulate drying of biomass in Aspen Plus. The most used method is based on coal drying, which is provided by Aspen Plus as a tutorial [19],[20],[58]. This method involves an RSTOIC reactor and a calculator block to simulate the moisture content of the feedstock after drying. The RSTOIC reactor in Aspen Plus models stoichiometric reactions with a specified reaction extent or conversion. This approach doesn't utilize the full potential of Aspen Plus, as it leaves the user with the task of computing aspects like the energy needed in the dryer, the amount of air required and the dimensions of the dryer. Manoucherinejad et al. [17] implemented the dryer operation block in Aspen Plus to simulate drying of biomass. The dryer was simulated as a co-current dryer. This approach improves the drying model in comparison to the Aspen Plus tutorial by automatically taking the drying kinetics into account. It also delivers information on the solid and gas composition and temperature profiles in the dryer [17].

Experimental drying data is required for the dryer block to adequately simulate the drying in Aspen Plus. Dhanushkodit et al. [59] compared 11 different equations for drying fitting, which included Lewis, Page, modified Page and Henderson and Pabis. Their results regarding the statistical correlation of the drying models with

experimental data are presented in Table 2.3. They concluded that all equations achieved R^2 values above 0.873, with Page obtaining the highest R^2 with 0.998. All equations also had a root mean square error (RMSE) below 0.0921 and a X^2 below 0.1060, with Page having the lowest RMSE (0.0247) and lowest X^2 (0.0017).

Table 2.3: Drying fitting comparison

Model name	R^2	RMSE	X^2
Lewis	0.916	0.0773	0.0313
Page	0.998	0.0247	0.0017
Modified page	0.943	0.0712	0.0032
Henderson and Pabis	0.911	0.0921	0.0046
Logarithmic	0.972	0.0638	0.0082
Two term	0.933	0.0376	0.0041
Exponential two term	0.920	0.0375	0.1060
Wang and Singh	0.873	0.0316	0.0238
Thompson	0.911	0.0855	0.0412
Diffusion Approximation	0.891	0.0332	0.0132
Midilli etal.	0.923	0.872	0.0712

Source: [59]

2.3 Torrefaction reactor

Torrefaction is a thermal treatment in which biomass is heated to a temperature between 200 °C and 300 °C [60]. Typical torrefaction times range from 10 minutes up to 1 hour [55],[61],[62],[63]. During the torrefaction process a part of the solid biomass is converted to volatiles. The aim of torrefaction is to create a solid with a higher calorific value, increased hydrophobicity and higher grindability than regular biomass [16],[17]. The higher calorific value makes the biomass attractive as a fuel. Higher hydrophobicity results in less moisture uptake after production, preventing a decline in the HHV [17]. Grindability is useful for pelletization after torrefaction. The density of the solids decreases during torrefaction, leaving a light, brittle material unsuitable for transportation [64]. Pelletization of the solids increases the volumetric energy content and offers more options for transportation [64]. No concluding information on an ideal particle sizes for torrefaction was found. In research on the influence of the particle size on the torrefaction process the particle size were in the range of 1 mm to 25 mm [65],[66].

Torrefaction is a process which is in many ways similar to drying, as both processes heat up biomass to a certain temperature and hold the biomass for a certain time. Equipment for torrefaction is based on drying equipment [67]. The torrefaction reactor can be heated directly or indirectly. This study focuses on volatiles valorization. To ensure that the volatiles do not mix with the heating agent, only indirectly heated torrefaction reactors are discussed in this section.

2.3.1 Moving bed reactor

Figure 2.5 presents an overview of a combined dryer and moving bed reactor. The moving bed reactor is similar to the moving bed dryer in that the feed moves through the reactor. Solids enter the reactor at the top after which they are indirectly heated by hot air or a flue gas. The torrefied product leaves the reactor at the bottom. The main advantage of this design is its simplicity. The main disadvantage is the difficult temperature control, resulting different solids conversions [67].

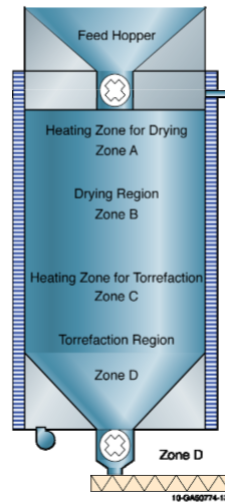


Figure 2.5: Moving bed reactor

Source: [68]

2.3.2 Rotating drum reactor

Figure 2.6 presents an overview of a rotating drum reactor. A heating jacket is used to provide heat to the reactor instead of a heating agent. The dryer rotates the biomass via flights to improve heat transfer characteristics. The indirectly heated rotating drum reactor operates similarly to the directly heated one discussed in the dryer section, but in this case the heating agent flows outside of the drum in a shell around it. The temperature of the heating agent should be close to the operational temperature of the biomass to prevent burning of the biomass when it touches the walls. An advantage of this reactor type is the uniform heat distribution and thus uniform torrefaction of the biomass [67]. A disadvantage is the large footprint and associated high costs [67].

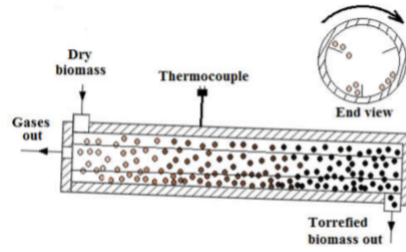


Figure 2.6: Rotating drum reactor

Source: [69]

2.3.3 Screw conveyor

Figure 2.7 presents an overview of a screw conveyor reactor. Feedstock is fed to the reactor from the top. A screw is used to transport the biomass through the torrefaction reactor. Outside of the screw, a hull is placed so that the biomass can be indirectly heated. An advantage of this reactor is its cheap price. Disadvantages are the charring of biomass in contact with the reactor walls and the absence of mixing, resulting in an uneven heat distribution [67].

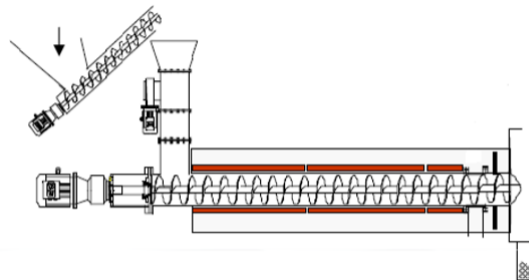


Figure 2.7: Screw conveyor

Source: [70]

2.3.4 Scale

Two conflicting aspects of a torrefaction plant influence the ideal size of a torrefaction plant. Because of the high moisture content and low bulk density, it is difficult to transport biomass, making centralized torrefaction plants with a large catchment area unfeasible due to the long transportation distances [71]. On the other hand, upscaling is an easy way to reduce costs of equipment like the dryer and

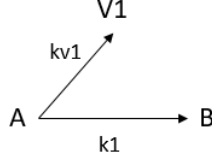
torrefaction reactor [71]. On average, the optimal production capacity of pelletized biomass was found to be around 100 kton/year [17],[71],[72],[73],[74].

2.3.5 Torrefaction modelling

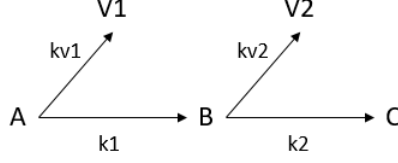
Modelling the torrefaction process consists of modelling the solid weight loss kinetics, volatiles generation kinetics and volatiles composition. The (solid) weight loss refers to the biomass (solids) converted to volatiles (gasses) during torrefaction. Experimental data on solid weight loss and volatiles production during torrefaction is required in order to simulate the torrefaction process [17].

Weight loss modelling

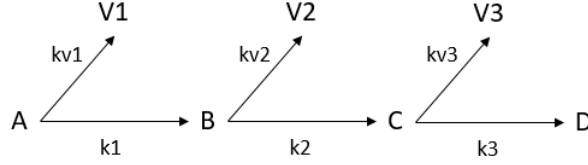
Torrefaction is a complex reaction mechanism which is difficult to model using reaction kinetics. Therefore, often simplified models are used to model the weight loss kinetics of torrefaction [63]. Examples of a simplified mechanism are 1-step, 2-step and 3-step mechanisms, presented in Figures 2.8a to 2.8c.



(a) 1-step mechanism



(b) 2-step mechanism



(c) 3-step mechanism

Figure 2.8: Torrefaction mechanisms

The 1-step mechanism, presented in Figure 2.8a, is used to determine the solid weight loss rate via a 1-step mechanism. It accounts for solid weight loss and volatiles generation [75]. The 2-step mechanism, presented in Figure 2.8b, originally developed by Di Blasi et al. [75], is the most used mechanism for torrefaction modelling [17],[63],[76]. This mechanism is based on the assumption that torrefaction can be modelled as a 2-step reaction mechanism. This is an improvement over the 1-step model, as it more accurately predicts volatile generation [75]. The 3-step mechanism, presented in Figure 2.8c, is a further development of the 2-step mechanism, adding an extra weight loss step. The mechanisms are solved using differential equations. Eq. (2.1) presents the differential equation which describes the first step for all three mechanisms. Similar differential equations are valid for the other steps in the 2- and 3-step mechanisms. All differential equations can be solved analytically, yielding equations on weight loss and volatiles generation dependent on time.

$$\frac{dA}{dt} = -(k_1 + k_{v1})A \quad (2.1)$$

The 1-step, 2-step and 3-step mechanism, when solved, are used to obtain general equations on the the weight loss kinetics and volatiles generation, but it is not possible to provide insight into the volatiles composition.

Volatiles composition

Several ways were found to model the volatiles composition during torrefaction. One method is the following one, presented originally by Tumuluru et al. [22]. It optimizes the matrix calculation, presented in Eq. (2.2) to fit the experimental data on volatiles composition as well as possible.

$$\begin{bmatrix} W_{V1}^{T_1} & W_{V2}^{T_1} \\ W_{V1}^{T_2} & W_{V2}^{T_2} \\ \vdots & \vdots \\ W_{V1}^{T_i} & W_{V1}^{T_i} \end{bmatrix} \cdot \begin{bmatrix} X_{i,V1} & X_{j,V1} & \dots & X_{z,V1} \\ X_{i,V2} & X_{j,V2} & \dots & X_{z,V2} \end{bmatrix} = \begin{bmatrix} Y_i^{T_1} & Y_j^{T_1} & \dots & Y_z^{T_1} \\ Y_i^{T_2} & Y_j^{T_2} & \dots & Y_z^{T_2} \\ \vdots & \vdots & \ddots & \vdots \\ Y_i^{T_i} & Y_j^{T_i} & \dots & Y_z^{T_i} \end{bmatrix} \quad (2.2)$$

Here $W_{V1}^{T_1}$ is the weight fraction in terms of % of the dry weight of the biomass of V1 at temperature T_1 . $X_{i,V1}$ is the fraction of component i in V1 and $Y_1^{T_1}$ is the weight fraction of component i at temperature T_1 in terms of % of the dry weight of the biomass. Since the weight fractions (W) of V1 and V2 at various temperatures are known through the employment of the 1-step, 2-step or 3-step mechanisms as discussed before, as well as the weight fractions (Y) of the compounds at various temperatures through experimental data, the compositions (X) of V1 and V2 can be determined using an optimization tool. The optimization tool optimizes the composition of V1 and V2 for all temperatures for a certain torrefaction time. By using this method on experimental data with various torrefaction times and temperatures, it is possible to set up general equations on the compositions of V1 and V2 as a function of time [22]. As the ratio between the sizes of V1 and V2 varies with temperature, because the mass flow of V1 and V2 changes with temperature (Section 3.3.2 provides a more elaborate discussion on the relation between the size of V1 and V2 with temperature), the combined volatiles composition is dependent on time and temperature. An advantage of this method is its wide applicability on different kinds of biomass, and the ability relate the volatiles composition with temperature and time.

A different way of obtaining a volatiles composition is through the work of Neves et al. [77]. They gathered a lot of experimental data on the torrefaction of a lot of different types of biomass to set up general equations on the volatiles composition. A disadvantage of this method is that it only correlates the volatiles yields with temperature, not with time. Subsequently, it often finds a quite low correlation between the model and the experimental data because of the high amount of different crops used in this study.

A third method is used by Ranzi et al. [78]. They found individual reaction rates for the formation of each volatile component (e.g. CO_2 or H_2), which were obtained by curve fitting Arrhenius equations for the formation of the volatiles out of specific solid fraction (e.g. cellulose, hemicellulose) to experimental data. The reaction rates obtained by this method are only valid for the biomass used in Ranzi et al. [78]. This limits the applicability of this method.

2.3.6 Torrefaction in Aspen Plus

There is no equipment in Aspen Plus which is designed to model torrefaction. To implement torrefaction in Aspen Plus, other authors use the models described above to model the weight loss kinetics and the volatiles composition in Aspen Plus through a calculator block and a reactor block. They either use an RSTOIC reactor ([79]) or RYIELD reactor ([20],[58],[80]), or a combination of the two ([19],[17],[81]) along with a calculator block which implements the solid weight loss and volatile yields. The RSTOIC block is operated by assuming a reaction in which the biomass breaks apart in various volatiles. The conversion of the reaction and the volatiles composition can be specified in a calculator block [17]. The RYIELD reactor model in Aspen Plus can be used to simulate the yield of various components after torrefaction. When used to simulate the torrefaction of biomass, the resulting compounds are the torrefied biomass and the volatiles.

2.4 Volatiles valorization

Volatiles valorization is the main subject of this study. A limited amount of research was done on this topic, especially in comparing different ways of valorization. As stated in the introduction, this study will focus on three methods of valorization:

1. Combustion
2. Chemical looping combustion
3. Chemical looping steam reforming

This section reports on the theory behind these three methods and gives examples on how this was simulated in Aspen Plus.

2.4.1 Combustion

Combustion of the volatiles is the most used method of volatiles valorization [17]. In the earliest techno-economic analyses on torrefaction volatiles combustion is

already used to provide (part of) the heat required in the dryer and torrefaction reactor [13]. The volatiles are sent to a combustor in which they are burned in the presence of air. Manoucherinejad et al. [17] and Arteaga-Pérez et al. [19] modelled this in Aspen Plus using an RGibbs block, which minimizes the Gibbs free energy of the reaction. An excess of air was used by both to ensure full combustion. No other sources were found which elaborate on the combustion of volatiles in Aspen Plus.

2.4.2 Chemical looping combustion

Chemical looping combustion is a technique which originates from the coal industry, where it is a way of generating electricity while also reducing CO_2 emissions [82],[83]. CO_2 emissions are reduced through the generation of a pure CO_2 stream (over 90 % pure) in the CLC process [82]. The CO_2 stream has potential for transportation and sequestration because of its high purity. A schematic overview of the process is shown in Figure 2.9.

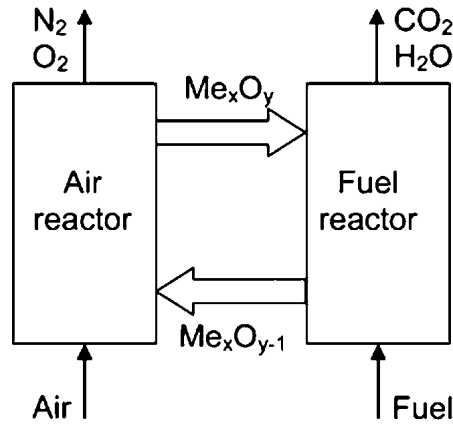


Figure 2.9: Schematic overview of chemical looping

Source: [84]

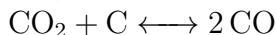
The fuel in Figure 2.9 is fed on the right side in the fuel reactor (FR), where it is converted into CO_2 , CO , H_2 and water using $MeOx$, which is an oxidized metal which acts as an oxygen carrier. The reaction mechanisms are very complex, but the following simplified reactions give an overview.

1. Volatiles $\longrightarrow CO + H_2 + H_2O + CO_2$,
2. $MeOx \longrightarrow Me$

Thermodynamic analyses have shown that the most suitable oxygen carriers when volatiles produced during torrefaction of biomass are used as feedstock are hematite, Fe_2O_3 , or nickel oxide, NiO [85],[86],[87]. Nickel oxide is generally preferred over iron oxide due to its higher reactivity and longer lifetime [88], [89]. The amount of oxygen carrier required depends on the type of oxygen carrier used. Bimbela et al. [90] found that a weight ratio between the oxygen carrier and volatiles passing the reactor per hour of 0.0025 was optimal for syngas production through chemical looping of acetic acid over NiO . Heng et al. [91] found a molar ratio between oxygen carrier and volatiles passing per hour in the reactor of 3 was optimal for hydrogen production through chemical looping of condensed volatiles obtained through torrefaction and steam reforming. The oxygen carrier is regenerated in the air reactor (AR), where the oxygen in the air is used to oxidize the oxygen carrier. The FR and AR operate at atmospheric pressure and the temperature varies depending on the oxygen carrier. For example, between 850 and 950 °C if iron oxides are used [91] and between 500 and 700 °C if nickel oxides are used [90]. The process in the FR is endothermic [91], thus requiring energy. Heng et al. [91] and Deshpande et al. [92] suggested that this energy demand can be met by feeding the fuel at a higher temperature than the temperature of operation in the FR, thereby providing the energy necessary in the FR. The AR is exothermic, and produces heat [91].

Boudouard reaction

A challenge in chemical looping combustion is the Boudouard reaction due to coke deposition. This reaction describes the balance between CO_2 , CO and solid carbon, via the following mechanism:



The formation of solid carbon and CO_2 is promoted at lower temperatures leading to coke deposition, thereby causing erosion to machinery and oxygen carrier deactivation [91]. The equilibrium constant of this reaction is equal to 0 at 702 °C or 975 K [93].

Chemical looping combustion in Aspen Plus

Like torrefaction, chemical looping combustion is not easily simulated in Aspen Plus. Various reactor blocks are used to simulate the process. Heng et al. [91] used an RGibbs reactor to simulate the CLC. Deshpande et al. [92] used an RGibbs reactor to simulate the gasification of the biomass, after which an RSTOIC was used to simulate the chemical looping combustor. The reactions for the RSTOIC are shown below for iron oxide as an oxygen carrier. These reactions were gathered from Heng et al. [91]. No reaction mechanism was found for nickel oxides.

1. Volatiles \longrightarrow CO + H₂ + H₂O + CO₂,
2. $4.504 \text{ Fe}_2\text{O}_3 + \text{CH}_4 \longrightarrow 9.512 \text{ FeO}_{0.9470} + 2 \text{ H}_2\text{O} + \text{CO}_2 \quad \Delta H^0 = 289.3 \text{ kJ/mol},$
3. $3 \text{ Fe}_2\text{O}_3 + \text{CO} \longrightarrow 2 \text{ Fe}_3\text{O}_4 + \text{CO}_2 \quad \Delta H^0 = -47.006 \text{ kJ/mol},$
4. $3 \text{ Fe}_2\text{O}_3 + \text{H}_2 \longrightarrow 2 \text{ Fe}_3\text{O}_4 + \text{H}_2\text{O} \quad \Delta H^0 = -49.856 \text{ kJ/mol},$
5. $1.202 \text{ Fe}_3\text{O}_4 + \text{CO} \longrightarrow 3.807 \text{ FeO}_{0.9470} + \text{CO}_2 \quad \Delta H^0 = 47.600 \text{ kJ/mol},$
6. $1.202 \text{ Fe}_3\text{O}_4 + \text{H}_2 \longrightarrow 3.807 \text{ FeO}_{0.9470} + \text{H}_2\text{O} \quad \Delta H^0 = 88.100 \text{ kJ/mol},$
7. $1.202 \text{ Fe}_3\text{O}_4 + \text{CH}_4 \longrightarrow 3.807 \text{ FeO}_{0.9470} + 2 \text{ H}_2 + \text{CO} \quad \Delta H^0 = 294.650 \text{ kJ/mol},$
8. $4.807 \text{ Fe}_3\text{O}_4 + \text{CH}_4 \longrightarrow 15.266 \text{ FeO}_{0.9470} + 2 \text{ H}_2\text{O} + \text{CO}_2 \quad \Delta H^0 = 18.472 \text{ kJ/mol},$
9. $3 \text{ Fe}_2\text{O}_3 + \text{CO} \longrightarrow 2 \text{ Fe}_3\text{O}_4 + \text{CO}_2 \quad \Delta H^0 = -43.200 \text{ kJ/mol},$
10. $3 \text{ Fe}_2\text{O}_3 + \text{H}_2 \longrightarrow 2 \text{ Fe}_3\text{O}_4 + \text{H}_2\text{O} \quad \Delta H^0 = -2.7 \text{ kJ/mol}.$

The simulation of Deshpande et al. [92] used an FR temperature between 895 °C and 985 °C and a AR temperature of 950 °C. Both reactors operated at atmospheric pressure.

2.4.3 Chemical looping steam reforming

An additional configuration of the chemical looping process is to produce hydrogen. This is done via steam reforming. The process is presented in Figure 2.10.

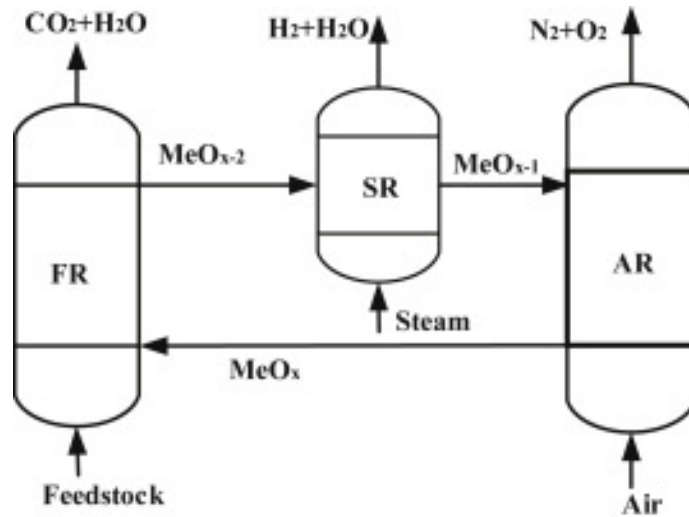
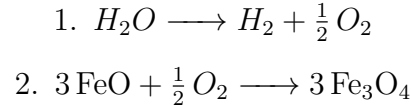


Figure 2.10: Schematic overview of chemical looping

Source: [91]

In Figure 2.10, an additional reactor is placed as opposed to Figure 2.9: the steam reactor (SR). Here, steam is reformed to hydrogen by partly oxidizing the reduced oxygen carrier. Having the hydrogen production take place in a separate reactor instead of in the fuel reactor ensures easy separation of the hydrogen [91]. Iron oxides used as an oxygen carrier in this process, as they can be reduced to wüstite (FeO) from hematite (Fe_2O_3) in the FR, and then partly oxidized in the SR to magnetite (Fe_3O_4) [91]. The reaction in the SR is presented below [91].



An increase in formation of wüstite will also increase the yield of hydrogen. For this purpose, in Figure 2.11 the phase diagram of FeOx is shown as a function of temperature and the partial pressures of CO (dashed lines) and H_2 (unbroken lines) in respect to the partial pressures of CO_2 and water. It is observed that the region with overlapping wüstite formation is small, which makes the production of wüstite challenging. Nevertheless, at a temperature around 850 °C, the partial pressures, and thus the mol % of both CO and H_2 are similar to the partial pressures and mol % of CO_2 and water. Because of this, the fuel reactor operates at a temperature of at least 850 °C.

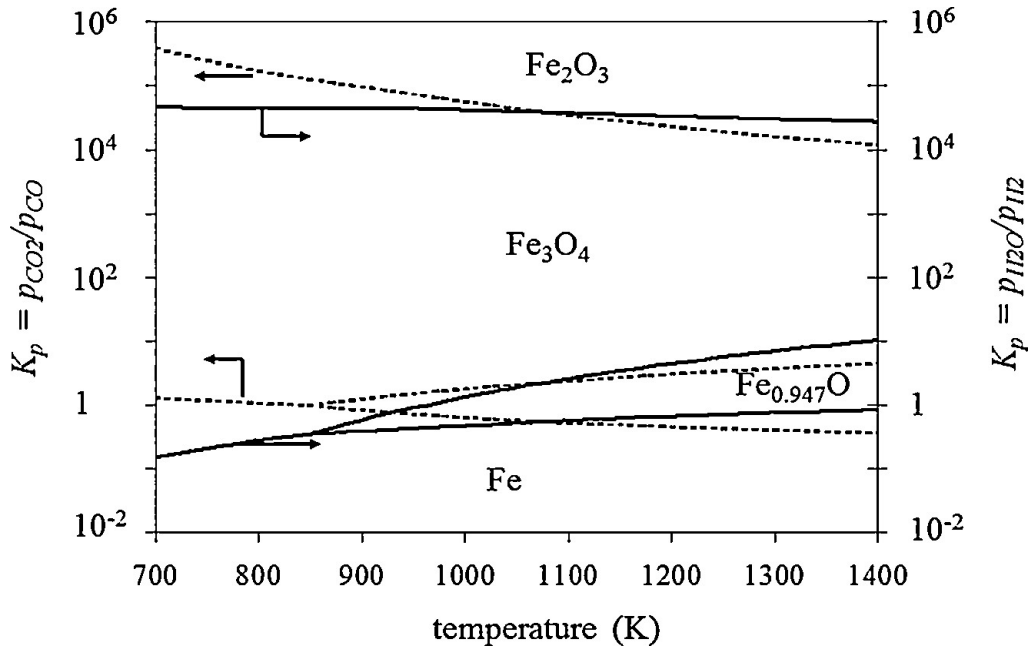


Figure 2.11: Phase diagram of FeOx

Source: [94]

The SR typically operates between 500 °C and 750 °C to converse FeO to Fe_3O_4 [91],[95]. This part of the process can be operated under high pressures of up to 90 bar [96]. Operating the SR under high pressures is attractive because it is less energy intensive to pressurize the water and solids before they enter the SR as opposed to pressurizing the hydrogen after it was produced [96]. Delivering pressurized hydrogen is preferred due to the low density of hydrogen at standard conditions (1 atm, 25 °C).

The benefit of this configuration is the production of hydrogen. There are several downsides to a configuration with the aim of hydrogen production, the most noticeable one being the lack of energy carrier production in the form of CO or CH_4 . Less combustible compounds are formed in the FR because of the high operational temperature [91], which means no combustor can be used to generate energy from this stream and less heat is generated for other units in the torrefaction plant. If the heat demand of the torrefaction plant is already met, valorizing the volatiles with the aim of hydrogen production can prove to be a valuable technique.

Chemical looping steam reforming is simulated in Aspen Plus in a similar manner as chemical looping combustion. Heng et al. [91] used an RGibbs reactors for the FR, SR and AR. In Heng et al. [91], the FR operates at 850 °C, the SR at 750 °C and the AR between 950-1100 °C, all at atmospheric pressure. The resulting hydrogen had a purity of 99.99 %.

Chapter 3

Methodology

This chapter presents the modelling approach for simulating the drying and torrefaction process in Aspen Plus, as well as the methodology used for the design of different process configurations for the valorization of the volatiles. Aspen Plus was chosen as the model environment, as it contains an extensive database (thermodynamic data and equipment models) and user-friendly interface for evaluation of a great variety of chemical processes. It also provides tools for economic evaluation of the equipment used, both in terms of capital expenditures (CAPEX) and operational expenditures (OPEX). First, this chapter discusses the types of biomass for which a simulation in Aspen Plus was made along with a brief overview of the process as it was modelled in Aspen Plus. Secondly, this chapter presents the simulation approach in Aspen Plus for the drying and torrefaction. Thirdly, this chapter discusses the different process configurations for the valorization of the volatiles. Fourthly, the approach to economic analysis is discussed.

3.1 Biomass selection

As stated in Section 2.2.5 and Section 2.3.5, experimental data on drying and torrefaction is required to simulate these processes in Aspen Plus. Out of the seven types of biomass discussed in Section 2.1, only for two types of biomass enough experimental data was found on drying and torrefaction. These two were corn stalk and sugarcane bagasse. Sunflower stalk lacked data on torrefaction, while for sugar beet pulp, corn cobs, rape stalk and sunflower seed shells lacked data on drying. It has therefore been decided to only include corn stalk and sugarcane bagasse for the simulations in Aspen Plus. CS and SCB are used as abbreviations for corn stalk and sugarcane bagasse throughout this Thesis.

3.2 Aspen Plus modelling

One of the main reasons to choose Aspen Plus as the modelling software of choice was the option to model the behaviour of biomass in this program. Aspen Plus has an enormous database of chemical compounds, but the version used for simulations in this Thesis (8.8) does not have biomass pre-defined due to its non-standard composition. Nevertheless, Aspen Plus offers the option to define non-conventional compounds. Biomass was defined through this feature. Biomass is similar to coal, as both materials are composed of mainly carbon, hydrogen and oxygen. Thus, biomass was modelled using the standard coal property models HCOALGEN and DCOALIGT. The simulation of biomass using these two models was validated with experimental data by Manoucherinejad et al. [17]. These property models require the proximate, ultimate and sulfur analyses of the fuel. The proximate and ultimate analyses were obtained from the available literature (see Section 2.1). The sulfur fraction of biomass consists purely of organic sulphur, and does not require additional specification.

3.2.1 Environmental conditions

Before simulation of the torrefaction process, the standard conditions of the simulation were specified for several input streams. For example, adequate simulation of air used for drying or combustion required a specific temperature and humidity. The air temperature outside and humidity are dependent on the location of the torrefaction plant. Since transportation of raw biomass is expensive, as was discussed in Section 2.3.4, the torrefaction plant was placed near the production location of either corn stalk or sugarcane bagasse. Corn is usually grown in colder climates, like Europe and the US. Sugarcane, on the other hand, thrives in tropical regions. One production location for both types of biomass would make an equal comparison of outcome possible, and is therefore preferred over two separate locations. One country grows both varieties of biomass: Brazil [97]. Furthermore, to ensure easy exportation of the produced pellets, it was beneficial to locate the torrefaction plant near the coast, but also near the production sites in Brazil. Most of the production of corn and sugarcane takes place in the southern part of Brazil [98]. Also large ports, like the port of Santos, are located nearby, thus it was decided to locate the torrefaction plant in the southern part of Brazil, specifically near the town of Curitiba. The average temperature of Curitiba ranges between 10 °C-25 °C, with a yearly average of 17 °C [99], while the average humidity is 80 % [100]. The input conditions for air in Aspen Plus were set at 17 °C, 80 % humidity and 1 bar.

3.2.2 Basic simulation model

To simulate the torrefaction plant and valorization of the volatiles in Aspen Plus, three main types of equipment are required: a dryer, a torrefaction reactor and a valorization unit. Figure 3.1 presents the basic block scheme for the torrefaction process. Hot air and biomass enter the dryer unit, out of which wet air and dried biomass leave. The dried biomass is sent to the torrefaction reactor, where it is torrefied. The torrefied biomass leaves the torrefaction reactor to be processed further. The volatiles generated during torrefaction are sent to the valorization unit. The valorization unit was a combustor or chemical looping combustor, depending on the process configuration selected. The flue gasses leaving the valorization unit are used to provide heat to the air used in the dryer. The remaining thermal energy is used to heat air used to provide thermal energy the torrefaction reactor.

Every process configuration was optimized to operate at a torrefaction temperature as low as possible, while remaining self-sufficient, which means it aims to reduce the amount of auxiliary fuels required for providing heat to the dryer and torrefaction reactor as much as possible. If auxiliary fuel was required, the torrefaction temperature was first increased to obtain a larger volatile fraction, which was used to generate more thermal heat required by the dryer or torrefaction reactor. Only if raising the torrefaction temperature to 300 °C still wasn't sufficient in providing enough thermal energy for the dryer and torrefaction reactor, auxiliary fuels were used. A lower torrefaction temperature is beneficial as this increases the solid yield (torrefied biomass + ash) in the torrefaction reactor, thereby reducing the feedstock required. Less feedstock reduces the dimensions of the dryer and torrefaction reactor, which is beneficial in economic terms. Furthermore, it was assumed that apart from the energy needed in the form of heat for the dryer and the torrefaction reactor, no additional energy for auxiliary equipment, for example pumps and conveyor belts, is needed. For example, mechanical energy requirements to rotate the dryer or transport the solids through the torrefaction reactor. Whenever data or models were not available in Aspen Plus, this was assumed or calculated.

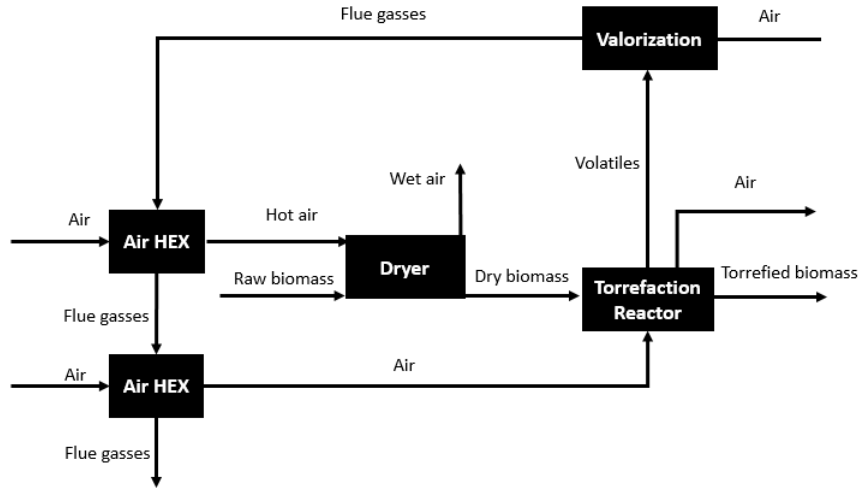


Figure 3.1: Basic block scheme

3.3 Dryer

The following parameters regarding the dryer were required by Aspen Plus to be defined prior to simulating the dryer: length, cross-sectional area, residence time, fill grade, porosity, Sherwood number, gas velocity, equilibrium moisture content, critical moisture content and (normalized) drying data. First the equilibrium moisture content, critical moisture content, drying data and residence time are discussed through an analysis of the drying kinetics. Secondly, fill grade, porosity, length, cross-sectional area, Sherwood number and gas velocity are discussed.

3.3.1 Drying kinetics

Drying kinetics are key in understanding and developing a process for the torrefaction of biomass. The aim of this section is to obtain information on the critical and equilibrium moisture content of biomass and to draw general equations for drying dependent on time, temperature and particle size, so that the drying time, normalized drying data, critical and equilibrium moisture content were implemented in the dryer simulation in Aspen Plus.

Critical and equilibrium moisture content

The critical and equilibrium moisture content are parameters required for adequate drying simulation. The equilibrium moisture content is the residual moisture left in the biomass after drying at a certain temperature [101]. Figure 3.2 presents an

overview of three drying regimes typical of solids drying. The x-axis represents the moisture content, X , in the solid while the y-axis represents the drying rate, N , in terms of moisture lost due to evaporation per time unit. The right side drying regime, from A to B, is associated with the entrance effect of the heating of the solid, and therefore increasing drying rate. This entrance effect was assumed to be insignificant in this Thesis, due to the rather long drying times encountered. The middle regime, from B to C, represents a constant drying regime, with a constant, maximum drying rate, N_{max} . In this regime, the surface of the particle is fully covered in moisture, making the drying process limited by heat transfer from the drying agent to the moisture. The moisture content at which, during drying, the surface of the particle is not completely saturated anymore is the critical moisture content [102]. This point is marked by X_c on the x-axis in Figure 3.2. The point of critical moisture is noticed in experimental drying data as the moisture content at which the drying rate decreases. The point of critical moisture content signals a change in the drying regime, from a heat transfer limited process in the first part to a mass transfer limited process in the last part [102]. The drying rate decreases between point C and D in Figure 3.2, until the equilibrium moisture content X_e is reached.

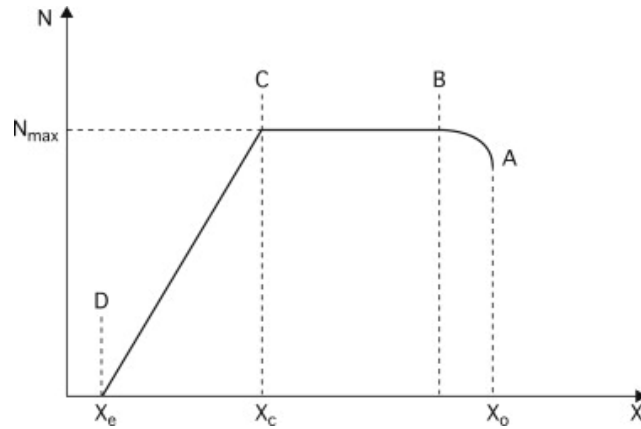


Figure 3.2: Drying regimes

Source: [103]

The normalized moisture content, or moisture ratio, NMC , is determined by eq. (3.1).

$$NMC = \frac{X - X_e}{X_c - X_e} \quad [104] \quad (3.1)$$

Where NMC is the normalized moisture content, X is the moisture content, X_c is the critical moisture content and X_e is the equilibrium moisture content. The normalized drying data was obtained by using Eq. (3.2).

$$NDR = \frac{\text{Current drying rate}}{\text{Drying rate 1st period}} \quad [104] \quad (3.2)$$

Drying equations

The drying data for CS and SCB were obtained from the most recent literature data available. Figure 3.3 presents the drying data for CS [101] and SCB [105].

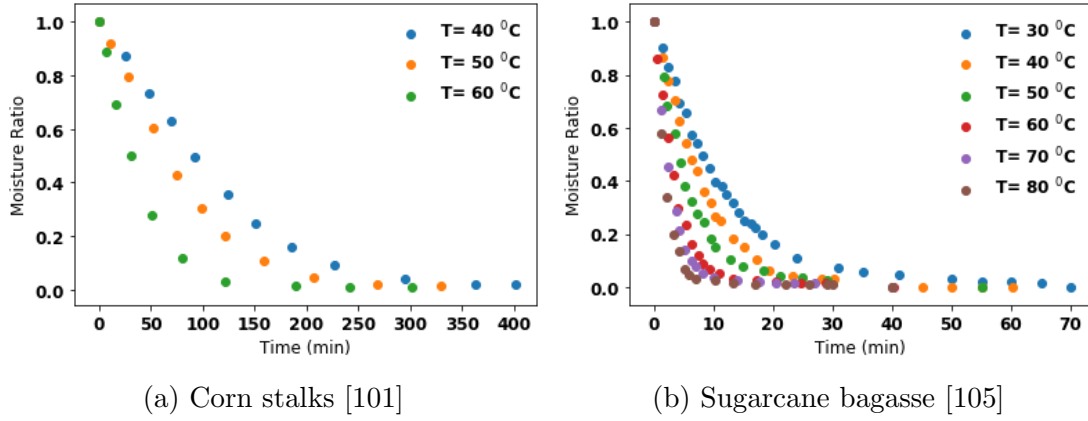


Figure 3.3: Drying data

The important characteristics from both types of biomass are presented in the Table 3.1. This Table presents the particle size of the biomass used in the experiments, along with the initial moisture content (X_i) and the equilibrium moisture content (X_e). The critical moisture content (X_c) for data presented Figure 3.3 is between 25 % (wb.) and 36 % (wb.) for CS and 19 % (wb.) and 40 % (wb.) for SCB.

Table 3.1: Properties CS and SCB from literature

Parameter	Corn stalks [101]	Sugarcane bagasse [105]
Diameter	12.5 mm	0.43 mm
X_i (% wb.)	40 %	25 %
X_e (% wb.)	3 %	1 - 4%

Curve fitting of the drying data is necessary to obtain general formulae for the drying of biomass, dependent only on temperature and time. These formulae are used to determine the residence time of the biomass in the dryer. The drying data was fitted to the Henderson-Pabis method presented in (3.3). This method was selected because of the good fitting results obtained using it, both by the literature

presented in Section 2.2.5 and in this Thesis. The fitting was done for the drying data by using the curvefit function from the scipy.optimize package in Python. This resulted in the following curves, shown in Figure 3.4.

$$MR(t) = A \cdot e^{-k \cdot t} \quad (3.3)$$

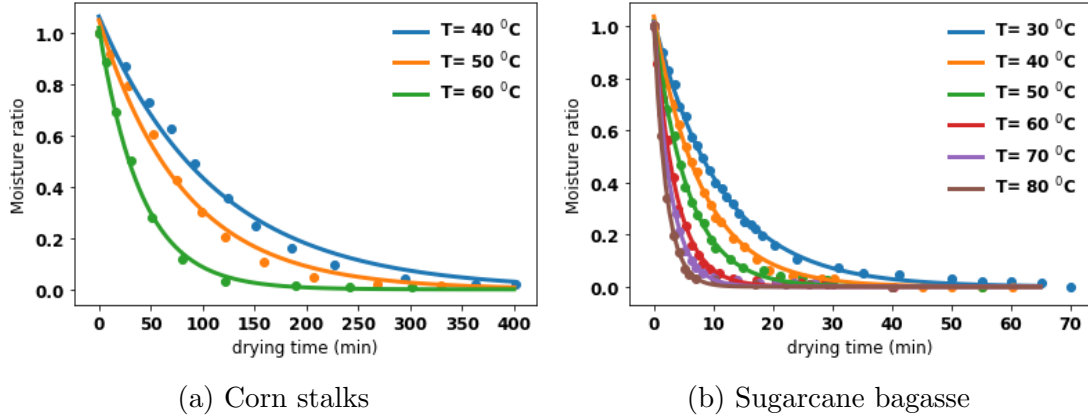


Figure 3.4: Curves fitted to drying data (see Table 3.4 for input values)

The results of the curve fitting are presented in Table 3.2 and 3.3 as the statistical parameters R^2 and X^2 . The R^2 value is above 0.988 for all curves fitted to the drying data of CS and at least 0.996 for the curves fitted to the drying data of SCB. The X^2 is below 0.11 for all curves fitted to the drying data of CS and below 0.1 for all curves fitted to the drying data of SCB. The difference in experimental data provides a reason for the fact that the fitting for SCB had a larger correlation with the experimental data than the CS fitting.

Table 3.2: Curve fitting results corn stalk

Temperature	A	k	R^2	X^2
40 °C	1.065	0.0089	0.989	0.103
50 °C	1.051	0.012	0.992	0.0707
60 °C	1.021	0.025	0.998	0.0391

Table 3.3: Curve fitting results sugarcane bagasse

Temperature	A	k	R^2	X^2
30 °C	1.021	0.089	0.998	0.058
40 °C	1.038	0.12	0.998	0.033
50 °C	1.017	0.18	0.998	0.052
60 °C	1.012	0.27	0.996	0.071
70 °C	1.015	0.36	0.997	0.082
80 °C	1.011	0.48	0.997	0.076

In Figure 3.5, values for A and k are plotted versus temperature to obtain an expression for A and k dependent on temperature. This was done to obtain more general version of equation 3.3, dependent on time and temperature.

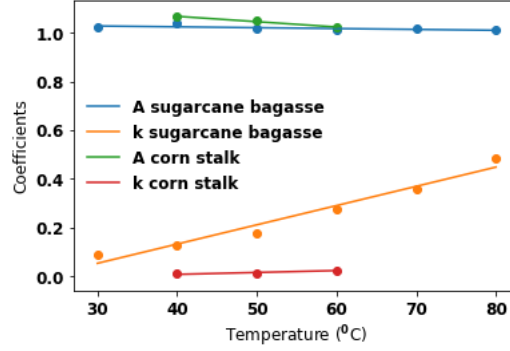


Figure 3.5: Drying Coefficients A & k versus temperature

A linear relationship between A, k and temperature was used to obtain an expression for A and k based on temperature as presented below.

$$A_{cs} = 1.16 - 2.19 \cdot 10^{-3} \cdot T \quad (3.4)$$

$$k_{cs} = -2.39 \cdot 10^{-2} + 7.84 \cdot 10^{-4} \cdot T \quad (3.5)$$

$$A_{scb} = 1.04 - 3.54 \cdot 10^{-4} \cdot T \quad (3.6)$$

$$k_{scb} = -1.84 \cdot 10^{-1} + 7.91 \cdot 10^{-3} \cdot T \quad (3.7)$$

Eq. (3.8) was used to relate the length L of the particle to the moisture ratio. When Eq. (3.8) is compared to Eq. (3.3), it becomes clear that the length of the particle in Eq. (3.8) is related to the k-value in Eq. (3.3).

$$MR(t, D, L) = \frac{8}{\pi^2} \cdot e^{\frac{D \cdot t}{4 \cdot L^2}} \quad (3.8)$$

The k-value dependence on L was calculated using Eq. (3.9). Here, L_{old} refers to the particle length presented in Table 3.1.

$$k_{new} = \left(\frac{L_{new}}{L_{old}} \right)^2 \cdot k_{old} \quad (3.9)$$

Eq. (3.4) - (3.7) and Eq. (3.9) were implemented in the general equation for the moisture ratio, Eq.(3.3), to obtain a specific equation for the moisture ratio of CS and SCB based on temperature, drying time and particle size. Eq.(3.10) and

eq.(3.11) presents the relationship between moisture ratio, drying temperature, drying time and particle size for CS and SCB, respectively. T is the temperature in $^{\circ}\text{C}$ and t is time in minutes.

$$MR_{CS}(T, t, L) = (1.16 - 2.19 \cdot 10^{-3} \cdot T) \cdot e^{-(7.84 \cdot 10^{-4} \cdot T - 2.39 \cdot 10^{-2}) \cdot (\frac{L_{new}}{L_{old}})^2 \cdot t} \quad (3.10)$$

$$MR_{SCB}(T, t, L) = (1.04 - 3.54 \cdot 10^{-4} \cdot T) \cdot e^{-(7.91 \cdot 10^{-3} \cdot T - 1.84 \cdot 10^{-1}) \cdot (\frac{L_{new}}{L_{old}})^2 \cdot t} \quad (3.11)$$

Particle characteristics in Aspen Plus

Table 3.4 presents the input parameters for the particle size, initial moisture content and equilibrium moisture content for the Aspen Plus model. Before transportation of the CS from the farm to the torrefaction plant, the CS is often shredded to make transportation more convenient [106]. Sokhansanj et al. [106] found that shredding to 6 mm was required before transportation of the CS. 6 mm was set as the diameter of the CS particles for the simulations in Aspen Plus. Costa et al. [107] found that the fresh particle size of sugarcane bagasse ranged from 0.3 mm to 4.75 mm, with a mean of 1.5 mm. The particle size of sugarcane bagasse thus was set at 1.5 mm in Aspen Plus. The initial moisture content of SCB was taken from the proximate analysis, while the initial moisture content of CS was assumed to be 40 %, based on research by Bonner et al. [101]. The equilibrium moisture content for CS was found be constant within the temperature range of 40 $^{\circ}\text{C}$ to 60 $^{\circ}\text{C}$ at 3 % wb. The equilibrium moisture content of sugarcane bagasse was determined by curve fitting the data from Scheufler et al. [105] to a 2nd degree polynomial. The data and curve fit are presented below in Figure 3.6. Equation (3.12) shows the fitted equation.

$$X_{e_{scb}} = 5.36 \cdot 10^{-6} \cdot T^2 - 5.16 \cdot 10^{-3} \cdot T + 0.566 \quad (3.12)$$

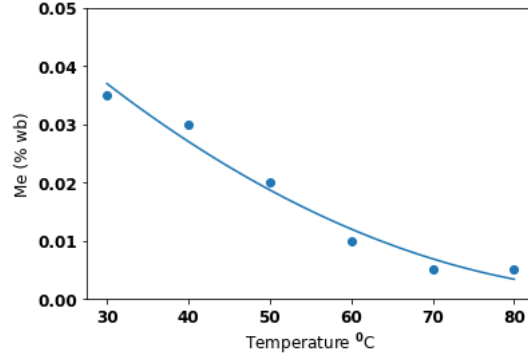


Figure 3.6: Equilibrium moisture content sugarcane bagasse

Table 3.4: Standardized length parameters drying in Aspen Plus

Parameter	Corn stalks	Sugarcane bagasse
Diameter	6.0 mm	1.5 mm
X_i (% wet wt.)	40 %	48.25 %
X_e (% wet wt.)	3%	1-4 %

Energy balance dryer

To obtain the residence time of the biomass in the dryer, Eq. (3.10) and Eq. (3.11) were applied in Aspen Plus. In order to calculate the residence time, information on dryer temperature and moisture ratio after drying were required. The moisture after drying was set to 6 %, which is in accordance with the literature discussed in Section 2.2. The temperature of the dryer was determined via an energy balance. Figure 3.7 shows the schematic illustration of the drying process as a black box model. The temperature of the biomass before drying was set at 17 °C, which is based on the local weather conditions as discussed in Section 3.2. The temperature of the air used for drying, T_{a1} , was set to 400 °C, which is in accordance with the temperature range of drying agents in rotary drum dryers as found in the literature review of the dryer in Section 2.2. The amount of air needed in the dryer, \dot{m}_{a1} , was determined via a design spec in Aspen Plus. A design spec is used in Aspen Plus to obtain a certain design specification (e.g. moisture content after drying of 6 %) through varying a stream or block parameter (e.g. air temperature, air mass flow or dryer length). The target of the design spec was defined as the outlet moisture content of the biomass leaving the dryer and the target value was set to be equal to 6 % with a tolerance of 0.1 %. The black box model is presented for the CS configuration. The mass flow of air entering the dryer was adjusted to reach this target. The $c_{P,bio}$ was assumed 1.426 and independent of temperature, based on research by Dupont et al. [108].

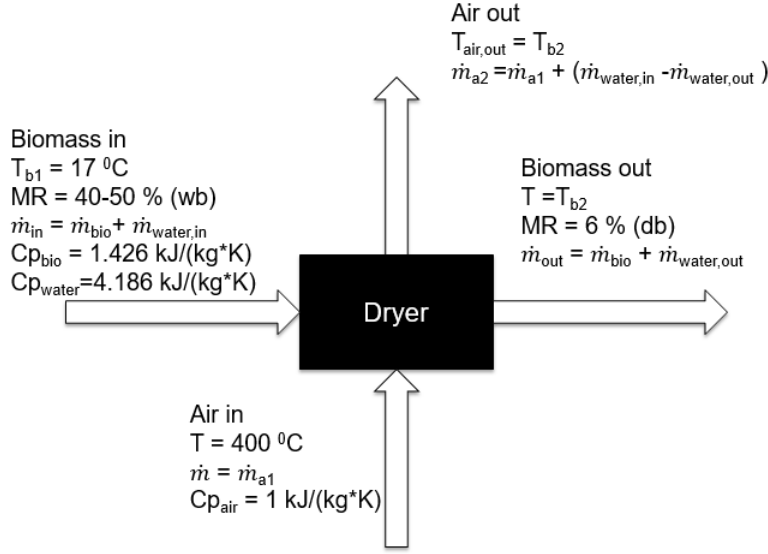


Figure 3.7: Black box model for the dryer

The energy balance of the dryer is described by equations (3.13) to (3.15).

$$\Delta E_{biomass} = -\Delta E_{air} \quad (3.13)$$

$$\Delta E_{biomass} = (\dot{m}_{bio} \cdot c_{p,bio} + \dot{m}_{water,in} \cdot c_{p,water}) \cdot \Delta T_{biomass} + (\dot{m}_{water,out} - \dot{m}_{water,in}) \cdot LH \quad (3.14)$$

$$\Delta E_{air} = \Delta T_{air} \cdot \dot{m}_{air} \cdot c_{p,air} \quad (3.15)$$

Here, E is energy in J/hr , \dot{m} is the mass flow in kg/hr , LH is latent heat required for vaporization of water, in Joule/kg , c_p is the specific heat capacity in $\text{Joule}/(\text{kg}\cdot\text{K})$ and $\Delta T_{biomass}$ is the temperature difference of the material between the entrance of the dryer and the end of the dryer ($T_{b2}-T_{b1}$) and ΔT_{air} is the temperature difference of the air between the entrance and end of the dryer. It is assumed that the air and the solids have the same temperature at the end of the dryer, so that $T_{a2}=T_{b2}$. The operational temperature of the dryer, T_{b2} , was calculated using Eq. (3.16).

$$T_{b2} = \frac{T_{b1} \cdot (c_{p,bio} \cdot \dot{m}_{bio} + c_{p,water} \cdot \dot{m}_{water,in}) + T_{a1} \cdot c_{p,air} \cdot \dot{m}_{a1} - LH \cdot (\dot{m}_{water,out} - \dot{m}_{water,in})}{c_{p,bio} \cdot \dot{m}_{bio} + c_{p,water} \cdot \dot{m}_{water,in} + c_{p,air} \cdot \dot{m}_{a1}} \quad (3.16)$$

Figure 3.8 presents the relation between operational temperature of the dryer versus drying times for CS and SCB. CS requires less drying than SCB, due to its lower M_i and the difference in structure between CS and SCB. SCB, being a

processed product, consists of fibrous material, lowering its diffusion coefficient, resulting in longer drying times.

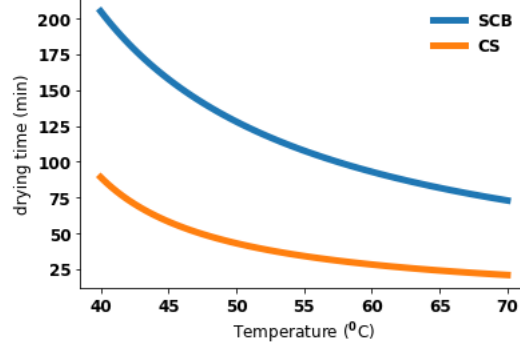


Figure 3.8: Drying time comparison (6 % final moisture, particle details in Table 3.4)

The drying temperature in Aspen Plus was limited in range by the experimental data obtained from literature. It was assumed that the dryer for all configurations operates between 60 °C and 70 °C, to reduce drying, as is clear in Figure 3.8, higher temperatures require less drying time, while refraining from pushing the extends of the experimental data too much. The exact temperature of the dryer was determined by the energy balance between the hot air entering the dryer and the energy required for heating the biomass and evaporating the moisture.

Dryer dimensions

The porosity and fill grade were set at 85 % and 15 % [17]. The area and length of the dryer are both dependent on the feed flow of raw biomass into the dryer, fill grade, porosity and residence time. Equations (3.17)-(3.19) present the calculations required to estimate the length of the dryer.

$$V_s = \dot{m}_{biomass} \cdot \tau \quad (3.17)$$

$$V_d = \frac{V_s}{(1 - \epsilon) \cdot \phi} \quad (3.18)$$

$$L = \frac{V_d}{A} \quad (3.19)$$

Where V_s is the volume of the solid biomass in m^3 , $\dot{m}_{biomass}$ is the flow of biomass entering the dryer in m^3/hr , τ is the drying time (hr), V_d is the volume of the dryer

in m^3 , ϵ is the fill grade of the dryer, ϕ is the porosity of the dryer, L is the length of the dryer (m) and A is the cross-sectional area of the dryer in m^2 .

The Sherwood number and the gas velocity were calculated by equation (3.20) to (3.26).

$$Sh = \sqrt{Sh_{laminar}^2 + Sh_{turbulent}^2} \quad [17] \quad (3.20)$$

where

$$Sh_{laminar} = 0.664 \cdot \sqrt{Re} \cdot Sc^{1/3} \quad [17] \quad (3.21)$$

and

$$Sh_{turbulent} = \frac{0.037 \cdot Re^{0.8} \cdot Pr}{1 + 2.433 \cdot Re^{-0.1} \cdot (Pr^{2/3} - 1)} \quad [17] \quad (3.22)$$

Eq. (3.21) holds for laminar flow over a flat surface for $Re \gg 1$ and $Sc \gg 1$ [109]. Eq. (3.22) holds for turbulent flow over a flat surface for $Sc \gg 1$ [109]. Because the particle size is much smaller (mm range) than the characteristic length of the dryer (m range), flow of biomass particles relative to the dryer surface is assumed to be like flow over a flat surface. The Reynolds number (Re), Prandtl number (Pr) and Schmidt number (Sc) are calculated using Equations (3.23)-(3.25):

$$Pr = \frac{\mu_G \cdot c_{P,G}}{h} \quad [17] \quad (3.23)$$

$$Re = \frac{u_{GP} \cdot \rho_G}{\mu_G} \quad [17] \quad (3.24)$$

$$Sc = \frac{\mu_G}{D \cdot \rho_G} \quad [17] \quad (3.25)$$

Where μ_G is the viscosity of water in $kg/(m \cdot s)$, $c_{P,G}$ is the heat capacity in $J/(K \cdot kg)$, h is the heat transfer coefficient in $W/(K \cdot m)$, u_G is the velocity in m/s , d_P is the characteristic length of the dryer in m , ρ_G is the density of the biomass in kg/m^3 and D is the mass diffusivity in m^2/s . The gas velocity u_{gas} was calculated by using equation (3.26):

$$u_{gas}(m/s) = \frac{\dot{V}_{air}}{A} \quad (3.26)$$

Where \dot{V}_{air} is the amount of air entering the dryer in m^3/s and A is the cross-sectional area of the dryer in m^2 . The cross-sectional area of the dryer is required to calculate the length in Eq. (3.19) and (3.26).

Manoucherinejad et al. [17] assumed a dryer length of 14 m and diameter of 2.4 m. It was decided to use a dryer of 14 m length and 3 m diameter to determine the amount of dryers required in parallel. This was done by assuming a diameter

of 3 m and dividing the total dryer length as calculated by Eq. (3.19) by 14 m (and rounding up to an integer).

The heat loss through the surface of the dryer was calculated based on the heat transfer coefficient (h_{conv}) and the curved surface area of the dryer (A_{dryer}):

$$h_{conv} = 1.32 \cdot \left(\frac{\Delta T}{D}\right)^{0.25} \quad [110] \quad (3.27)$$

$$Q = h_{conv} \cdot A_{dryer} \cdot \Delta T \quad (3.28)$$

Here, h_{conv} is in W/m^2K , ΔT is the difference between the temperature of the dryer and the outside temperature in $^{\circ}C$ and D is the diameter of the dryer in m. Q is the heat loss in W and A_{dryer} is in m^2 . All calculations implemented in the calculator block in Aspen Plus concerning the determination of the length, cross-sectional area, residence time, fill grade, porosity, Sherwood number, gas velocity, equilibrium moisture content, critical moisture content and (normalized) drying data for the dryer are presented in Appendix 1.5.1.

3.3.2 Torrefaction

Weight loss kinetics

The aim of this section is to draw general equations for the torrefaction weight loss kinetics and volatiles generation and composition dependent on torrefaction time and temperature which can be used in Aspen Plus to model torrefaction. It was assumed that heating rate had no influence on weight loss kinetics, volatiles generation and composition. The experimental data used to model the weight loss and volatiles generation during torrefaction in Aspen Plus is presented in Figure 3.9a and 3.9a.

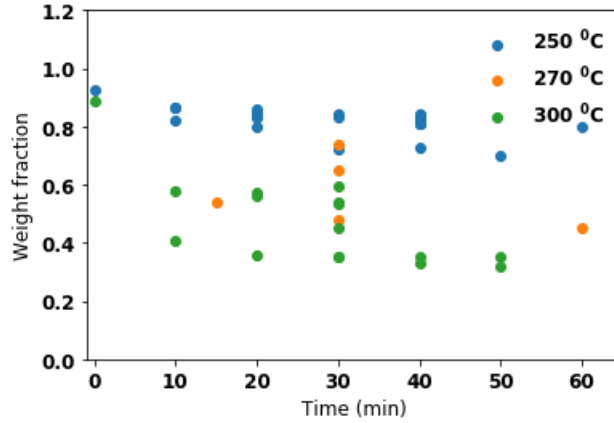


Figure 3.9a: Weight loss data torrefaction corn stalks

Sources: [27],[111],[112],[113][114],[115],[116],[117]

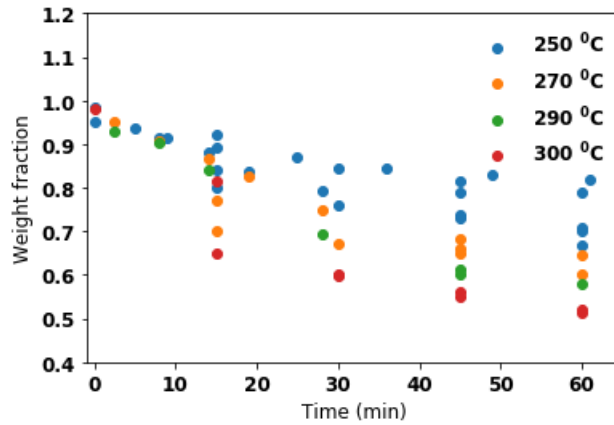


Figure 3.9b: Weight loss data torrefaction sugarcane bagasse

Sources: [118],[119],[120],[121],[122],[123],[124]

The literature review presented in Section 2.3.5 yielded three mechanisms which had potential to be used to simulate weight loss during torrefaction: the 1-step, 2-step and 3-step mechanisms. The three mechanisms assume that torrefaction and volatiles generation are modelled using either 1, 2 or 3 weight loss steps, while generating either 1, 2 or 3 volatile streams. The solid yield equations, which were calculated using the analytical solutions to the mechanisms, of all three mechanisms were fitted to the experimental data presented in Figures 3.9a and 3.9b. The results in terms of statistical correlations are presented in Table 3.5. SCB

has a larger R^2 value (0.872 to 0.924) than CS (0.512 to 0.679). This is because the torrefaction data is less wide-spread for sugarcane bagasse, which is visible in Figures 3.9a and 3.9b. The reason of the spread of experimental data regarding the weight loss of SCB and CS during torrefaction is due to different heating rates employed by the different sources and the differences in particle samples of CS and SCB used for the experiments by the different sources. The R^2 and X^2 values improve both for SCB and CS as higher order mechanism (3-step over 2-step, 2-step over 1-step) are used. The R^2 value for SCB increases from 0.872 to 0.918 when a 2-step mechanism is used instead of a 1-step mechanism. The X^2 value of sugarcane bagasse decreases from 0.0488 to 0.0357 when a 2-step mechanism is fitted to the experimental data instead of a 1-step mechanism. The R^2 for CS increases from 0.512 to 0.597 when a 2-step mechanism is applied instead of a 1-step mechanism. The X^2 value for corn stalk decreases from 0.964 to 0.390 when the 2-step mechanism is used instead of a 1-step one. Using a 3-step mechanism over a 2-step mechanism results in a smaller increase of the R^2 for SCB (0.06 difference with the 2-step mechanism), as opposed to the 0.109 increase between the 1-step and 2-step mechanisms. The X^2 value decreases 0.0059 when the 3-step mechanism is used instead of the 2-step one. When the 3-step mechanism is used for CS, the R^2 value increases by 0.082 in comparison to 2-step value, while the X^2 value decreases by 0.095. The change in the X^2 value for both CS and SCB is much larger when the 2-step mechanism is used instead of the 1-step mechanism (0.574 and 0.0131, respectively) than it is for when the 3-step mechanism is used instead of the 2-step one (0.095 and 0.0059, respectively). The change in the R^2 value is similar for CS between the 1-step mechanism and the 2-step mechanism (0.085) and between the 2-step mechanism and the 3-step mechanism (0.082), while the change for in the R^2 value for SCB is much larger between the 1-step and 2-step mechanisms (0.046) than between the 2-step and 3-step mechanisms (0.006). Because using the 3-step mechanism instead of the 2-step mechanism only improves the R^2 value of CS, while achieving the same results as the 2-step mechanism in for the R^2 values of SCB and for the X^2 values for both types of feedstock, in addition to the fact that the literature review in section 2.3.5 showed that the 2-step mechanism is employed more often in literature, it was decided to implement the results of 2-step mechanisms in Aspen Plus.

Table 3.5: Comparison of fitting methods for torrefaction

Mechanism	Sugarcane bagasse		Corn stalk	
	R^2	X^2	R^2	X^2
1-step	0.872	0.0488	0.512	0.964
2-step	0.918	0.0357	0.597	0.390
3-step	0.924	0.0298	0.679	0.295

The kinetic model of the 2-step mechanism is presented in Eq. (3.29)-(3.33).

$$\frac{dA}{dt} = -K1 \cdot A \quad (3.29)$$

$$\frac{dB}{dt} = kb \cdot A - K2 \cdot B \quad (3.30)$$

$$\frac{dC}{dt} = kc \cdot B \quad (3.31)$$

$$\frac{dV1}{dt} = kv1 \cdot A \quad (3.32)$$

$$\frac{dV2}{dt} = kv2 \cdot B \quad (3.33)$$

Where $K1=kb+kv1$ and $K2=kc+kv2$. These differential equations were solved analytically with the following boundary conditions:

1. $A(t=0)=1$
2. $B(t=0)=0$
3. $C(t=0)=0$
4. $V1(t=0)=0$
5. $V2(t=0)=0$

The solutions are as follows:

$$A = e^{-K1 \cdot t} \quad (3.34)$$

$$B = \frac{kb}{K1 - K2} \cdot (e^{-K2 \cdot t} - e^{-K1 \cdot t}) \quad (3.35)$$

$$C = \frac{kb \cdot kc}{(K1 - K2) \cdot K1 \cdot K2} \cdot (K1 - K2 - K1 \cdot e^{-K1 \cdot t} + K2 \cdot e^{-K2 \cdot t}) \quad (3.36)$$

$$V1 = \frac{kv1}{K1} \cdot (1 - e^{-K1 \cdot t}) \quad (3.37)$$

$$V2 = \frac{kv2 \cdot kb}{K1 - K2} \cdot K1 \cdot K2 \cdot (K1 - K2 - K1 \cdot e^{-K2 \cdot t} + K2 \cdot e^{-K1 \cdot t}) \quad (3.38)$$

Eq. (3.37) and (3.38) are two general equations which together describe the volatiles generation during torrefaction. The final amount of torrefied biomass was calculated by adding A, B and C, resulting in Eq. (3.39) :

$$Solids = \left(1 + \frac{kb \cdot K1 - kb \cdot K2}{K1 \cdot (K2 - K1)}\right) \cdot e^{-K1 \cdot t} + \frac{kb \cdot kc - kb \cdot K2}{K2 \cdot (K2 - K1)} \cdot e^{-K2 \cdot t} + \frac{kb \cdot kc}{K1 \cdot K2} \quad (3.39)$$

Figures 3.10a and 3.10b present the result of the curve fitting according to the 2-step mechanism.

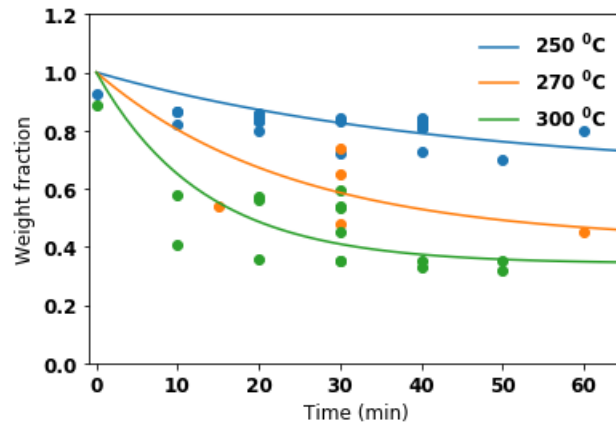


Figure 3.10a: Weight loss torrefaction CS fitted to a 2-step mechanism

Sources: [27],[111],[112],[113],[114],[115],[116],[117]

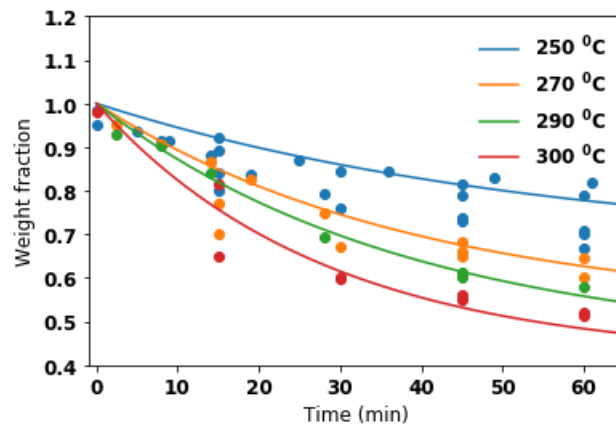


Figure 3.10b: Weight loss torrefaction SCB fitted to a 2-step mechanism

Sources: [118],[119],[120],[121],[122],[123],[124]

Equations (3.37), (3.38) and (3.39) are general equations for the generation of volatiles weight loss of solids during torrefaction for different torrefaction times, but have to be solved for each individual temperature to account for temperature. The curve fits for different temperatures presented in Figures 3.10a and 3.10b yielded different values for k_b , k_c , k_{v1} and k_{v2} . The k 's (k_b , k_c , k_{v1} and k_{v2})

were related to torrefaction temperature to obtain a general equation for weight loss kinetics and volatiles generation based on time and temperature. Equation (3.40) presents the relation between the k 's and temperature.

$$k_i(T) = A \cdot e^{\frac{-b}{R \cdot T}} \quad (3.40)$$

Here k_i is the activation coefficient used in Eq. (3.29)-(3.33), A is the pre-exponential factor, b is the activation energy in J, R is the gas constant in $J/(mol \cdot K)$ and T is the temperature in Kelvin. The k 's obtained after the curve fitting of the 2-step mechanism to the weight loss data were curve fitted to Eq. (3.40). The results of this are plotted below in Figure 3.11. For clarity, this was done using the Ln of the coefficient versus $1000/T$. Figure 3.11a shows that k_b and k_c remain constant versus temperature for CS while k_{v1} and k_{v2} increase with temperature. k_b for SCB is stable versus temperature as is shown in Figure 3.11b, while k_c , k_{v1} and k_{v2} increase with temperature. It becomes clear from Figure 3.11 that k_c is much larger than k_b , and thus the conversion from A to B is much slower than the conversion from B to C. Furthermore, k_{v2} is smaller than k_{v1} in at all temperatures in Figure 3.11a, thus V_1 is larger than V_2 in all cases of torrefaction for CS and SCB.

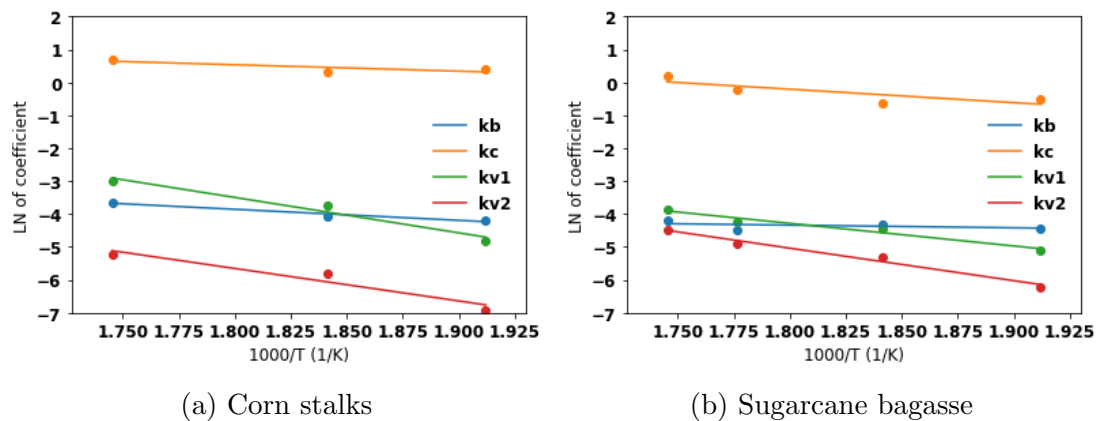


Figure 3.11: Torrefaction coefficients versus temperature

The values of A and b obtained from Eq. 3.40 for the different k 's are presented in the Table 3.6. The different k 's were implemented in Eq. (3.37), (3.38) and (3.39) to obtain the general volatiles generation and weight loss equations during torrefaction equations dependent on time and temperature, which in turn were implemented in Aspen Plus.

Table 3.6: K relations for each type of biomass

K value	A	b
k1 CS	1.21E+01	2.93E+04
k1 SCB	6.36E-02	7.29E+03
k2 CS	9.17E+01	1.83E+04
k2 SCB	1.18E+04	4.42E+04
kv1 CS	3.42E+05	7.49E+04
kv1 SCB	2.20E+03	5.53E+04
kv2 CS	5.85E+04	6.61E+04
kv2 SCB	1.72E+05	7.89E+04

Volatiles composition

The general equation for the volatiles composition was obtained by using the first method in Section 2.3.5, which used the approach by Tumuluru et al. [22], and by expending this method by adding time dependence. The method of Tumuluru et al. [22] was preferred over the other two methods discussed in section 2.3.5, as this method could be used for all types of biomass, while also allowing for a modification of the method so that the volatiles composition could be made dependent on time. Eq. (3.41), which was presented before in section 2.3.5, is shown again to elaborate on how a general equations for the compositions of V1 and V2 were obtained.

$$\begin{bmatrix} W_{V1}^{T_1} & W_{V2}^{T_1} \\ W_{V1}^{T_2} & W_{V2}^{T_2} \\ \vdots & \vdots \\ W_{V1}^{T_i} & W_{V1}^{T_i} \end{bmatrix} \cdot \begin{bmatrix} X_{i,V1} & X_{j,V1} & \dots & X_{z,V1} \\ X_{i,V2} & X_{j,V2} & \dots & X_{z,V2} \end{bmatrix} = \begin{bmatrix} Y_i^{T_1} & Y_j^{T_1} & \dots & Y_z^{T_1} \\ Y_i^{T_2} & Y_j^{T_2} & \dots & Y_z^{T_2} \\ \vdots & \vdots & \ddots & \vdots \\ Y_i^{T_i} & Y_j^{T_i} & \dots & Y_z^{T_i} \end{bmatrix} \quad (3.41)$$

Like stated in section 2.3.5, $W_{V1}^{T_1}$ is the weight fraction in terms of % of the dry weight of the biomass of V1 and V2 at temperature T_i . $X_{i,V1}$ is the fraction of component i in V1 and $Y_i^{T_1}$ is the weight fraction of component i at temperature T1 in terms of % of the dry weight of the biomass. The W terms of V1 and V2 were obtained by the using the general equations on weight loss kinetics as presented in Section 3.3.2. The Y terms were obtained using experimental data presented in Figures 3.9a and 3.9b. As multiple sources were used to obtain data on volatiles composition, and multiple data points were obtained for the same torrefaction time and temperature, it is not possible to solve Eq. (3.41) by division. Rather, optimization needs to be conducted to find the best fit of the compositions of V1 and V2 to the experimental data. The optimization was performed using the CVXPY package in Python. The CVXPY package allows for convex hull optimizations via a least square solution, while also offering the opportunity to set boundaries on the solutions [125],[126]. The boundary condition desired in this

problem is that the fractional compositions of V1 and V2 should each add up to 1. Using CVXPY allowed for acquiring an optimal composition of V1 and V2 for the experimental data, while taking the boundary condition into consideration by constraining the solution in such a way that $\sum_i X_{i,V1} = \sum_i X_{i,V2} = 1$.

To obtain a general equation for the volatile composition based on temperature and time, the experimental data on volatile composition was split according to torrefaction time. For each torrefaction time, a separate composition of V1 and V2 was generated by using the CVXPY package as explained above.

A first degree polynomial equation (3.42) was used to relate the fraction of compound i in V1 or V2 to time. The values of these coefficients for every compound are shown in the Appendices 1.1. The coefficients, along with equation (3.42), were implemented in Aspen Plus to determine the volatiles composition in Aspen Plus.

$$V1_i \text{ or } V2_i = a \cdot \text{time} + b \quad (3.42)$$

Figure 3.12 presents the relation of the compositions of V1 and V2 with time as presented in equation (3.42). The dots mark the V1 and V2 compositions as optimized with the CVXPY tool for the times for which experimental data was available. The broken line represents the result of fitting Eq (3.42) through the marked dots. The non-condensable compounds are marked with nc, and the condensable compounds with c. Two prominent outliers are observed in Figure 3.12b. These are attributed to optimization errors. From Figures 3.12a and 3.12b it is observed that for CS the majority of V1 (wt. %) and V2 (wt. %) is formed by CO_2 and water. Other prominent compounds present in V1 and V2 are CO and acetic acid. The majority of V1 and V2 for SCB, as is observed in Figures 3.12c and 3.12d is formed by CO_2 . It is also interesting to note the differences in CS and SCB regarding the composition of condensable volatiles. CS torrefaction yields small fractions of acetol ($C_3H_6O_2$), formaldehyde (CH_2O) and formic acid ($HCOOH$), whereas SCB torrefaction results in small fractions of furane (C_4H_4O), phenol (C_6H_6O) and HMF (hydroxymethylfurfural) ($C_6H_6O_3$). The reason that some compounds are only produced during torrefaction of CS, like formaldehyde, and other during the torrefaction of SCB, like HMF, lies in the different structural composition of both types of biomass and differences in experimental research which influence the compounds found in the volatiles.

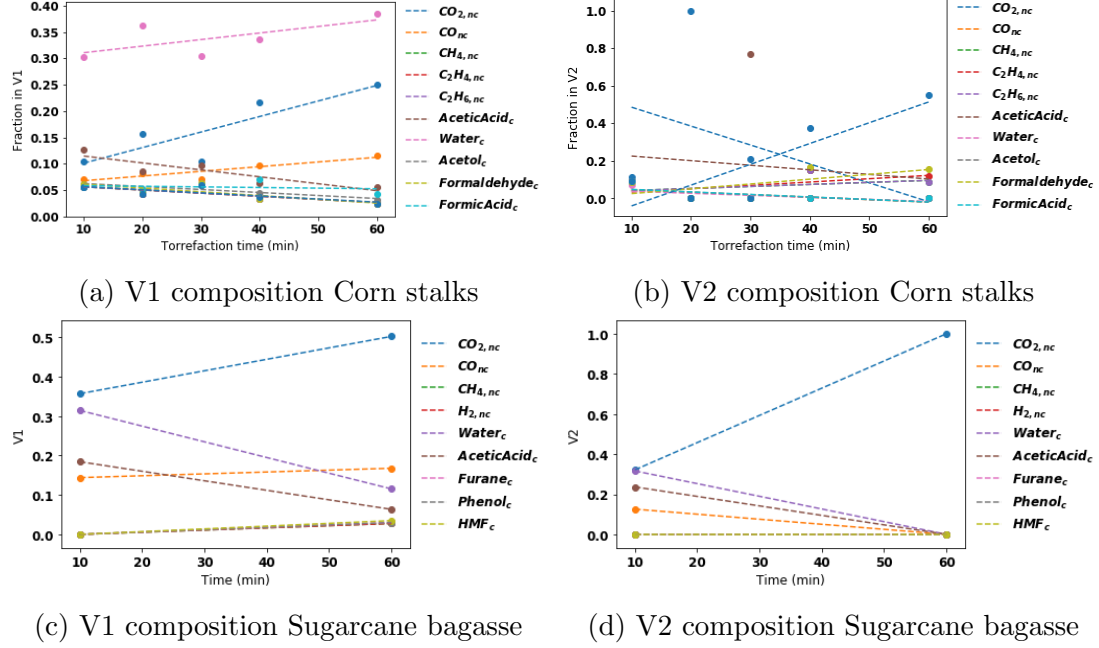


Figure 3.12: Compositions of V1 and V2 versus time

General equations for the weight loss and volatiles generation and volatiles composition were obtained through this process. The volatiles listed in Figure 3.12 only consist of carbon and hydrogen. The elemental composition of the solids was changed in Aspen Plus according to the loss of carbon and hydrogen to volatiles. As the elemental composition changes due to carbon and hydrogen losses, the calorific value of the the solids also changes.

Heating values & Efficiencies

The higher heating value (HHV) represents the calorific value of a fuel in terms of energy per mass unit. The lower heating value (LHV) also represents the calorific value, but assumes that the energy required to vaporize any water in the fuel is not recovered. Experimental data for HHV during torrefaction extracted from Ren et al. [111] and Valix et al. [127] was fitted to the Boie correlation, Eq. (3.43). The Boie correlation is a correlation to relate the higher heating value of an organic fuel to its elemental composition [128]. As biomass is an organic fuel, the Boie correlation was used to predict the higher heating value of the biomass depending on its elemental composition.

$$HHV_T^{Boie} = 100 \cdot (a_1 \cdot x_C^{dm} + a_2 \cdot x_H^{dm} + a_3 \cdot x_S^{dm} + a_4 \cdot x_O^{dm} + a_5 \cdot x_N^{dm}) + a_6 \quad [128] \quad (3.43)$$

In this formula, a_1 to a_6 represent the different coefficients to be fitted. x_i^{dm} represents the weight fraction of each element in the biomass: C, H, S, O and N.

As the elemental composition of the biomass changes during torrefaction, so does its higher heating value. By fitting the equation above to the experimental data, a general Boie equation was obtained for both CS and SCB. The results are shown below in Figure 3.13, along with the experimental data plotted by dots.

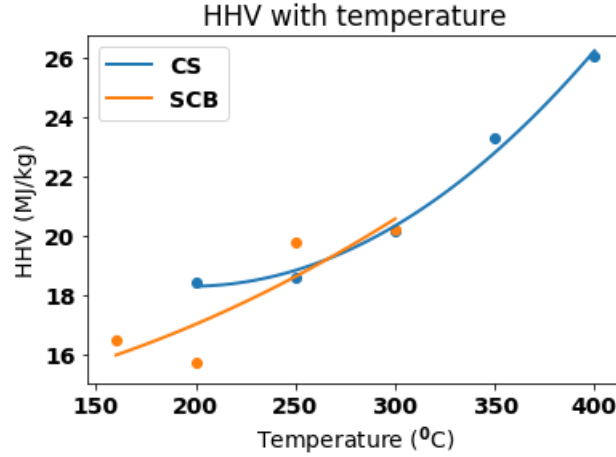


Figure 3.13: HHV for corn stalk and sugarcane bagasse during torrefaction

CS and SCB have roughly the same HHV (20 MJ/kg) in the torrefaction range, between 250 °C and 300 °C. The reason for this is the similar elemental composition found by Valix et al. [127] and Ren et al. [111] in this temperature range. The values for a_1 to a_6 are shown below in Table 3.7.

Table 3.7: Estimated coefficients for Boie correlation

Parameter	CS	SCB
a_1	0.155	0.00265
a_2	-3.87	-0.00533
a_3	78.5	-0.0717
a_4	0.374	0.000320
a_5	-16.7	0.00558
a_6	13.9	6.66

The LHV of the torrefied biomass was calculated using the following formula:

$$LHV = HHV - \frac{18.02}{2} \cdot H \cdot 2.24 [129] \quad (3.44)$$

Here, LHV is in MJ/kg, HHV is in MJ/kg and H is the fraction of hydrogen in the elemental composition of the torrefied biomass. 18.02 refers to the molecular weight of water (18.02 g/mol), which is divided by 2 to account for the two hydrogen atoms in each water molecule. 2.24 to the vaporization enthalpy of water (2.24 MJ/kg).

The Boie coefficients as found in Table 3.7 were implemented in Aspen Plus to account for the change in calorific value during torrefaction. The HHV and LHV of the torrefied biomass were used to determine the thermal efficiency of the torrefaction plant.

The gross thermal efficiency of the torrefaction plant was determined by Eq. (3.45) and (3.46).

$$\eta_{th,gross(HHV)} = \frac{E_{pellets(HHV)}}{E_{\text{raw biomass(HHV)}} + E_{\text{consumed}}} \quad (3.45)$$

$$\eta_{th,gross(LHV)} = \frac{E_{pellets(LHV)}}{E_{\text{raw biomass(LHV)}} + E_{\text{consumed}}} \quad (3.46)$$

Here, E_{pellets} is the thermal energy content of the pellets produced, $E_{\text{raw biomass}}$ is the thermal energy content of the raw biomass entering the model and E_{consumed} is the thermal or mechanical energy consumed by the configuration. The HHV of the raw biomass on a dry basis is 17.98 MJ/kg for CS [111] and 17.83 MJ/kg for SCB [127]. The HHV of H_2 is 141.7 MJ/kg. The LHV of raw CS, on a dry basis, is 15.76 MJ/kg [111] and 15.42 MJ/kg for raw SCB on a dry basis [127], [130]. The LHV of H_2 is 121 MJ/kg.

The net higher and lower efficiency were determined by taking the left over energy into consideration. Eq. (3.47) and (3.48) were used to determine the net higher and lower efficiency. The energy left over, E_{leftover} , is defined as the difference in thermal energy between the thermal energy left in the air stream used to provide thermal energy to the torrefaction reactor and the thermal energy of the outside air. The leftover thermal energy thus represents the surplus of energy used in the torrefaction reactor. The temperature of the air used to heat the torrefaction reactor influences the potential of thermal valorization of this stream. Low temperature left over air is harder to utilize than high temperature left over air.

$$\eta_{th,net(HHV)} = \frac{E_{\text{pellets(HHV)}} + E_{\text{leftover}}}{E_{\text{raw biomass(HHV)}} + E_{\text{consumed}}} \quad (3.47)$$

$$\eta_{th,net(LHV)} = \frac{E_{\text{pellets(LHV)}} + E_{\text{leftover}}}{E_{\text{raw biomass(LHV)}} + E_{\text{consumed}}} \quad (3.48)$$

Torrefaction plots

Figures 3.14 and 3.15 summarize the results from the previous sections on solids and volatiles yields. The crosses mark the solid yields from experiments. The amount of volatiles, both condensables and non-condensables, increase when torrefaction time and temperature increase, while the amount of solids left decreases. This

is because more solid conversion occurs at higher temperatures and longer torrefaction times. The largest amount of non-condensable volatiles are produced during the torrefaction of SCB. Furthermore, SCB torrefaction is slower than CS, as SCB has larger amounts of solids left after the same time and temperature of torrefaction. The modelling results for SCB have a better agreement with the experiments since, as was presented in Figure 3.9a and 3.9b, the experimental data on solids weight loss during SCB torrefaction is less wide-spread than the same data for CS torrefaction. The efficiency of the torrefaction unit is shown in the right side figures. Here, the following formula is used:

$$\eta_{th} = \frac{HHV_{torrefied} \cdot Yield}{HHV_{raw}} \quad (3.49)$$

Where η_{th} is in %, HHV in MJ/kg and yield in %.

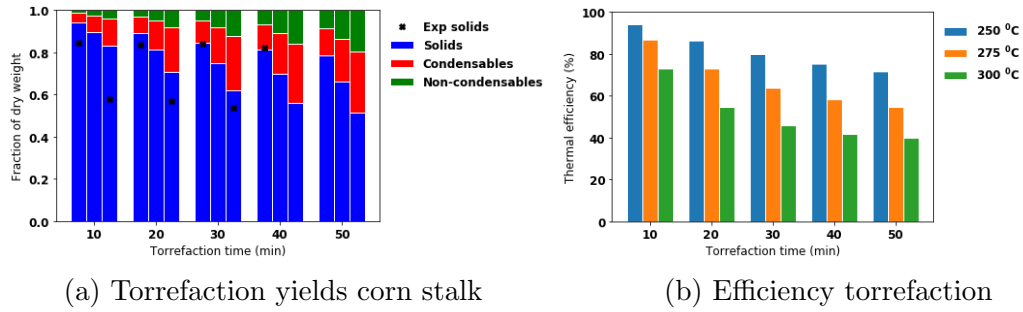


Figure 3.14: Torrefaction plots corn stalks

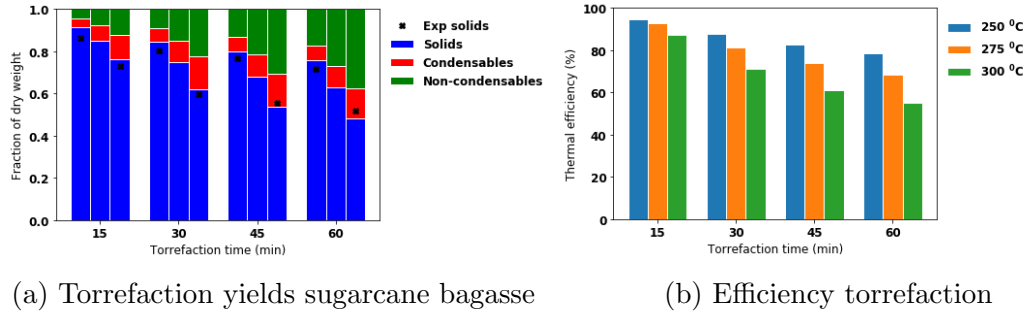


Figure 3.15: Torrefaction plots sugarcane bagasse

3.3.3 Simulating the torrefaction reactor in Aspen Plus

As the general equations on the weight loss kinetics, volatiles generation, volatile composition and calorific content of the solids during torrefaction were obtained,

it was possible to model the torrefaction in Aspen Plus. Based on the outcomes of the literature review in section 2.3.5, it was decided to simulate an indirectly heated rotating drum reactor as the torrefaction reactor, because of the better temperature distribution in the solids as opposed to the screw conveyor and moving bed reactor. Figure 3.16 presents an overview of a cross section of the indirectly heated rotating drum reactor. The reactor consists of two concentric cylinders: the inner cylinder used for the transport of the solids and where biomass is torrefied, while the outer cylinder is where air flows, providing heat to the process. The air flows counter flow relative to the solids to shorten the length of the reactor.

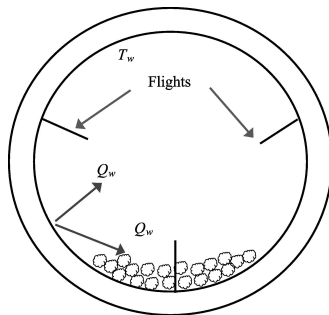


Figure 3.16: Torrefaction reactor cross section

Source: [131]

The indirectly heated rotating drum reactor consist of two parts: an inner cylinder and an outer cylinder. The inner cylinder contains the biomass and the outer cylinder contains the air used for heating. The temperature of the wall, T_w , was kept at the operational temperature of the torrefaction reactor. Heat is transferred from the outer cylinder through the wall to the solids and the gasses in the inner cylinder, represented in Figure 3.16 by the Q_w arrows. Flights are installed in the inner cylinder to rotate the solids through the reactor and improve heat transfer. The kinetics of the torrefaction reactor were modelled using a 2-step torrefaction mechanism (see Section 2.3.5). This was modelled in Aspen Plus using an RStoic reactor because of its ability to simulate weight loss of the solids and the generation of the volatiles by a single reaction (see Section 2.3.6). Since the 2-step torrefaction mechanism divides the volatiles into two streams, V1 and V2, two RSTOIC reactors were defined to simulate each devolatilization step. Each reactor was set up with a calculator block, in which the general equations on weight loss kinetics, volatiles generation and volatiles composition were implemented to simulate the torrefaction process. The calculations specified in the calculator block are presented in appendix 1.5.2. It was assumed that both reactors operate at the same temperature and pressure. The temperature varies

between 200 °C and 300 °C, the torrefaction temperature range as obtained from literature (see Section 2.3.5) while the pressure was kept constant at 1 bar. The heat required in the torrefaction reactor is provided by the left-over heat from the flue gasses which were used to heat up the air entering the dryer. Because of the high heat of the flue gasses, the biomass would burn if flue gasses were used directly. Furthermore, if flue gases were fed into the reactor, these would dilute the volatiles and make valorization more difficult, as the moisture content of the volatiles increases, reducing its calorific value [131]. To prevent this from happening, a heat exchanger network was devised, in which air is heated to 40 °C above the operational temperature in the torrefaction reactor. 40 °C was assumed the maximum temperature difference between the air and the operational temperature of the torrefaction reactor because Nhuchhen et al. [131] conducted experiments for heat transfer in torrefaction reactors up to 340 °C, while it was concluded from literature, as discussed in section 2.3, that the maximum torrefaction temperature was 300 °C. The amount of air heated by the flue gasses was determined by the energy content of the flue gasses. A design spec was set up in Aspen Plus, which used a vapour fraction of 1 as target for the flue gasses which had passed the heat exchanger, while adjusting the amount of air entering the heat exchanger. This way, as much thermal energy from the flue gasses as possible was used to heat up the air for the torrefaction reactor, while preventing condensation in the heat exchanger. Condensation in the heat exchanger is unfavourable because this would create different flow regimes in the heat exchanger.

Torrefaction reactor dimensions

In order to calculate the dimensions of the torrefaction reactor, the length of the torrefaction reactor was determined. The first part of the reactor is the part where the biomass is heated to the required torrefaction temperature. The length of this part (L_{heat}) was calculated by the eq. 3.50. Heat transfer from the heated air to the solids is comprised of heat transfer from the air to the wall, heat conduction in the wall and heat transfer from the wall to the solid biomass and gas inside the inner cylinder. It was assumed that the overall heat transfer process was limited by the heat transfer between the wall and the solid biomass and gas in the inner cylinder, which is in accordance with the findings of Nhuchhen et al. [131].

$$L_{heat} = \frac{E}{U \cdot \pi \cdot D \cdot \Delta T_{ln}} [109] \quad (3.50)$$

Here, L_{heat} is the length in meter required to heat up the biomass, E the energy required to heat up the biomass in watt, U the overall heat transfer coefficient ($W/(m^2K)$), D the diameter in meter. U is assumed to be 15.50 $W/(M^2K)$, a value found by experimental research on the effective heat transfer coefficient in

indirectly heated rotary torrefaction reactors [131]. ΔT_{ln} is expressed by Eq (3.51).

$$\Delta T_{ln} = \frac{\Delta T_1 - \Delta T_2}{\ln \frac{\Delta T_1}{\Delta T_2}} \quad (3.51)$$

Here, ΔT_1 is the difference in temperature between the air leaving the reactor and the biomass entering the reactor. ΔT_2 is the difference in temperature between the air entering the reactor and the biomass leaving the reactor.

The total length of the reactor also includes the part of the reactor where the biomass is torrefied under operating conditions. The length of this part, L_{tor} was calculated with Equation (3.52) to (3.54):

$$V_s = \dot{m}_{biomass} \cdot \tau \quad (3.52)$$

$$V_t = \frac{V_s}{(1 - \epsilon) \cdot \phi} \quad (3.53)$$

$$L_{tor} = \frac{V_t}{A} \quad (3.54)$$

V_s is the volume of the solids, $\dot{m}_{biomass}$ is the mass flow rate of the biomass and τ is the torrefaction time. V_t is the volume of the torrefaction reactor, ϵ is the filling grade and ϕ the porosity. A is the cross-sectional area of the torrefaction reactor in eq. (3.54). The standard diameter of the reactor was assumed to be 3 m, a value obtained from the literature review of Section 2.3.5. Assuming a standard diameter of 3 m resulted in a standard cross-sectional area of 7.07 m^2 . The cross-sectional area was used in both length calculations (L_{heat} and L_{tor}), along with the other parameters already specified, a filling grade of 0.15 and a porosity of 0.4. By adding the two lengths (L_{heat} and L_{tor}) together, the total length of the torrefaction reactor was determined. It was assumed that the torrefaction reactor is perfectly insulated, and no heat losses occur.

Similar to the approach in 3.3, it was decided to assume a standard reactor length and diameter and determine the amount of reactors required in parallel by assuming a standard diameter, calculating the total length of the torrefaction reactors and dividing the total length as calculated by Eq. (3.52) and (3.54) by a standard length. Manoucherinejad et al. [17] and Bergman et al. [13] both assumed a torrefaction reactor diameter of 3 m. The length of the reactor varied between 32 m [13] and 43 m [17]. A reactor diameter of 3 m and length of 43 m were set as the standard dimensions of the reactor.

The volatiles and the solids produced in the RSTOIC reactors were separated using a cylinder block in Aspen Plus. Once the volatiles were separated from the

torrefied biomass, they were sent to the valorization unit (combustor or a chemical looping combustor, or a combination of both). Finally, solids were cooled, grinded and pelletized.

3.3.4 Grinding & pelletization

After torrefaction, the torrefied material was first cooled down. This was simulated in Aspen Plus via a heat exchanger, which was used to determine the amount of cooling water needed for this process. Then, torrefied biomass was subjected to a grinding process. The grinding and pelletization process were modelled using in-house scripts. The amount of energy needed for grinding and pelletization was assumed to be 18 kWh/ton and 150 kWh/ton, respectively [17].

3.4 Valorization unit: scenarios

Four scenarios were designed to valorize the volatiles resulting from the torrefaction process. The following enumeration gives an overview of the various scenarios considered in this Thesis. Each scenario was evaluated for both corn stalk and sugarcane bagasse as input fuel, resulting in 8 different process configurations. The abbreviations which will be used in the rest of this Thesis to refer to each of the scenarios are listed in the enumeration. The abbreviations first state the type of biomass (CS or SCB) followed by the valorization scenario.

1. Torrefaction followed by combustion of all volatiles (CS_{comb} and SCB_{comb})
2. Torrefaction followed by chemical looping combustion of all volatiles (CS_{clc} and SCB_{clc})
3. Torrefaction followed by combustion for non-condensable volatiles and chemical looping combustion for condensables volatiles ($CS_{comb+clcl}$ and $SCB_{comb+clc}$)
4. Torrefaction followed by chemical looping for all volatiles coupled with hydrogen production (CS_{H_2} and SCB_{H_2})

The best configuration was determined by comparing the different configurations using the following parameters: energy consumption, thermal efficiency, by-products production (H_2) and costs (CAPEX and OPEX).

3.4.1 Combustion of all volatiles

Figure 3.17 presents the schematic overview of the torrefaction process coupled with a combustor unit, where all volatiles are combusted. The flue gasses are used

to provide energy to the DRY HEX and TOR HEX to pre-heat the air that enters the dryer ($dryair_{1-2}$) and torrefaction reactor ($torair_{1-3}$), respectively. The air entering the dryer, $dryair_1$, is heated up to 400 °C, as discussed in Section 3.3, while the air entering the torrefaction reactor is heated 40 °C above the operational temperature of the torrefaction reactor as was discussed in Section 3.3.2. The dryer and torrefaction reactor were modelled using the the relevant equations obtained from experimental data and dimensioning equations as discussed in Sections 3.3 and 3.3.2.

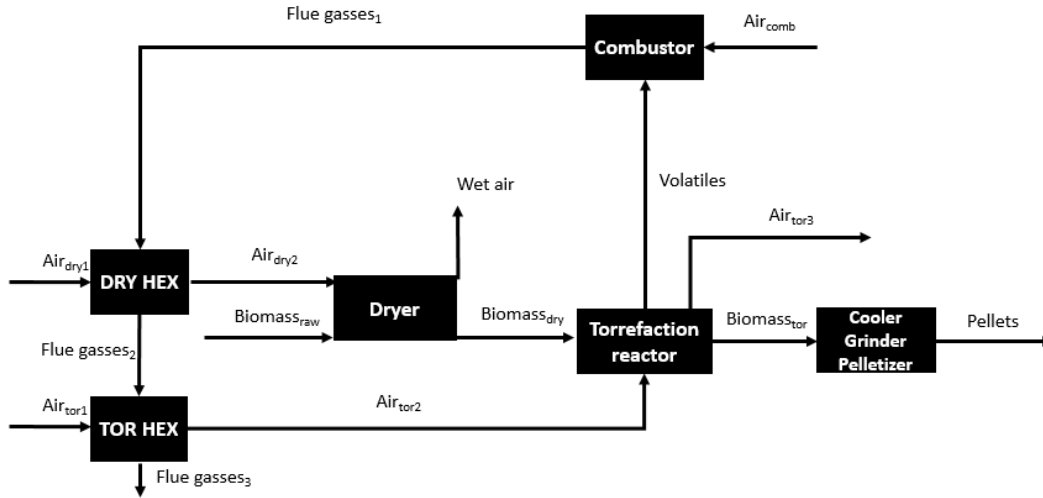


Figure 3.17: Combustion model

After the drying process, wet air and dried biomass leave the dryer. Dried biomass is sent to the torrefaction reactor and after torrefaction, is sent to the grinder and pelletizer. Of these blocks the energy demands were determined using the approach explained in section 3.3.4.

The volatiles are sent to the combustor. The combustor was modelled in Aspen Plus as an RSTOIC reactor. This type of reactor enables the specification of combustion reactions. Complete combustion of all volatiles was assumed, such that all volatiles are converted, in the presence of oxygen, to CO_2 and H_2O . The amount of air entering the combustor (air_{comb}) was regulated using a calculator block. The calculator block adjusted air_{comb} based on the flammability limits of the volatiles mixture entering the combustor. The flammability limits indicate the range of fuel concentration in air in which fuels are combustible [132]. The flammability range is bounded by a higher and lower flammability limit, which indicate the fuel concentrations in air at which too much fuel (higher flammability limit) or too little fuel (lower flammability limit) is present for ignition [132]. The

flammability limits were determined by using Le Chateliers mixing rule [133], Eq. (3.55). Only combustible compounds such as H_2 , CO and CH_4 , are considered in Eq. (3.55).

$$LFL_{mix} = \frac{1}{\sum_i \frac{x_i}{LFL_i}} \quad [133] \quad (3.55)$$

The presence of incombustible compounds in the volatiles stream, like water and CO_2 , raises the low flammability limit (LFL), thereby lowering the zone in which combustion is possible. The composition of the volatile stream from torrefaction in combination with Le Chateliers mixing principle were used to determine the LFL and HLF of the volatile stream.

The amount of air required for combustion air_{comb} was adjusted to approach the lower flammability limit which maximizes air_{comb} . This, in order to maximize the energy delivered to the torrefaction unit and dryer. To ensure that the LFL was not exceeded, a calculator block in Aspen Plus determined the maximum amount of air as calculated via the LFL and divided this by 1.5.

3.4.2 Chemical looping of all volatiles

Figure 3.18 presents an overview of the chemical looping combustion (CLC) configuration as modelled in Aspen Plus. The DRY HEX, TOR HEX, Dryer and Torrefaction reactor operate the same as explained in Section 3.4.1.

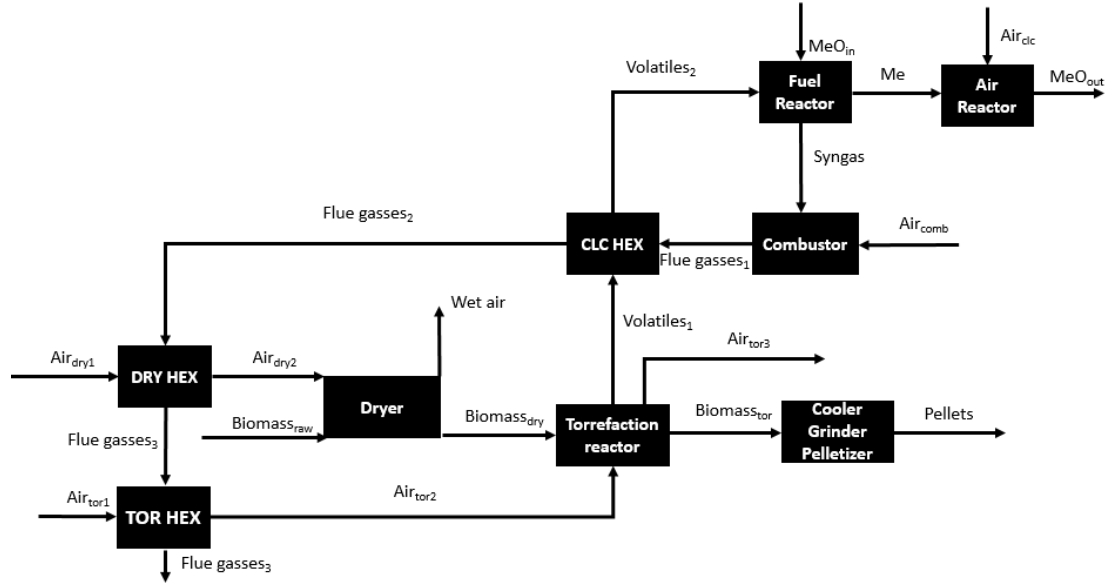


Figure 3.18: CLC model

After torrefaction, volatiles ($Volatiles_1$) are pre-heated in the CLC HEX to a temperature $50\text{ }^{\circ}\text{C}$ above the operational temperature of FR to reduce its heat duty. After volatiles are heated, $Volatiles_2$ are sent to the CLC unit. The simulation of CLC was modelled based on the methodology presented by Heng et al. [91]. A RGIBBS reactor was selected to simulate the FR and AR. The temperature of the FR was set to $650\text{ }^{\circ}\text{C}$, based on the work by Bimbela et al. [90]. The Boudouard reaction was assumed to be negligible, as research by Bimbela et al. [90] indicated that the formation of solid carbon was limited.

NiO was selected as the oxygen carrier for CLC due to the lower operational temperatures ($500\text{ }^{\circ}\text{C}$ - $700\text{ }^{\circ}\text{C}$) in the FR in comparison to the other catalyst considered in Section 2.4.2, Fe_2O_3 , ($850\text{ }^{\circ}\text{C}$ to $950\text{ }^{\circ}\text{C}$). Furthermore, as discussed in Section 2.4.2, the higher reactivity and longer lifetime of NiO compared to Fe_2O_3 , make it one of the most suitable oxygen carriers for CLC [88],[89]. The amount of oxygen carrier (MeO_{in}) entering the FR was determined using a calculator block, which adjusted the oxygen carrier stream such that the molar ratio of oxygen carrier to "active" carbon in the volatiles (R) remains at 0.0025 (see Section 2.4.2). Here, "active" carbon refers to the carbon content in combustible compounds like CO , CH_4 . This excludes the CO_2 fraction in $Volatiles_2$, as the CO_2 is not reformed in the FR.

The stream out of the FR is split using a cyclone block in Aspen Plus. The gasses (*syngas*) are sent to the Combustor, which is operated based on the same principles regarding the amount of excess air as presented in Section 3.4.1. The

flue gasses exiting the Combustor ($Fluegasses_1$) are used to heat: $Volatiles_1$ to 700 °C, Air_{dry1} to 400 °C and Air_{tor1} to 40 °C above the operational temperature of the torrefaction reactor. The solids (Me) are sent to the AR, which operated at the same temperature as the FR (650 °C). The amount of air supplied to the AR, Air_{clcin} is determined via a calculator block, through which an excess of air is supplied at 650 °C. The air (Air_{clcout}) and solids MeO_{out} is separated after leaving the AR via a cyclone.

Purpose of CLC

The aim of the CLC section was to generate a syngas. It was decided not to generate energy in the FR as is usually aimed for [82]. The reason is the maturity of this technique. Although CLC is a rapidly advancing technique, it has not yet been commercialized [134]. As torrefaction on its own is in the beginning of commercialization, it was decided that adding another still un-commercial technique would reduce the applicability of this Thesis too much. It has therefore been decided to aim for the generation of syngas over oxygen carriers, a technique proved and commercialized for a long period of time [60]. A disadvantage to this approach is that it disables the sequestration of CO_2 , as air is used for combustion of the syngas. A potential advantage of CLC over regular combustion is the lower LFL of syngas in comparison to the volatiles. This allows for a larger air stream to be used in the combustor, and higher conversion of combustion energy produced by the volatiles to thermal energy. A higher conversion of combustion energy to thermal energy means less volatiles are required to provide heat to the dryer and torrefaction reactor. Therefore, the process has potential to be operated at a lower torrefaction temperature in comparison to a process where all volatiles are straight up combusted. A lower torrefaction temperature, as explained in Section 3.2, requires less feedstock, thereby reducing the dimensions of the dryer and torrefaction reactor, which yields economic benefits.

NiO validation in Aspen Plus

Experimental data from Bimbela et al. [90] on the chemical looping of acetic acid over NiO catalysts was used to validate the results of the RGIBBS reactor. Acetic acid is used as a model compound to ensuring the repeatability of experiments regarding the performance of catalysts in CLC of volatiles [90]. It was assumed that the validation through the experimental data of Bimbela et al. [90] for acetic acid applies to the CLC of all volatiles produced by torrefaction. The results of the experiments by Bimbela et al. [90] and Aspen Plus are presented in Figure 3.19a and 3.19b.

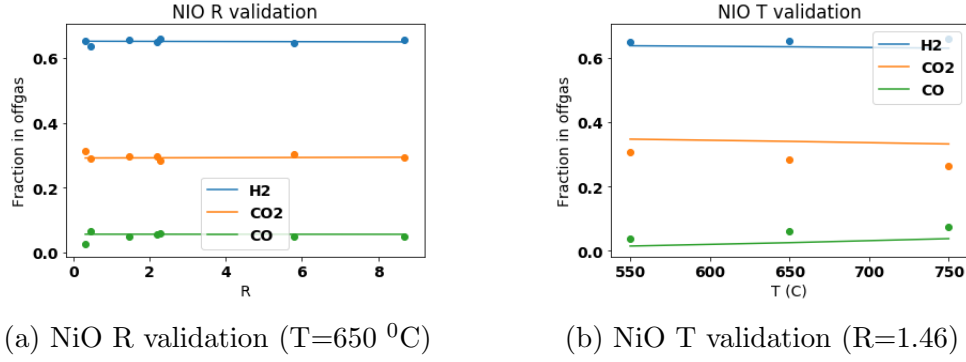


Figure 3.19: NiO validation

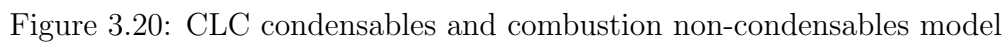
Table 3.8: Correlation NiO validation

Validation	R			Temperature		
	H_2	CO_2	CO	H_2	CO_2	CO
R^2	0.96	0.99	0.99	0.98	0.99	0.93
X^2	0.00057	0.0022	0.021	0.0019	0.033	0.052

The results from Aspen Plus show a positive correlation with the results by Bimbela et al. [90], as is presented in Table 3.8. All R^2 values are above 0.93 and all X^2 are below 0.052. Therefore, the RGIBBS reactor adequately simulates CLC of all volatiles using NiO as a catalyst.

3.4.3 Combustion of non-condensable volatiles and CLC of condensable volatiles

Figure 3.20 presents an overview of this configuration. In comparison to the previous two process configurations (see Sections 3.4.1 and 3.4.2), this configuration separates the volatiles resulting from torrefaction in two streams for valorization: combustion of the non-condensables and CLC for the condensables. The non-condensable volatiles are volatiles which are not condensable at standard conditions (298 K and 1 atm), for example CO_2 and CO . Condensable volatiles are condensable at standard conditions, for example acetic acid and water. The aim of this process configuration is to evaluate if the separation of the volatiles provides additional benefits (e.g. higher thermal efficiency) as opposed to stand-alone combustion or CLC of all volatiles. The DRY HEX, TOR HEX, Dryer, Torrefaction reactor operate according to the same principles as the ones described in Section 3.4.1. The Fuel Reactor, Air Reactor, Combustor and CLC HEX operate similar to the units described in Section 3.4.2, with the same operational conditions.



```
graph LR; V1[Volatiles1] --> C1[Cooler]; C1 -- Volatiles2 --> GLS[Gas/Liquid Separator]; GLS -- Volatiles3 --> CCS1[Compressor Cooler & Separator]; GLS -- Condensables1 --> C5[Condensables5]; CCS1 -- Volatiles4 --> CCS2[Compressor Cooler & Separator]; CCS1 -- Condensables2 --> C3[Condensables3]; CCS2 -- Non-condensables --> NC[Non-condensables]; CCS2 -- Condensables4 --> C4[Condensables4];
```

After torrefaction, the volatiles ($Volatiles_1$) are cooled to 25 °C using cooling water, which condenses part of the volatiles. The condensed volatiles ($Condensables_1$) are separated from the gaseous volatiles using a gas/liquid separator. $Volatiles_3$ are sent to the compressor, cooler and separator units to recover acetic acid. In the compressor unit, $Volatiles_3$ are compressed to 6.8 bar in two steps, since at this value, 90 % of the acetic acid (a major condensable volatile) is condensed. After the first step, the compressed volatiles are cooled and separated, and the condensed volatiles ($Condensables_2$) are mixed with $Condensables_1$ to form $Condensables_3$. The remaining gaseous volatiles ($Volatiles_4$) are sent to the second compression

step. After further compression to 6.8 bars, the volatiles are cooled and separated. *Condensables*₄ are mixed with *Condensables*₃ to form *Condensables*₅ and sent to the CLC section. *Non – condensables* exiting the second compressor, cooler & separation unit are sent to the Combustor. The FR reactor was set to operate to same conditions as the CS scenario (Section 3.4.2) to generate syngas which is then burned, together with the *Non – condensables* in the Combustor.

3.4.4 Chemical looping of all volatiles coupled with hydrogen production

A scenario in which CLC is applied to all volatiles in combination with hydrogen production is considered to investigate the prospect volatiles valorization through hydrogen production. Hydrogen production add value to the volatiles as hydrogen can readily be sold. The model for this configuration is presented in Figure 3.22. The TOR HEX, Dryer and Torrefaction reactor operate using the same conditions as the ones discussed in Sections 3.4.1 - 3.4.3.

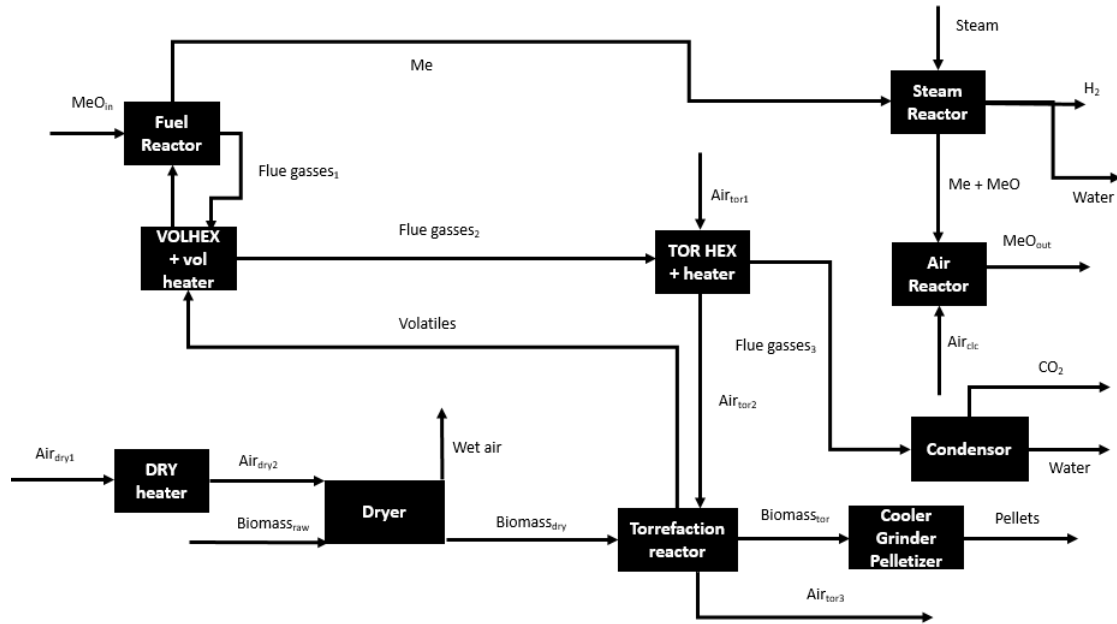


Figure 3.22: CLC and hydrogen production model

The DRY HEX was replaced by a DRY heater due to the fact that this configuration doesn't produce heat through volatiles valorization, as stated in Section 2.4.3. It was assumed that auxiliary fuel is required to heat Air_{dry1} to 400 °C. The volatiles are pre-heated in the VOLHEX+vol heater. Instead of using NiO as oxygen carrier, as was done in Sections 3.4.2 and 3.4.3, this configuration used

Fe_2O_3 as oxygen carrier. This, since Fe_2O_3 allows for reduction to FeO in the FR and allows simple separation of hydrogen after steam reforming. Furthermore, the fact that Ni is not able to partially oxidize to an intermediate form, like Fe_3O_4 is the intermediate form between FeO and Fe_2O_3 , makes steam reforming not possible when NiO is used as oxygen carrier.

The reduced oxygen carrier (FeO) in the Me stream exiting the FR, is then sent to Steam Reactor where it is partly oxidized by steam to Fe_3O_4 (see Section 2.4.3, 3.22). The steam entering the Steam Reactor is reformed to hydrogen, which is later separated from the remaining water stream using a condenser. An overview of the Steam Reactor sector is presented in Figure 3.23. To provide hydrogen at high pressure, it was decided to operate the SR at 30 bar, which is in accordance with the pressure range presented in Section 2.4.3. $Water_1$ was pressurized in the pump to 30 bar. Using residual heat from the water and hydrogen out of the Steam Reactor, plus an additional heater, $Water_4$ was heated to 540 °C. $Water_4$ and Me_1 were combined in the Steam Reactor, in which water was reformed to hydrogen. The oxygen carrier, water and hydrogen ($Me_2 + Water + H_2$) leaving the SR were separated using a cyclone. $Water + H_{2,1}$ were used to provide heat to $Water_2$. $Water + H_{2,2}$ were separated by a condenser, resulting in $Water_5$ and H_2 , both at 30 bar. Me_3 was sent to the AR.

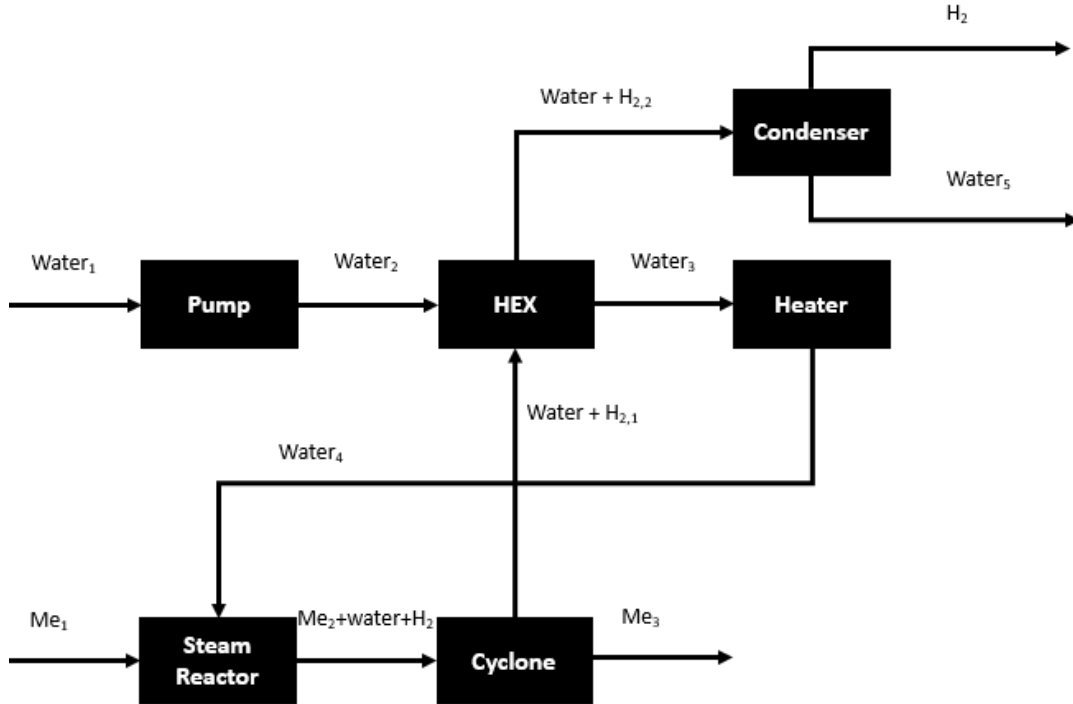


Figure 3.23: Steam reactor

The partly oxidized metal ($Me + MeO$) is sent to the Air Reactor to be re-generated back to Fe_2O_3 . As stated in Section 2.4.3, operational temperatures of the FR and AR are between 850 °C and 950 °C when Fe_2O_3 is used as oxygen carrier. Based on this, it was decided to model the FR with an operational temperature of 920 °C. Based on the literature review in Section 2.4.3, it was decided to follow the approach of Deshpande et al. [92] operate the AR 50 °C above the operational temperature of the FR to provide MeO_{in} to the FR above the operational temperature and thereby reduce the heat requirement of the FR. The operational temperature of the SR was set at 540 °C. 540 °C was selected as this was in accordance with the findings of the literature review as presented in Section 2.4.3 and yielded the highest hydrogen yield in the simulations in Aspen Plus. The volatiles are heated to 970 °C in the VOLHEX+vol heater unit. Like stated in Section 3.4.2, the volatiles are heated to 50 °C above the FR temperature to reduce the heat duty of the FR. Part of the heat required to heat the volatiles is provided by $Fluegasses_1$. Auxiliary heat is required to heat the volatiles to 970 °C. The remaining heat of the flue gasses ($Fluegasses_2$) is used to heat air required in the Torrefaction reactor. The TOR HEX operates with the same principles as the TOR HEX described in Section 3.4.1. The high operational temperature in the FR (920 °C) reforms volatiles to a large extent to CO_2 and water instead of creating a syngas like in Sections 3.4.2 and 3.4.3. The CO_2 and water in $Fluegasses_3$ are split after leaving the TOR HEX through condensation. This enables CO_2 sequestration, as the CO_2 stream has a high purity after the water has been separated.

Fe_2O_3 validation in Aspen Plus

The validation of Fe_2O_3 as an oxygen carrier in chemical looping is based on the validation by Kuo et al. [95]. Kuo et al. [95] compared the solid conversion of Fe_2O_3 to FeO and Fe_3O_4 as simulated by the RGIBBS reactor in Aspen Plus to the experimental work done by Li et al. [86]. The experimental work by Li et al. [86] focused on the influence of the molar ratio (R) of iron-oxides to volatiles on the conversion of Fe_2O_3 to FeO and Fe_3O_4 . Kuo et al. [95] found good agreement with the experimental results from Li et al. [86], thereby confirming that the simulation of the FR in Aspen Plus using a RGibbs reactor and Fe_2O_3 as a catalyst is valid. The results of Kuo et al. [95] were repeated and the results are presented in Figure 3.24. The statistical analysis of the validation is presented in Table 3.9. Although the R^2 value is lower than for the NiO validation (0.64 versus 0.93), and the X^2 is higher than in the NiO validation (2.48 over 0.052), the simulation results still qualitatively follow experimental values, as is presented in Figure 3.24. The difference between the experimental data and the Aspen Plus simulation for $R < 0.2$ is attributed to entrance and start up effects in the

experimental research by Li et al. [86]. The plateau in Figure 3.24 of no solid conversion ($R = 0.2-1$) were attributed to the gas conversion in these ranges by Li et al. [86]. As the Aspen Plus simulation follows the experimental data by Li et al. [86] qualitatively, it has been decided that the RGIBBS reactor accurately models the conversion of Fe_2O_3 to FeO and Fe_3O_4 .

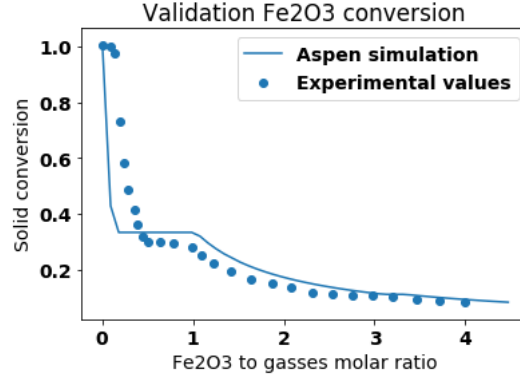


Figure 3.24: Fe_2O_3 validation

($T=850\text{ }^{\circ}\text{C}$, $P=1\text{ atm}$)

Table 3.9: Correlation Fe_2O_3 validation

Validation	X^2	R^2
Conversion	2.48	0.64

3.4.5 Scale

All equipment has been modelled and all incoming streams were regulated using calculator blocks (catalysts entering the fuel reactor, air entering the air reactor) or design specs (air used in the dryer and torrefaction reactor), except for the biomass. Section 2.3 discussed the scale of torrefaction plants. It was decided to model a torrefaction plant with a yearly production of 100 kton pellets. The operation of torrefaction plants is limited by the supply of CS and SCB. It is not possible to store biomass outside for long periods of time, as this will degrade the quality of the material. Usually, sugar production takes place from early April to early December in Brazil (a total of 8 months), resulting in a production of sugarcane bagasse during the same period [135]. Corn harvesting takes place twice a year: from February to March and from May to August, resulting in a total harvesting period of 6 months [136].

Torrefaction time

To allow for fair comparison between the different configurations, it has been decided that the only changing design parameter is the torrefaction temperature. As more or less excess heat is generated by volatile valorization, and accordingly energy is left over or auxiliary fuels are required, the torrefaction temperature was raised or lowered. The aim of every configuration was to be as self-sufficient as possible, as explained in Section 3.2. The range of the torrefaction temperature was set between 200 °C and 300 °C, as discussed in Section 3.3.2. The torrefaction time was set at 30 minutes for CS configurations and 40 minutes for SCB configurations. Both these times are well in the time range as obtained from literature and discussed in Section 2.3. The reason for the different torrefaction times is because, as discussed in Section 3.3.2, SCB torrefaction requires longer torrefaction times and higher torrefaction temperatures. To prevent all SCB configurations from operating at 300 °C, and thereby removing the potential of equal comparison with CS torrefaction, it was decided to set a longer torrefaction time.

3.5 Economic analysis

An economic evaluation is required to determine the economic performance of the configurations. The economic evaluation is divided in two parts: capital expenditures (CAPEX) and operational expenditures (OPEX). The prices of the equipment and other one-time expenditures are discussed in the CAPEX section, whereas the yearly expenditures are discussed in the OPEX.

3.5.1 Capital expenditures

The CAPEX of a torrefaction plants is largely determined by the expenditures required for equipment. Different methods for acquiring the equipment costs were used. For equipment well known to practically all industry, like heat exchangers and gas/liquid separators, Aspen Plus was used to obtain the costs. For other more specialized equipment, like dryers, torrefaction reactors and the CLC reactors, a different method was used. A way to calculate the price of a piece of equipment using a source of a similar piece of equipment in another study is to re-scale according to the following formula:

$$\text{Price 2} = \text{Price 1} \cdot \left(\frac{\text{Size 2}}{\text{Size 1}} \right)^m \quad (3.56)$$

Here, m is the exponential scale factor, which is 0.70 in this study for all types of equipment. It is important to note that the sizes in eq.(3.56) refer to flow of

material through the equipment in kg/hr. The amount of equipment, as determined in Sections 3.3 and 3.3.2 has not been used to determine the price of the equipment. The decision was made not to do this because of the influence of parameters assumed, for example particle size. The particle size has a large impact on the drying time, and thus in turn on total dryer length and amount of dryers required. Costs of equipment are better scalable through Eq. (3.56), in which assumed parameters like particle size have no influence on equipment costs.

The index of the journal of chemical engineering was used to correct the prices to the current year through eq.(3.57). The equipment index of 2019 was used, when it was at 740 [137].

$$\text{Price 2} = \text{Price 1} \cdot \frac{\text{Index 2}}{\text{Index 1}} \quad (3.57)$$

Using Eq. (3.56) and (3.57) and several sources, the prices of the dryer, torrefaction reactor, CLC reactor, pelletizer and grinder were calculated. The different pieces of equipment along with the relevant sources are shown in Table 3.10. In case multiple sources were listed, the average price as calculated by Eq.(3.56) and Eq.(3.57) was used for further analysis.

Table 3.10: Sources equipment prices

Equipment	Sources
Dryer	[71], [138], [13]
Torrefaction Reactor	[71],[139],[13]
CLC Reactor	[140]
Pelletizer	[71], [141],[142]
Grinder	[71], [141],[142]

The total CAPEX was determined by using the equipment costs. The parameters shown below in Table 3.11 are self-explanatory. The second column presents the parameters as fractions of other parameters. The value of all of these parameters were gathered from Cooper [143].

Table 3.11: CAPEX factors

Parameter	Calculation
Equipment costs	Total equipment costs
Installed costs	43 % of equipment costs [143]
Instrumentation & controls	25 % of installed costs [143]
Piping	60 % of installed costs [143]
Building & site	20 % of installed costs [143]
Total physical investment	Installed, instrumentation & controls, piping and building & site costs combined [143]
Engineering & construction	25 % of physical investment costs [143]
Contingencies	15 % of physical investment costs [143]
Total CAPEX	Physical investment, engineering & construction and contingencies costs combined [143]

3.5.2 Operating expenditures

Several different factors influence the operating expenditures (OPEX) of a torrefaction plant. These include the price of the raw materials, the costs of utilities, maintenance costs, labor costs, indirect expenses, overhead and depreciation. These factors are discussed in this section.

Raw materials

Each configuration used at least one type of raw material: the biomass used as feedstock. SCB is used in Brazilian sugar mills to provide electricity. The SCB is used in a boiler to heat up steam, which is used in the sugar production process. The boiler produces approximately 664 kWh for every ton of dry SCB [144]. The economic value of the SCB is the same as the value of the electricity produced by burning it in the boiler. As the average electricity price was assumed to be 0.071 €/kWh [145], the price of a ton of dry SCB was assumed to be €47.14 or €24.40 per wet ton SCB. It is assumed that a torrefaction plant using SCB as a feedstock is build next to the sugarcane mill. Therefore, it was assumed that no additional transportation costs need to be taken into consideration.

Sokhansanj et al. [106] analysed the price of CS for torrefaction in America. They found that \$38 per ton CS is required to purchase the corn stalk from the farmers and to shred, bail and stack it [106]. A typical transportation distance of 70 km was assumed by Sokhansanj et al. [106], which was also assumed in this Thesis. The transportation costs were assumed to be \$10 [106]. A total price of \$48 or €42.72 per ton of CS was assumed in this study. The total costs for the raw

materials were calculated by a multiplying of the amount of raw biomass required in the dryer times the average price of the raw (wet) biomass.

All configurations using a CLC reactor also have the price of the catalyst used in the CLC reactor. The price of the catalysts used in the CLC reactors was calculated by eq.(3.58).

$$\text{Costs catalysts} = \frac{\text{kg catalyst in system}}{\text{lifetime of catalyst}} \cdot \text{price catalyst} \cdot \text{Operational time during the year} \quad (3.58)$$

Table 3.12 presents the lifetime and the price required in eq.(3.58).

Table 3.12: Prices catalysts

Catalyst	Lifetime (hours)	Price (€/kg)
NiO	5000 [89]	12.64 [146]
Fe_2O_3	1000 [89]	10.68 [147]

Utilities

Table 3.13 presents the prices for the different types of utilities used in the configurations. Electricity was required for the volatiles separation system of configurations $CS_{comb+clc}$ and $SCB_{comb+clc}$. Cooling water was required in all configurations to cool down the torrefied biomass. Steam is a standard utility in Aspen Plus which was provided as an utility for configurations requiring auxiliary heat. Steam is assumed to be provided at 1000 °C and cooled to 400 °C during usage.

Table 3.13: Utility prices

Utility	Price	Unit	Source
Electricity	0.071	€/kWh	[145]
Cooling water	0.0078	€/m ³	Aspen Plus
Steam	0.0022	€/kWh	Aspen Plus

Maintenance

Because a torrefaction plant includes the handling of solids and operates a medium high temperatures, yearly maintenance costs were assumed to be 8 % of the total CAPEX [143].

Labor

Labor expenses are dependent on the total amount of different pieces of equipment present in a plant and on the costs of employees. Eq.(3.59) was used to determine

the operating labor in man-hours per processing step (Y) as a function of plant capacity in ton/day (X):

$$Y = 10^{-0.738 \cdot \text{LOG}_{10}(X)} \quad [143] \quad (3.59)$$

By multiplying the amount of processing steps, B, by Y, and dividing by the operating time per day (24 hours), the amount of employees which need to be present at each time (C) was determined, rounded up to a integer.

$$C = \frac{B \cdot Y}{C} \quad (3.60)$$

The amount of employees needed for one employee at work was determined by determining the total shifts per week (21, as there are 3 shifts per day 7 days a week), and the amount of shifts each employee takes, which was assumed to be 4. The total amount of employees in service was determined by multiplying the amount of shifts an employee takes per week by the amount of employees at work at all times (C). To determine the costs of all employees, an annual salary, which was assumed to be €72,000/yr, was multiplied by all employees in service.

Supervision & operating supplies

In addition to employees working at the plant, some supervision is necessary in the form of department supervisors and foremen. Their costs were assumed to be 25 % of the labor costs [143]. Operating supplies like paper and computers were assumed to be 7 % of labor costs [143].

The total direct OPEX are the costs of raw materials, utilities, labor and supervision & operating supplies combined.

Indirect expenses

Indirect expenses are expenses like insurance, fire protection and several taxes. They were assumed to be 4 % of the direct expenses [143].

Overhead

Apart from the labor costs of the employees and the foremen, additional labor costs are present in the form of salaries of sales offices, engineers, administration and managers. They were assumed to be 6 % of the total direct expenses [143].

Depreciation

Depreciation is the cost of a decrease in the value of the plant. Each year, the plant is worth less due to wear and tear of the equipment. The lifetime of the

plant was set at 15 years, so the depreciation was calculated by dividing the total capital investment by the lifetime.

As all configurations have now been discussed, along with their equipment and the scale of the plant and the method of economic analysis, it is now possible to run the simulations and evaluate their results in terms of efficiency, production of by-products and economics

3.5.3 Net present value

The NPV (net present value) is defined as the difference between the cash outflows and inflows over a period of time [148]. NPV is used to determine the profitability of a project, since it accounts for return of investment of a project. This information helps investors and stakeholders decide if a project is attractive for investment [148]. The NPV is determined by eq.(3.61).

$$NPV = \sum_t^{\text{lifetime}} \frac{\text{Cash flow}}{(1 + r)^t} - CAPEX[148] \quad (3.61)$$

Here, t is the time period in years, r is the internal rate of return (IRR), which was assumed to be 10 %, the cash flow is the difference between the income generated by selling the pellets and the expenses due to production costs. CAPEX is the total initial investment. The lifetime of the plant was assumed to be 15 years. It was assumed that no working capital was required at the start of the project. In order for the configurations to be a profitable investment, the NPV should be positive at the end of the lifetime of the project. Equaling the NPV to 0 at the end of the lifetime of the torrefaction plant returns the minimum selling price of pellets at which the project is attractive to investors.

3.5.4 End use

The torrefaction plant in this Thesis is assumed to be in Brazil, but it is assumed that they are destined for the European or US energy market. Because of the high demand for energy in these regions, which is 5 times larger than the energy demand in Latin America [149], a higher demand for pellets is present in these regions. Furthermore, the wide spread of coal powered power plants in the US and EU allow for co-firing of torrefied pellets and coal [150]. Because of the coal-like properties of torrefied pellets, a high co-firing percentage of 50 % is achievable [151].

Costs associated with transportation, power station upgrades and conversion of pellets to electricity were taken into consideration in the economic analysis. In

accordance with research by Uslu et al. [151], costs associated with transport between Brazil and Europe were assumed to be €2.92/MWh. It is assumed that costs of transportation to the US and Europe are comparable with each other. Costs associated with the power station (e.g. electric cables, retrofitting of equipment to enable co-firing, conveyor infrastructure) were assumed to be €0.43/MWh, based on research by Beets [152]. The thermal efficiency was assumed to be 45 %, which is the efficiency of modern, state-of-the-art coal power plants [153].

Chapter 4

Results & Discussion

This chapter presents the results and discussion of the simulations of the different process configurations discussed in 3.4. All different scenarios were modelled for a pellet production of a 100 kton/yr. Firstly, the results of the dimensioning of the dryer and torrefaction reactor are presented for every configuration. Secondly, the results of the modelling of the process configuration are presented and evaluated in terms of volatiles generation, pellet production, energy consumption and efficiency. Thirdly, this chapter provides an economic evaluation of all studied configurations. Table 4.1 presents the notations that were used to address the different process configurations. The PFD (process flow diagram) of each configuration is presented in Appendix 1.2.

Table 4.1: Configuration summary

Number	Type of biomass	Valorization volatiles
CS_{comb}	Corn stalk	Combustion
$CS_{comb+clc}$	Corn stalk	CLC condensables Combustion non-condensables
CS_{clc}	Corn stalk	CLC
CS_{H_2}	Corn stalk	CLC + H_2 production
SCB_{comb}	Sugarcane bagasse	Combustion
$SCB_{comb+clc}$	Sugarcane bagasse	CLC condensables Combustion non-condensables
SCB_{clc}	Sugarcane bagasse	CLC
SCB_{H_2}	Sugarcane bagasse	CLC + H_2 production

4.1 Equipment dimensioning

4.1.1 Dryer

Table 4.2 presents the main results of the dryer modelling in Aspen Plus. Table 4.2 includes the drying times, combined length of the dryers, amount of dryers,

and the corresponding heat loss and thermal energy required for heating the air which enters each dryer system. The combined dryer length is the length of all dryers combined, which was calculated using the equations presented in Section 3.3. The exit moisture content of the dryer for all scenarios was set to 6%.

Table 4.2: Dryer results

Configuration	Feedstock (kg/hr)	Drying time (min)	Total dryer length (m)	Amount of dryers	Heat loss (kW)	Heat duty dryer (kW)
CS_{comb}	63,512	48	84.1	7	96	19,602
$CS_{comb+clc}$	63,044	43	82.4	6	96	19,515
CS_{clc}	43,280	44	57.7	5	66	13,291
CS_{H_2}	80,313	46	111.2	8	123	24,640
SCB_{comb}	52,853	105	291.6	21	329	19,953
$SCB_{comb+clc}$	47,080	107	264.5	19	292	17,718
SCB_{clc}	42,707	106	237.1	17	265	16,040
SCB_{H_2}	69,700	104	382.3	28	433	26,254

The drying time for SCB configurations (around 100 minutes) is much longer than the drying time for corn stalk (around 45 minutes). This difference is attributed to the lower diffusion coefficient in SCB compared with CS due to the differences in structure, which results in longer drying times (see Section 3.3). The drying time differs a couple of minutes between different process configurations for the same type of biomass due to the tolerance of the design spec in Aspen Plus which regulated the air entering the dryer (see Section 3.3). The long drying time of SCB configurations of over 100 minutes results in a high number of dryers required for drying, between 17 and 28 for SCB_{clc} and SCB_{H_2} , respectively. The amount of dryers required has potential to be reduced by decreasing the particle length or increasing the drying temperature.

Under the assumptions made in this work (see Section 3.3), longer drying times and higher feedstock flows resulted in a longer total dryer length and a higher amount of dryers. The high feed of biomass in configuration CS_{H_2} and SCB_{H_2} resulted in the most dryers (8 and 28) required for these configurations for their respective types of biomass.

Comparison dryer results with literature

The results presented in Table 4.2 are different compared to the results of other studies on drying and torrefaction modelling. The research by Manoucherinejad et al. [17] modelled drying and torrefaction of pine wood chips with an initial moisture content of 50 % and particle size of 15 mm. Drying 34,500 kg/hr of pine wood chips from 50 % to 10 % using air initially at 300 °C and 50 % relative humidity required only one dryer, 14 m in length and 2.4 m in diameter. The difference in dryers required between Manoucherinejad et al. [17] and the results from

this Thesis is attributed to the higher moisture content after drying (10 % over 6 %) and lower drying time (5.7 min over 44-105 min) used by Manoucherinejad et al. [17] as compared to this Thesis. The difference in drying time is attributed to the difference in the methods used for the determination of the drying time. The research by Manoucherinejad et al. [17] determined the drying time by using calculations involving length, diameter and rotational speed of the dryer, whereas the residence time in this study was calculated via drying kinetics as a function of drying temperature, drying time and particle size. Bergman et al. [13] modelled the drying and torrefaction process of wood chippings with a initial moisture content of 50 % and a particle size of 10 mm. No information on the drying agent in terms of temperature and humidity were supplied by Bergman et al. [13]. The research by Bergman et al. [13] found 4 parallel dryers (20 m length, 5 m diameter) were required to reduce the moisture content from 50 % to 15 % for a feedstock of 64,625 kg/hr. These results are of the same order of magnitude as the results presented in Table 4.2 for CS configurations. The difference in results of Bergman et al.[13] with the SCB configurations is attributed to the low diffusion coefficient in SCB, resulting in longer drying times and consequentially more dryers.

The calculated heat loss in the drying section is not significant compared to the heat required for heating the air which enters the dryer as a drying agent (0.5 % for the CS configurations and 1.7 % for SCB configurations). The low heat loss is attributed to the low operational temperature of the dryer, which was in the range of 60 °C to 70 °C for all configurations. The low operational temperature was selected due to the absence of experimental data on drying of CS at higher temperatures (see Section 3.3).

4.1.2 Torrefaction unit

Table 4.3 presents the volatiles composition for CS and SCB process configurations. As discussed in Section 3.3.2, the fractional composition of V1 and V2 changes with time and is constant for temperature. Because the ratio between V1 and V2 is dependent on the torrefaction temperature, the combined volatiles composition (V1 and V2 combined) is dependent on temperature and time. However, as stated in Section 3.3.2, V1 is far larger than V2 for all torrefaction temperatures and times, both for CS as for SCB. This is due to the faster generation of V1 due to the higher k-values found for V1 as opposed to V2, as discussed in Section 3.3.2 . As a consequence of V1 being far larger than V2, the combined volatiles stream (sum of V1 and V2) is almost fully comprised of V1. As the fractional composition of V1 is independent of temperature, the combined composition is almost fully independent of temperature. The torrefaction time was kept constant at 30 minutes and 40 minutes, respectively for all CS and SCB configurations. This resulted in a constant total volatiles composition for all CS and SCB configurations.

The CS volatiles is for a large fraction comprised of water (53 %) and CO_2 (13 %). The large fraction of these incombustible volatiles devalue the potential of the volatiles stream, as these compounds have no possibility to be used in energy generation. The considerable fractions of CO (9 %), CH_4 (5 %) and formaldehyde (5 %) increase the potential of the volatiles stream, as these compounds are combustible. The SCB volatiles are also comprised for a considerable part of water (28 %) and CO_2 (26 %). The large fraction combustible compounds like hydrogen (22 %) and CO (15 %) increase the potential of the volatiles stream for energy generation. Differences in the compounds of which the volatiles of CS and SCB torrefaction are comprised were discussed in Section 3.3.2.

Table 4.3: Volatiles compositions

(a) CS volatiles composition		(b) SCB volatiles composition	
$(t_{torrefaction} = 30min)$		$(t_{torrefaction} = 40min)$	
Compound	Molar fraction (wt.)	Compound	Molar fraction (wt.)
CO_2	0.13	CO_2	0.26
CO	0.09	CO	0.15
CH_4	0.05	CH_4	0.03
C_2H_4	0.03	H_2	0.22
C_2H_6	0.03	Water	0.28
Water	0.53	Acetic acid	0.05
Acetic acid	0.03	Phenol	0.00
Acetol	0.01	Furane	0.01
Methanol	0.02	HMF	0.00
Formaldehyde	0.05		
Formic acid	0.02		

The results of the torrefaction reactor modelling are presented in Table 4.4. Results are discussed in terms of total reactor length and the amount of reactors required by each process configuration. As mentioned in Section 3.3.2, the dimensions of one reactor were set to 43 m in length and 3 m in diameter, perfectly insulated.

Table 4.4: Torrefaction reactor results

Configuration	Combined reactor length (m)	Amount of reactors
CS_{comb}	509	12
$CS_{comb+clc}$	503	12
CS_{clc}	222	6
CS_{H_2}	663	16
SCB_{comb}	270	7
$SCB_{comb+clc}$	221	6
SCB_{clc}	206	5
SCB_{H_2}	479	12

As can be seen from Table 4.4, the combined length of the torrefaction reactors

for CS configurations are much longer compared to the rest of studied configurations because of the higher input feedstock (see Table 4.2), as a results of the shorter operational time during the year and higher operational torrefaction temperatures. The highest number of torrefaction reactors for their respective types of biomass are required for configuration CS_{H_2} (16 reactors) and SCB_{H_2} (12 reactors).

Comparison results torrefaction reactor with literature

Research by Manoucherinejad et al. [17] on drying and torrefaction of wood pine chips found that one torrefaction reactor with a length of 43 m, diameter of 3 m, biomass residence time of 30 min, operational temperature of 270 °C sufficed for the production of 100 kton pellets per year. This is less than the results presented in Table 4.4, in which 6 torrefaction reactors are required for CS_{cle} , which uses the same production level of 100 kton/yr and 30 minutes residence time, but with a lower operational temperature of 250 °C. The difference in torrefaction reactors is attributed to the higher temperature of the gas used to supply heat to the torrefaction reactor. The research by Manoucherinejad et al. [17] used flue gas at 950 °C to supply heat to the torrefaction reactor, as opposed to the 40 °C difference between the operating temperature of the reactor and the heating air used in this Thesis. Because of the large temperature difference between the flue gas and the operational temperature of the torrefaction reactor, Manoucherinejad et al. [17] assumed a heating rate of 100 °C/min of the solids in the torrefaction reactor. Rapid heating of the solids resulted in a short reactor length for Manoucherinejad et al. [17]. The calculations in this Thesis assumed a temperature difference of 40 ° between the heating agent and operational temperature of the torrefaction reactor. The length of the reactor was calculated assuming this low temperature difference, resulting in a long reactor length relative to Manoucherinejad et al. [17].

4.2 Operating conditions & production

Table 4.5 presents the results of the modelling for the different process configurations regarding feedstock, torrefaction temperature, volatiles generation, LFL of the volatiles, pellet production, energy consumption and efficiency. The LFL of the volatiles is presented for all configurations in which volatiles are combusted, thus excluding CS_{H_2} and SCB_{H_2} . As stated in Section 3.4.5, the torrefaction temperature was varied between 200 °C and 300 °C to aim for self-sufficiency of the configurations. All process configurations were designed for a production capacity of 100 kton/yr. The gross thermal LHV efficiency of the different configurations

was estimated based on the energy consumed by the process configurations, energy content of the torrefied biomass, the energy content of any H_2 produced and the energy content of the raw biomass (see Section 3.3.2). The gross LHV efficiency was selected, as the left over thermal energy of the air used for providing heat to the torrefaction reactor was of low quality due to its low temperature of 75 °C in SCB_{H_2} (see Appendix 1.2). To allow for equal comparison between the configurations, it has been decided to focus on the gross LHV efficiency.

Table 4.5: Summary of operational conditions and production

Configuration	Feedstock (kg/hr)	T torrefaction (°C)	Volatiles generation (kg/hr)	LFL (%)	Pellets production (kg/hr)	Energy consumption (MW)	Gross Efficiency (LHV) (%)
CS_{comb}	63,512	290	17,630	17	22,911	3.8	67%
$CS_{comb+clc}$	63,044	290	17,643	11	22,834	4.4	67%
CS_{clc}	43,280	250	4,859	8	22,837	3.8	92%
CS_{H_2}	80,313	300	25,680	-	22,467	33.3	48%
SCB_{comb}	52,853	280	11,974	11	17,108	2.9	72%
$SCB_{comb+clc}$	47,080	270	8,814	9	17,126	3.4	78%
SCB_{clc}	42,707	260	6,393	9	17,037	2.9	84%
SCB_{H_2}	69,700	300	21,219	-	17,120	34.9	48%

The operational temperature of the configurations was set by optimizing for self-sufficiency while reducing the amount of any left-over energy as discussed in Section 3.2. As discussed in Section 3.4.2, a lower LFL is preferred over a higher LFL, as a low LFL yields the potential to use more air in a combustor. This increased the conversion of energy generated by combustion to thermal energy, resulting in less volatiles required for combustion to generate the heat demanded by the dryer and torrefaction reactor. As less volatiles were required for combustion, it was possible to lower the torrefaction temperature, which in turn increased the solid yield in the torrefaction reactor. As the solid yield increased, less feedstock was required to obtain a pellet production of 100 kton/yr. Finally, less feedstock reduced the dimensions of the dryer and torrefaction reactor. The lower LFL of SCB volatiles in case of SCB_{comb} of 11 % and $SCB_{comb+clc}$ of 9 % as opposed to the LFL of CS_{comb} of 17 % and $CS_{comb+clc}$ of 11 % resulted in lower operational torrefaction temperatures of 280 °C and 270 °C for SCB_{comb} and $SCB_{comb+clc}$ as opposed to 290 °C required in CS_{comb} and $CS_{comb+clc}$. CS_{H_2} and SCB_{H_2} operate at the highest torrefaction temperature (300 °C), resulting in increased devolatilization and reduced torrefied solid yields. Therefore, in order to reach a pellet production of 100 kton/yr, CS_{H_2} and SCB_{H_2} have the largest biomass demand compared to the other scenarios, 80,313 kg/hr and 69,700 kg/hr, respectively. CS_{H_2} and SCB_{H_2} produced 505 kg/hr and 404 kg/hr of H_2 , respectively. The influence of the produced H_2 on the efficiency was taken into consideration. The lowest biomass demand is required for CS_{clc} (43,280 kg/hr) and SCB_{clc} (42,707 kg/hr) because these configurations operate at the lowest torrefaction temperatures, 250

$^{\circ}\text{C}$ and 260°C , respectively. The low torrefaction temperatures were obtained through optimization. The low LFL, of 8 % and 9 %, respectively, yielded the potential to increase the air fed to the combustor, converting more of the energy released during combustion to thermal energy. CS_{clc} and SCB_{clc} , due to the low torrefaction temperatures and low biomass demand, result in the least volatiles produced, 4,859 kg/hr and 6,393 kg/hr, respectively. The difference in hourly pellet production between the different types of biomass, 22,647-22,911 kg/hr for CS and 17,037-17,120 kg/hr for SCB, is due to different operational times were considered for corn stalk (4392 h) and sugarcane bagasse (5856 h) torrefaction plants.

4.2.1 Energy consumption

With respect to the energy consumption for each of the scenarios, the amount of energy required by each configuration was determined by the difference between the energy generated by the valorization of the volatiles and the energy demand of the torrefaction plant. Figure 4.1 presents an overview of the resulting energy consumption for each configuration. For the torrefaction plant, the model considers that the grinder and pelletizer were the only major processes requiring mechanical energy.

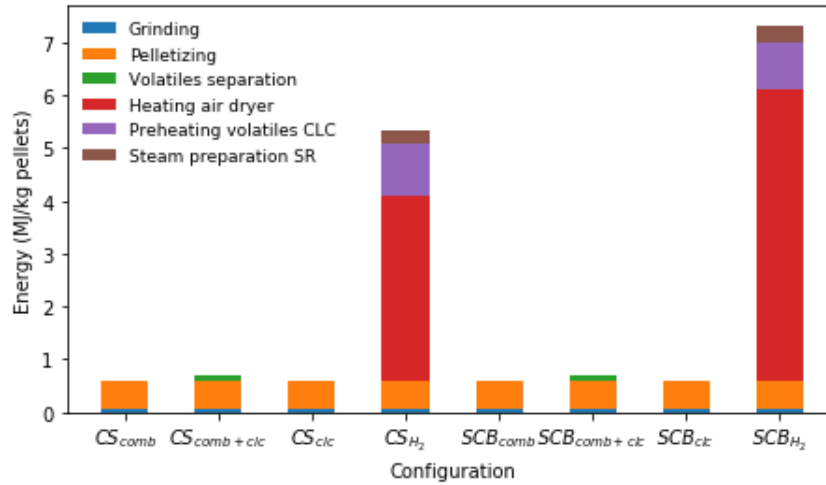


Figure 4.1: Energy consumption

The resulting energy requirement for grinding and pelletization was 0.6 MJ/kg of pellets produced for all configurations. All configurations have equal grinding and pelletization duties due to the same production capacity of 100 kton/yr. With respect to the valorization unit, process configurations involving volatiles

separation ($CS_{comb+clc}$ and $SCB_{comb+clc}$) require an additional mechanical energy requirement for compression of process streams, 0.09 MJ/kg and 0.1 MJ/kg, respectively. Results from the modelling indicate that the configurations oriented to H_2 production (CS_{H_2} and SCB_{H_2}) require additional energy in the form of heat compared to the other configurations required to heat the air entering the dryer, preheat the volatiles before the CLC section and to provide steam at high pressure in the SR. The heat duty of the dryer is the highest at 3.5 MJ/kg and 5.5 MJ/kg, respectively. Volatiles preheating in these two configurations required 1.0 MJ/kg and 0.8 MJ/kg, respectively. More energy is required to preheat the volatiles in CS_{H_2} as opposed to SCB_{H_2} due to the larger amount of volatiles produced by CS_{H_2} (see Figure 4.5). Steam preparation required 0.3 MJ/kg in both configurations. The demand for auxiliary energy is due to the lack of energy generated by the volatiles in CS_{H_2} and SCB_{H_2} , which limits the amount of energy that can be recovered from the volatiles. Because of the additional thermal energy required, the energy consumption of CS_{H_2} and SCB_{H_2} are larger than the energy demands of the other configurations, totaling at 5.3 MJ/kg and 7.3 MJ/kg, respectively.

With respect to efficiency, results from the modelling presented in Figure 4.5 show that the efficiency for CS_{clc} and SCB_{clc} were the highest at 92 % and 84 %, respectively, for all scenarios. These configurations report the highest efficiency due to the lack of additional energy required for volatiles separation as opposed to $CS_{comb+clc}$ and $SCB_{comb+clc}$ and low torrefaction temperatures as opposed to CS_{comb} and SCB_{comb} . Lower torrefaction temperatures result in higher torrefied solid yields (the ratio between pellets production and feedstock), and thus higher efficiencies.

4.3 Economics

4.3.1 Capital expenditures

The total capital expenditures (CAPEX) of the dryer, torrefaction reactor, CLC reactor, pelletizer and grinder were determined using Eq. (3.56) in Section 3.5.1. The costs of other equipment such as heat exchangers and coolers, were determined from the Economics tool in Aspen Plus . The total equipment costs for the different processes configurations using a torrefaction plant of 100 kton/yr are summarized in Figure 4.2. The price of the pelletizer was set constant for all configurations. Furthermore, it was assumed that all configurations of one type of biomass have the same output in terms of the weight of the pellets produced from the torrefaction reactor and thus require the same size pelletizer.

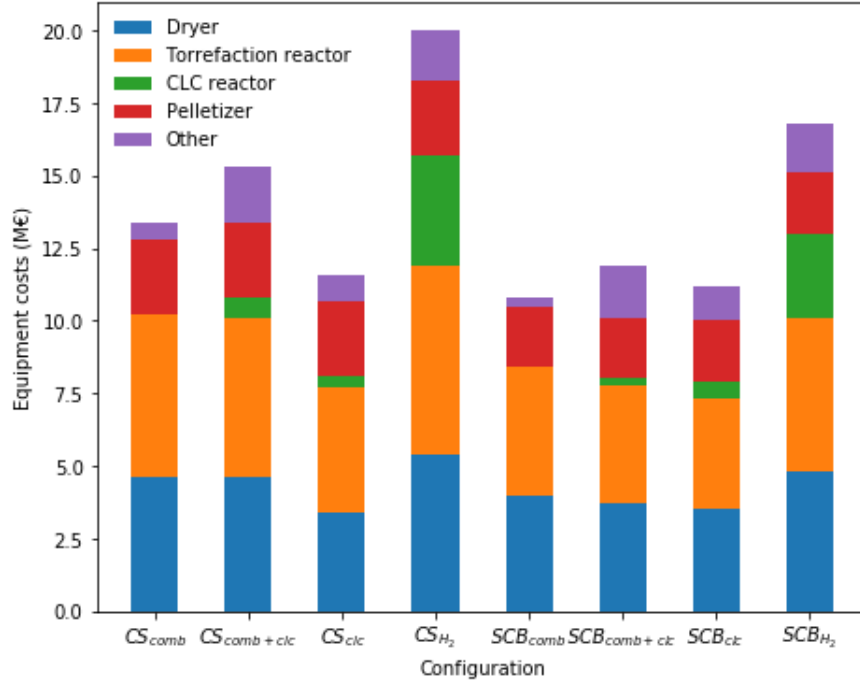


Figure 4.2: Equipment costs

Configurations CS_{clc} and SCB_{clc} demand the least feedstock ($<43,280$ kg/hr), resulting in the lowest capital expenditures required for the purchase of equipment for their respective torrefaction plants. This is reflected in the dryer costs (3.5 M€ for both) and torrefaction reactor costs of 4.3 M€ and 3.8 M€, respectively, for configurations CS_{clc} and SCB_{clc} . The lack of a CLC reactor reduces the equipment costs for CS_{comb} and SCB_{comb} in comparison to the other configurations regarding their respective types of feedstock. On the other hand, configuration CS_{H_2} and SCB_{H_2} , require high volumes of feedstock ($>69,700$ kg/hr, see Table 4.5), resulting in high costs for the dryer of 5.4 M€ and 4.8 M€ and torrefaction reactor of 6.5 M€ and 5.3 M€, respectively.

An interesting result to note is the relatively small up-front investment required for the CLC reactor in the CS_{clc} configuration compared to $CS_{comb+clc}$. This is due to the fact that even though all volatiles (condensable and non-condensable) were sent to the CLC reactor in configuration CS_{clc} , the lower torrefaction temperature reduces the requirement of feedstock, resulting in a lower amount of volatiles sent to the CLC reactor in CS_{clc} than in configuration $CS_{comb+clc}$.

With respect to the influence of the type of biomass, the total capital expenditures for all equipment for each configuration is lower for the sugarcane bagasse configurations. This is due to the lower feedstock requirements in these configurations due to longer production times during the year require smaller sized equip-

ment, reducing the costs of equipment.

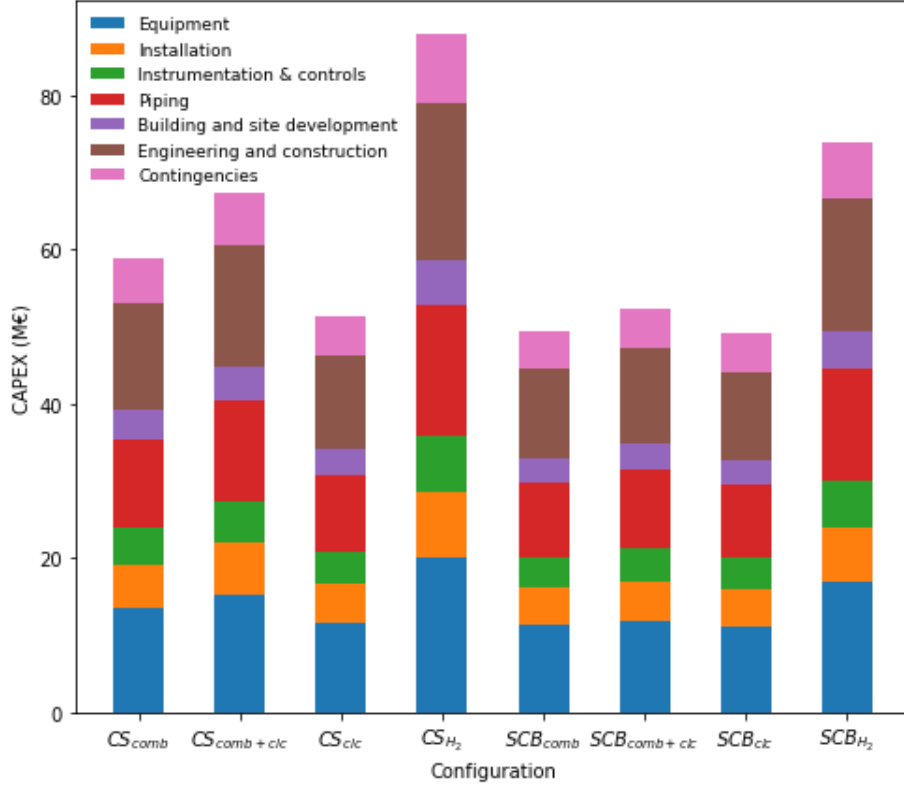


Figure 4.3: CAPEX

Figure 4.3 presents the disaggregated results for CAPEX calculations for each configuration. The total CAPEX is ultimately dependent on the equipment costs, as all other CAPEX factors are related to the equipment costs (see Section 3.5.1). Therefore, the processes with the highest equipment costs, CS_{H_2} and SCB_{H_2} , demand the highest total CAPEX as well. The process configurations CS_{clc} and SCB_{clc} , where all volatiles are sent to the CLC reactor, have the lowest equipment costs and are thus the least expensive CAPEX option for each type of biomass at 51.3 M€ and 49.1 M€ respectively. CS_{H_2} and SCB_{H_2} are the most expensive configurations, requiring 87.9 M€ and 74.0 M€ respectively.

Details of equipment costs and overall CAPEX can be found in Appendix 1.3.

4.3.2 Operating expenditures

The results of the operating expenditures (OPEX) calculations are presented in Figure 4.4. A detailed table of the OPEX for the configurations is presented

in Appendix 1.3. Configurations CS_{clc} and SCB_{clc} are the cheapest options in terms of total OPEX, at 20.8 M€/yr and 17.9 M€/yr, respectively. This is due to the lowest feedstock demand ($< 43,280$ kg/hr) and thus the smallest equipment required for these configurations. This reduced the costs for raw materials, maintenance and depreciation in comparison to the other configurations. Meanwhile, CS_{H_2} (42.1 M€/yr) and SCB_{H_2} (30.0 M€/yr) are the most expensive due to the large feedstock required ($> 69,700$ kg/hr), auxiliary heat demand and high capital expenditures, resulting in high OPEX for raw materials, maintenance and depreciation.

The majority of OPEX is due to feedstock costs, from 32 % for SCB_{H_2} to 46 % for CS_{comb} and CS_{H_2} . OPEX for CS configurations were higher than for their SCB counterparts due to higher costs for feedstock, €42.72/ton over €24.40/ton, respectively (see Section 3.5.2).

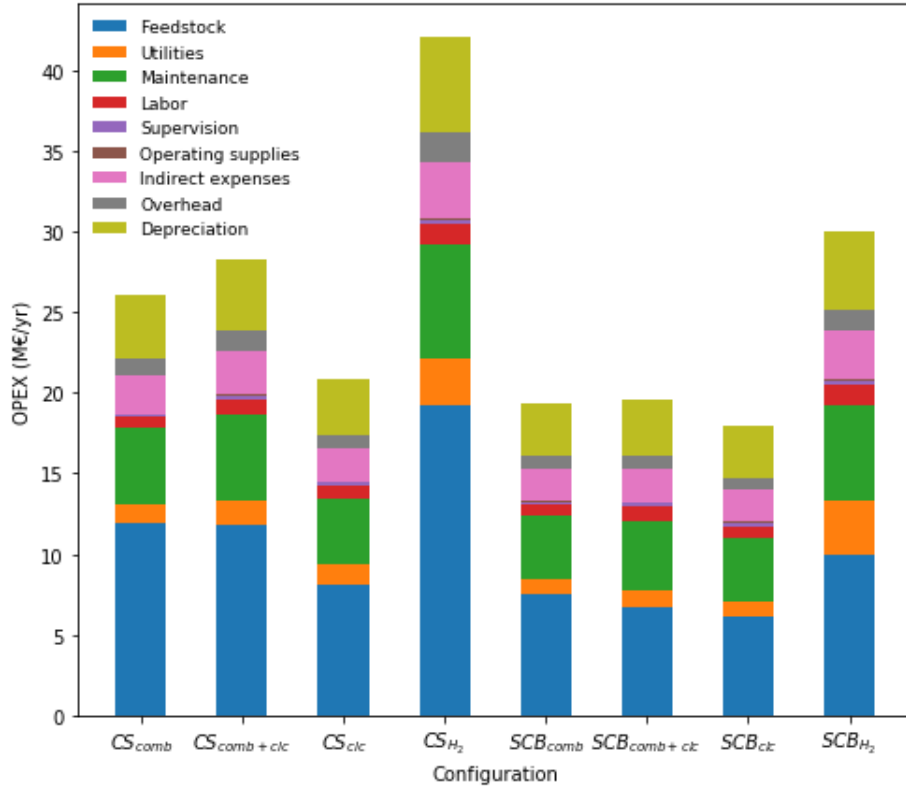


Figure 4.4: OPEX

Utilities OPEX

The OPEX for utilities are presented in Figure 4.5. The utility costs were dependent on the amount and type of utility required by the configurations. All configurations required electricity and cooling water for cooling down the torrefied biomass, grinding and pelletization.

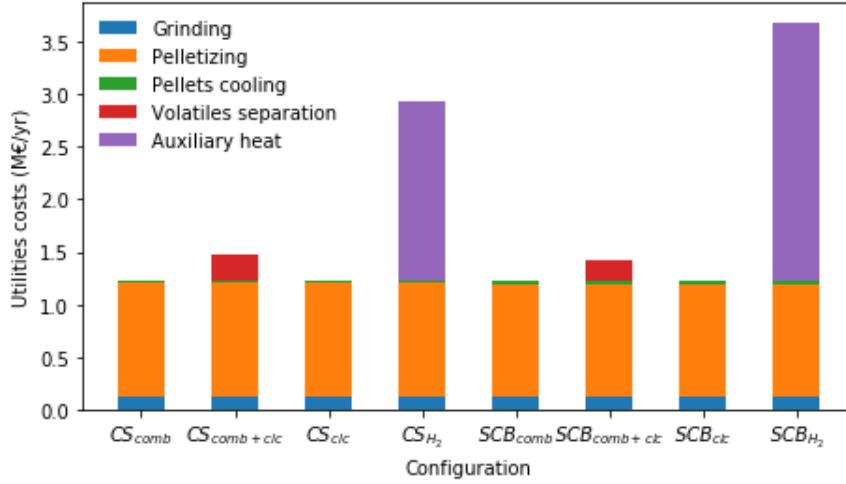


Figure 4.5: Utility costs

The resulting utility costs associated for these process steps were 1.2 M€/yr for all configurations. The utility costs associated with these process steps were dependent on the production capacity of the torrefaction plant, which was set at 100 kton/yr for every configuration, resulting in an equal utility cost for every configuration for these process steps. Cooling the pellets required 0.02 M€/yr, grinding 0.13 M€/yr and pelletizing 1.07 M€/yr. Volatiles separation increased the utility costs of $CS_{comb+clc}$ and $SCB_{comb+clc}$ by 0.3 M€/yr and 0.2 M€/yr, respectively, opposed to CS_{comb} and SCB_{comb} . The increase in the utility costs is due to electricity and cooling water demands for the compressors and coolers required in these configurations. The demand for auxiliary heat in configurations CS_{H_2} and SCB_{H_2} increased the costs for utilities for these two configurations by 1.7 M€/yr and 2.5 M€/yr as opposed to the other configurations. The higher utility OPEX associated with auxiliary heating for SCB_{H_2} as opposed to CS_{H_2} are due to the larger air demand in the dryer, 235,701 kg/hr and 221,209 kg/hr, respectively, and the longer operational time per year for SCB configurations of 8 months over 6 months for CS configurations.

4.3.3 Overall economic results and & comparison with literature

The most relevant results of the economic analysis were compared with findings from previous studies in Table 4.6. Table 4.6 presents CAPEX per kW and the production costs per MWh for each configuration. The CAPEX per kW is a means to relate the CAPEX to the production capacity. The production capacity is expressed as the amount of energy generated in the form of pellets per second, leading to an expression of production capacity in terms of kW. The CAPEX per kW was calculated to compare the CAPEX results to other sources, for example research by Svanberg et al. [71], while accounting for production capacity. The CAPEX per kW and production costs per MWh were calculated by using the LHV of the pellets, 16.81-18.76 MJ/kg for SCB and 16.29-18.59 MJ/kg for CS, depending on the torrefaction temperature. Higher torrefaction temperatures resulted in increased LHV.

Table 4.6: Overall results

Configuration	CAPEX/kW (€/kW)	Production costs (€/MWh)
CS_{comb}	549	55.45
$CS_{comb+clc}$	630	60.32
CS_{clc}	527	48.72
CS_{H_2}	787	85.80
SCB_{comb}	614	41.02
$SCB_{comb+clc}$	669	42.79
SCB_{clc}	650	40.55
SCB_{H_2}	863	59.80

Under the assumptions made in this work, process configurations CS_{clc} and SCB_{clc} report the lowest production costs at 48.72 €/MWh and 40.55 €/MWh. CS_{H_2} and SCB_{H_2} are the most expensive at 85.80 €/MWh and 59.80 €/MWh, respectively. The SCB configurations have lower costs per MWh than their CS counterparts due to the lower costs of raw material acquisition, as was discussed in Section 4.3.1 and 4.3.2. The CAPEX per kW is the lowest for CS_{clc} and SCB_{comb} , at €527/kW and €614/kW, respectively. The CS configurations are less expensive in terms of CAPEX/kW than their SCB counterparts due to the lower pellet production per hour of the SCB configurations. This means less energy is generated in the form of pellets per second, leading to a lower production capacity in terms of kW and thus a higher CAPEX/kW. Furthermore, more dryers were required for the sCB configurations as opposed to the CS configurations, increasing the CAPEX.

Comparison production costs with literature

The economic results of other research were updated to 2020 values by taking inflation into account [154]. Research by Radics et al. [155] compared four different studies on torrefaction economics in Europe and North America with a production capacity ranging between 40-100 kton/yr. All studies used volatiles combustion as valorization process. As SCB_{clc} yielded the best results in terms of production costs per MWh produced out of all configurations researched in this Thesis, it has been decided to compare the results of SCB_{clc} with others studies. Authors report average production costs per MWh of produced pellets of €26.26, with values ranging from €24.76 to €27.86/MWh. Results reported by Radics et al. [155] on production costs per MWh are on average 31% lower than the value obtained for SCB_{clc} , which was €40.55/MWh. This difference is attributed to the difference in the costs for the raw biomass, which varied between €5.32/MWh and €11.89/MWh in Radics et al. [155], as opposed to €13.79/MWh for SCB_{clc} used in this Thesis. Radics et al. [155] considered a low feedstock price of maximum €22.28/ton raw wood chips as opposed to €24.40/ton of raw SCB and €42.72/ton for CS. Information to further estimate the difference in production costs was not provided by Radics et al. [155].

Furthermore, a study by Svanberg et al. [71], which focused on the supply chain costs of torrefied wood pellets produced in a 200 kton pellet/yr torrefaction plant report production costs of €33.17/MWh. Their torrefaction plant used volatiles combustion as the valorization process of choice. Results from the modelling indicates that raw material acquisition accounts for 34 % of the production costs for SCB_{clc} , whereas raw material accounts for 59 % in findings by Svanberg et al. [71]. Moreover, Svanberg et al. [71] assumed maintenance expenses to be equivalent to 2 % of the CAPEX, whereas this Thesis assumed 8 %. Moreover, research by Svanberg et al. [71] included distribution costs after torrefaction and pellet production, which are equivalent to 9 % of the total production costs.

Comparison CAPEX with literature

CAPEX were estimated by Svanberg et al. [71] to be €340/kW. This is 35 % lower than the minimum value of €527/kW calculated in this Thesis for CS_{clc} . The difference is partly attributed to differences in production capacity, which provides scale advantages for Svanberg et al. [71] compared to values reported in Thesis. This resulted in lower CAPEX relative to energy production in the form of pellets per second. The difference in CAPEX/kW is further attributed to the larger amount of CAPEX factors, for example contingencies and engineering costs, taken into consideration in this Thesis. Furthermore, under the assumptions made in this work, the CAPEX factors "Installation & Control" and "Piping" were set

to 25 % and 60 %, respectively, of the installed equipment costs. Meanwhile, research by Svanberg et al. [71] assumed these factors combined to be 19 % of the installed equipment costs, resulting in a lower CAPEX/kW compared to the results produced in this Thesis.

4.3.4 Sensitivity analysis

The scale of the torrefaction plant has an influence on the production costs per MWh. Because of scale advantages, larger torrefaction plants require relatively lower CAPEX and OPEX per ton of pellets produced. To investigate the influence of scale, a sensitivity analysis on scale was performed. Configuration CS_{clc} was selected as the base cases for the sensitivity analysis. This configuration was chosen as it is the most competitive CS configuration. The size of the torrefaction plant was varied to cover three capacities as follows: small (10 kton/yr pellets), medium (100 kton/yr pellets) and large (300 kton/yr pellets). The main results of this sensitivity analysis are presented in Table 4.7.

Table 4.7: Sensitivity analysis

Scale	Feedstock (kg/hr)	Pellet production (kg/hr)	CAPEX (M€)	OPEX (M€/yr)	Production costs (€/ton)	Production costs (€/MWh)
Small	3,280	2,284	12.4	4.52	452	116.16
Medium	43,280	22,837	51.3	20.82	208	48.87
Large	138,810	68,511	118.8	55.34	184	43.30

The larger production scale yields scale advantages, as the production costs per ton pellets changes from €452/ton to €184/ton as the scale increases from small to large. The production costs per MWh decrease from €116.16/MWh to €43.30/MWh. Scale advantages are achieved as larger sized equipment yields scale advantages (see Section 3.5.1), while costs for labor, supervision and operating supplies are independent of scale. Especially the step from small to medium increases the competitiveness of a torrefaction plant, as the production costs per ton of pellets reduce by 54 %. It has been assumed that scale advantages of equipment sizing remain constant. In reality, instead of using ever larger equipment, parallel chains of operation will be designed. Doing so decreases the scale advantages, as multiple smaller lines of operation do not necessarily reduce equipment costs. Furthermore, restrictions on availability on land can potentially provide problems for up-scaling of torrefaction plants.

4.3.5 Net present value

The net present value (NPV) of the CS_{clc} and SCB_{clc} was determined via Eq. (8) in Section 3.5.3. CS_{clc} and SCB_{clc} were selected as these configurations required the least CAPEX and OPEX of their respective types of biomass. The potential profit by selling H_2 produced by CS_{H_2} and SCB_{H_2} was not taken into consideration for the NPV analysis, as these two configurations were 71 % and 51 %, respectively, more expensive in terms of total CAPEX and 102 % and 68 %, respectively more expensive in terms of total OPEX than CS_{clc} and SCB_{clc} . The gap was deemed to be too large for the production of H_2 to make up for. An internal rate of return (IRR) of 10 % and a lifetime of the plant of 15 years were assumed, which are typical values for a biomass plant in Brazil [156]. The NPV was set to 0 at the end of the lifetime of the plant by adjusting the selling price per ton of pellets to determine the point at which the project becomes profitable for investors. The selling price at the point where the NPV equals 0 after the lifetime of the plant was found to be €274.79 per ton of pellets for corn stalk pellets and €244.53 per ton of pellets for sugarcane bagasse pellets. Any selling price above €274.79/ton and €244.53/ton for CS and SCB pellets, respectively, would provide economic returns to investors. The difference between the selling prices of CS_{clc} and SCB_{clc} is due to the lower total CAPEX and OPEX of SCB_{clc} .

Figure 4.6 below shows the sensitivity of the price per ton to the IIR for CS_{clc} and SCB_{clc} . The y-axis presents the minimum price per ton that should be paid in order for the investment to be economically profitable. The IRR was varied between 9-16 %. In literature it was found that the IRR concerning biomass projects in Brazil varies between these values [157].

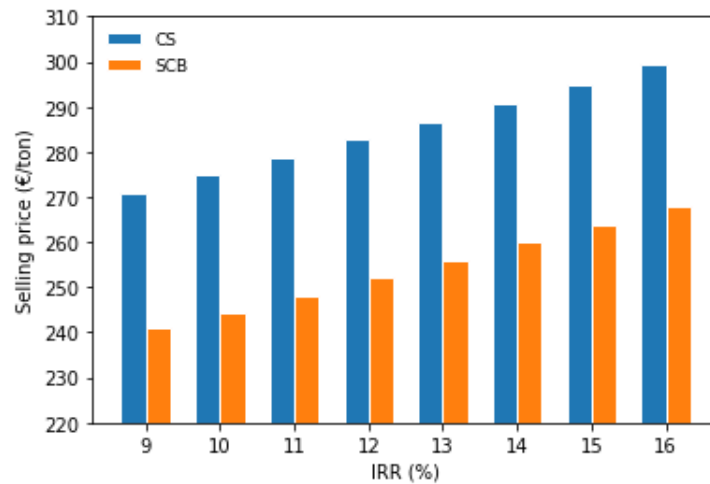


Figure 4.6: IRR sensitivity CS_{clc} and SCB_{clc}

The minimum selling price for a NPV of 0 after 15 years is €271.00/ton for CS_{clc} and €240.88/ton for SCB_{clc} , assuming an IRR of 9%. This is equivalent to a selling price of €51.37/MWh for CS_{clc} and €45.30/MWh for SCB_{clc} . Taking transportation costs into account (see Section 3.5.4), a deliverance selling price of €54.29/MWh for CS_{clc} and €48.22/MWh for SCB_{clc} were obtained. In 2020, a typical selling price of wood pellets delivered to Rotterdam was €35.65/MWh [158]. Compared with the reference market price, both CS_{clc} and SCB_{clc} are not competitive with market prices for the range of IRRs considered. The difference between the market price of €35.65/MWh and the selling price as calculated above of €54.29/MWh and €48.22/MWh can potentially be overcome via subsidies. Table 8 in Appendix 1.3 presents the detailed NPV per year of CS_{clc} and SCB_{clc} using these selling prices.

4.3.6 Comparison with other sources of energy

It has been assumed that the pellets are to be co-fired in a 50/50 coal/biomass power plant. After taking transportation costs of €2.92/MWh, power plant costs of €0.43/MWh and the efficiency of the power station of 45 % into account (see Section 3.5.4), the production costs of electricity by CS_{clc} and SCB_{clc} are €115.71/MWh for corn stalk and €97.55/MWh for sugarcane bagasse. It is assumed that there are no additional costs for the transportation of the pellets from the torrefaction plant to the harbor and from the harbor to the power plant. Furthermore, no costs regarding the combustion of pellets in a power station other than the extra costs associated with co-firing instead of pure coal combustion have been taken into consideration. Table 4.8 shows a comparison of the price of the torrefied pellets with other sources of energy. The economic analysis in this study was performed by using data from Europe and the US. Therefore, the results of the economic analysis were compared with cost for electricity generation by different fuel sources in Europe and the US. In this Thesis the location of the torrefaction plant was assumed to be in Southern Brazil, so this is also listed as the location in this study. All prices were updated to 2020.

Table 4.8: Cost comparison ($\eta_{th}=45\%$)

Type	Price (€/MWh)	Country
Pellets this study	97.55	Brazil
Biomass [159]	130.63	UK
Biomass [160]	86.95	US
Solar [159]	120.12	UK
Solar [160]	65.59	US
Wind (onshore) [159]	93.09	UK
Wind (onshore) [160]	49.66	US
Natural gas (conventional)[159]	99.01	UK
Natural gas (conventional) [160]	52.15	US
Natural gas (with CCS) [159]	165.17	UK
Natural gas (with CCS) [160]	80.46	US
Coal (with CCS) [159]	201.20	UK
Coal (conventional) [160]	84.64	US
Coal (with CCS) [160]	114.72	US

The most competitive price for energy generated by torrefied biomass in this study (€97.55/MWh) is in between the prices for the US €86.95/MWh and the UK (€130.63/MWh). It is less expensive than fossil fuels with CCS in the UK (€165.17/MWh for natural gas and €201.20/MWh for coal). It is more expensive than wind and solar energy in the US (€65.59/MWh and €65.59/MWh), while slightly more expensive than wind and less expensive than solar energy in the UK (€93.09/MWh and €120.12/MWh). A major benefit of biomass as opposed to wind and solar energy is its ability to be stored and transported easily. These factors were been considered in these prices. A comparison with the prices for fossil fuels without carbon capture reveals these are cheaper in all cases than the energy price found in this study, except for the price of natural gas in the UK (€99.01/MWh). The large difference in energy costs between all types of renewable energy in the UK and the costs calculated by this Thesis, plus the additional benefit of easy storage of pellets as compared to wind and solar energy, result in the conclusion that SCB_{clc} is competitive with the energy market in the UK.

Chapter 5

Conclusion

This Thesis was set up to fill the gap in literature on the valorization of volatiles produced during torrefaction. The approach was to design and evaluate different process models for torrefaction and volatiles valorization. The torrefaction and valorization process were simulated in Aspen Plus for two types of biomass: corn stalk and sugarcane bagasse. Four different process configurations regarding the valorization of volatiles were studied: (1) combustion of volatiles, (2) chemical looping combustion of all volatiles, (3) chemical looping combustion for the condensable volatiles and combustion for the non-condensable volatiles and (4) chemical looping for all volatiles in combination with hydrogen production.

The torrefaction plants modelled in this Thesis comprised of a dryer, torrefaction reactor and valorization unit. The simulation of drying and torrefaction were based on and validated through the use of experimental data. The drying of biomass has been improved relative to previous studies by using the dryer block in Aspen Plus in combination with drying equations based on experimental data. Drying equations with high correlations with experimental data, $R^2 > 0.99$ and $X^2 < 0.1$, were obtained and implemented in the Aspen Plus model. Torrefaction kinetics were modelled with good correlation ($R^2 > 0.6$ and $X^2 < 0.4$) to experimental data. The use of multiple sources for the torrefaction process increased the validity of the model. Valorization through CLC and valorization through steam reforming in combination with drying and torrefaction simulation were for the first time implemented in Aspen Plus. Results of CLC of all volatiles were promising.

The torrefaction temperature of the configurations was optimized to obtain self-sufficient configurations while reducing the leftover energy as much as possible. CS_{clc} and SCB_{clc} operated at the lowest torrefaction temperatures, 250 °C and 260 °C, respectively. The low torrefaction temperature increased the solids yield, during torrefaction, resulting in less feedstock required to meet the design capacity of 100 kton/year for CS_{clc} (43,280 kg/hr feedstock) and SCB_{clc} (42,707 kg/hr feedstock). Comparing results from modelling in terms of efficiency, CAPEX, OPEX

and price per MWh yields chemical looping of all volatiles as the best technique for volatiles valorization. Configurations CS_{clc} and SCB_{clc} obtained the highest LHV efficiency, of 92 % and 84 %, respectively, the lowest CAPEX, of 51.3 M€ and 49.1 M€, respectively and the lowest OPEX, of 17.6 M€/yr and 14.8 M€/yr, respectively. As a consequence, the lowest production costs per MWh were obtained for these configurations, of 41.09 €/MWh and 33.50 €/MWh, respectively.

It is concluded that valorization through steam reforming is undesirable as it prevents the opportunity to generate heat through valorization of volatiles. The lack of energy production by the volatiles in CS_{H_2} and SCB_{H_2} required large demands, 5.3 and 7.3 MJ/kg pellets produced, respectively, for auxiliary heat to provide heat to the dryer and preheat the volatiles before the chemical looping section. Volatiles valorization with the aim to obtain valuable compounds like hydrogen or acetic acid, which are used by the petrochemical industry, among others, is not deemed profitable in comparison to valorization through energy generation. Focus on the creation of valuable compounds instead of energy generation result in a high auxiliary heat demand for drying and torrefaction, increasing utility costs and reducing the profitability of the torrefaction plant.

Generally, configurations using SCB as feedstock were more competitive than configurations using CS. The difference was attributed to the higher costs for raw CS as opposed to SCB, and the reduced operational time for CS torrefaction plants, resulting in higher feedstock required per hour, requiring larger sized equipment, thereby increasing the costs.

Under the assumptions made in this work, SCB_{clc} and CS_{clc} are not profitable for an IRR of 9 % or higher. Profitability could be increased by subsidies or CO_2 emission trading. Increasing the scale of the torrefaction plant might provide economies of scale and increase profitability. Further research on economies of scale is required to confirm this. Furthermore, SCB_{clc} is competitive with other renewable energy sources.

Results from the modelling indicate that torrefaction provides an opportunity for renewable energy production. CLC is a technique that can further improve the valorization of volatiles produced during torrefaction and add value to the concept of torrefaction.

Chapter 6

Recommendations

The largest challenge during this Thesis was acquiring experimental data on composition, drying and torrefaction of different types of biomass. As stated in section 3.1, enough experimental data was only found for CS and SCB. All other types of biomass considered, except sunflower stalk, lacked sufficient data on low temperature drying. If someone wants to improve on this Thesis by modelling the drying and torrefaction process of other types of biomass, it is strongly advised to first obtain useful data on drying before collecting data on composition and torrefaction. The reason limited information on drying is available is because of the focus of research on the torrefaction of biomass instead of drying. Most researches either dry the biomass they use in torrefaction experiments by forced drying in an oven for 24 hours, removing all moisture, or by letting it dry by natural air. It is understandable that experiments on torrefaction, either on solid yield or volatiles generation or a combination of the two, are more exciting than drying experiments, but this has lead to a huge gap regarding drying kinetics, while this is an essential part in torrefaction studies. The recommendations are split in two sections depending on the technology employed: torrefaction and CLC. The following recommendations are made on torrefaction.

1. It is recommended that a table consisting of experimental data on composition, drying and torrefaction mass loss and volatile yields for a wide range of different feedstocks is created. This way, more types of biomass, including different types of agricultural residues, can be analysed for their potential pellet creation through torrefaction. As stated above, especially more experimental data on drying for different types of biomass is required.
2. Further research on torrefaction should incorporate the possibilities of natural air drying instead of using a dryer. Natural air drying can possibly get the moisture content in the feedstock down to much lower moisture contents than the 40 % and 50 % used in this study. This reduces the heat duty of the

dryer, reducing its dimensions. Moreover, further research on the possibility of placing a grinder to reduce particle size before drying and torrefaction should be considered, as a smaller particle size can significantly reduce the drying time, thereby reducing the dimensions of the dryer. A consideration should be made regarding the advantages of the reduction in drying time and consequently reduction in dryer dimensions and the disadvantages through increasing energy consumption by adding a grinder before the dryer. Furthermore, research should focus on providing heat to the torrefaction reactor. Increasing the temperature of the heating agent reduces the torrefaction reactor dimensions, but on the other hand increases the risk of biomass burning. The heat transfer between the reactor wall and the biomass is the rate determining step in this heat transfer problem. Apart from increasing the temperature of the heating agent, additional research could focus on using direct heating instead of indirect heating in the torrefaction reactor. This increases the heat transfer to the biomass, reducing the torrefaction reactor length. A disadvantage is the pollution of volatiles, as the heating agent will mix with the volatiles. This leads to reduced potential for combustion or CLC.

The following recommendations are made on CLC.

1. As was stated in the literature review, the common aim of CLC is to generate energy in the air reactor. In this thesis, a different approach was taken by aiming for syngas production in the fuel reactor, which was later burned in a combustor. Further research on energy generation in the air reactor in combination with implementation in the Aspen Plus model might offer potential improvement of the CLC compared to the implementation in this Thesis. Furthermore, additional research on the CLC process should be focused on the dimensioning of the CLC reactors. This way, more insight can be created in the heat exchange between the air reactor, fuel reactor and combustor, while also accounting for heat loss through the reactor walls. Further challenges also remain on the scalability of CLC and the separation of the syngas and reduced metal oxide generated by the different reactors in the CLC sections.

Bibliography

- [1] *Global Bioenergy Statistics 2019*. Tech. rep. World Bioenergy Association, 2019.
- [2] Didier B. *Biomass for electricity and heating Opportunities and challenges*. https://www.europarl.europa.eu/thinktank/en/document.html?reference=EPRS_BRI%282015%29568329. 2015.
- [3] N. homas. “CHAPTER 2 - Energy”. In: *Field Guide to Appropriate Technology*. Ed. by B. Hazeltine et al. San Diego: Academic Press, 2003, pp. 157–275. ISBN: 978-0-12-335185-2. DOI: <https://doi.org/10.1016/B978-012335185-2/50046-2>. URL: <http://www.sciencedirect.com/science/article/pii/B9780123351852500462>.
- [4] R. P. Chaudhary et al. “Chapter 12.2 - Deforestation in Nepal: Causes, Consequences, and Responses”. In: *Biological and Environmental Hazards, Risks, and Disasters*. Ed. by Jo. F. Shroder et al. Boston: Academic Press, 2016, pp. 335–372. ISBN: 978-0-12-394847-2. DOI: <https://doi.org/10.1016/B978-0-12-394847-2.00020-6>. URL: <http://www.sciencedirect.com/science/article/pii/B9780123948472000206>.
- [5] Marshall A.M. “First generation biofuels compete”. In: *New Biotechnology* 27.5 (2010), pp. 596–608. ISSN: 1871-6784. DOI: <https://doi.org/10.1016/j.nbt.2010.06.010>. URL: <http://www.sciencedirect.com/science/article/pii/S1871678410004863>.
- [6] C. Bonechi et al. “1 - Biomass: An overview”. In: *Bioenergy Systems for the Future*. Ed. by Francesco Dalena et al. Woodhead Publishing, 2017, pp. 3–42. ISBN: 978-0-08-101031-0. DOI: <https://doi.org/10.1016/B978-0-08-101031-0.00001-6>. URL: <http://www.sciencedirect.com/science/article/pii/B9780081010310000016>.
- [7] O. Ioannidou et al. “Investigating the potential for energy, fuel, materials and chemicals production from corn residues (cobs and stalks) by non-catalytic and catalytic pyrolysis in two reactor configurations”. In: *Renewable and Sustainable Energy Reviews* 13.4 (2009), pp. 750–762. ISSN: 1364-

0321. DOI: <https://doi.org/10.1016/j.rser.2008.01.004>. URL: <http://www.sciencedirect.com/science/article/pii/S1364032108000117>.
- [8] S.A. Channiwala et al. “A unified correlation for estimating HHV of solid, liquid and gaseous fuels”. In: *Fuel* 81.8 (2002), pp. 1051 –1063. ISSN: 0016-2361. DOI: [https://doi.org/10.1016/S0016-2361\(01\)00131-4](https://doi.org/10.1016/S0016-2361(01)00131-4). URL: <http://www.sciencedirect.com/science/article/pii/S0016236101001314>.
- [9] Leonel Jorge Ribeiro Nunes et al. “Chapter 13 - Future Developments and Derived Fuels”. In: *Torrefaction of Biomass for Energy Applications*. Ed. by Leonel Jorge Ribeiro Nunes et al. Academic Press, 2018, pp. 221 –229. ISBN: 978-0-12-809462-4. DOI: <https://doi.org/10.1016/B978-0-12-809462-4.00013-4>. URL: <http://www.sciencedirect.com/science/article/pii/B9780128094624000134>.
- [10] A. Dahija et al. *Bioenergy : Biomass to Biofuels*. Elsevier Science Technology, 2014, 2014.
- [11] M.L. Lopes et al. “Ethanol production in Brazil: a bridge between science and industry”. In: *Brazilian Journal of Microbiology* 47 (2016), pp. 64 –76. ISSN: 1517-8382. DOI: <https://doi.org/10.1016/j.bjm.2016.10.003>. URL: <http://www.sciencedirect.com/science/article/pii/S1517838216310346>.
- [12] *The development history of biomass pellets*. <http://www.gemcopelletmills.com/biomass-pellet-development.html>. Accessed: 14-05-2020.
- [13] P. Bergman et al. “Torrefaction for Biomass Co-Firing in Existing Coal-Fired Power Stations”. In: *Energy research Centre of the Netherlands* (Jan. 2005).
- [14] A. Salimbeni. “6 - Organic waste streams upgrading for gasification process optimization”. In: *Substitute Natural Gas from Waste*. Ed. by Massimiliano Materazzi et al. Academic Press, 2019, pp. 75 –103. ISBN: 978-0-12-815554-7. DOI: <https://doi.org/10.1016/B978-0-12-815554-7.00006-4>. URL: <http://www.sciencedirect.com/science/article/pii/B9780128155547000064>.
- [15] L. Fagernäs et al. “Drying of biomass for second generation synfuel production”. In: *Biomass and Bioenergy* 34.9 (2010), pp. 1267 –1277. ISSN: 0961-9534. DOI: <https://doi.org/10.1016/j.biombioe.2010.04.005>. URL: <http://www.sciencedirect.com/science/article/pii/S0961953410001297>.

- [16] S. Heidenreich et al. "Chapter 3 - Biomass Pretreatment". In: *Advanced Biomass Gasification*. Ed. by S. Heidenreich et al. Academic Press, 2016, pp. 11 –17. ISBN: 978-0-12-804296-0. DOI: <https://doi.org/10.1016/B978-0-12-804296-0.00003-8>. URL: <http://www.sciencedirect.com/science/article/pii/B9780128042960000038>.
- [17] M. Manouchehrinejad et al. "Process simulation of an integrated biomass torrefaction and pelletization (iBTP) plant to produce solid biofuels". In: *Energy Conversion and Management: X* 1 (2019). ISSN: 2590-1745. DOI: <https://doi.org/10.1016/j.ecmx.2019.100008>. URL: <http://www.sciencedirect.com/science/article/pii/S2590174519300066>.
- [18] L. Chai et al. "Comparing pelletization and torrefaction depots: Optimization of depot capacity and biomass moisture to determine the minimum production cost". In: *Applied Energy* 163 (2016), pp. 387 –395. ISSN: 0306-2619. DOI: <https://doi.org/10.1016/j.apenergy.2015.11.018>. URL: <http://www.sciencedirect.com/science/article/pii/S0306261915014592>.
- [19] L. E. Arteaga-Pérez et al. "Torrefaction of Pinus radiata and Eucalyptus globulus: A combined experimental and modeling approach to process synthesis". In: *Energy for Sustainable Development* 29 (2015), pp. 13 –23. ISSN: 0973-0826. DOI: <https://doi.org/10.1016/j.esd.2015.08.004>. URL: <http://www.sciencedirect.com/science/article/pii/S0973082615000824>.
- [20] R.S. Cherry et al. *Analysis of the Production Cost for Various Grades of Biomass Thermal Treatment*. Tech. rep. Idaho National Lab.(INL), Idaho Falls, ID (United States), 2013.
- [21] N. Nikolopoulos et al. "Modeling of Wheat Straw Torrefaction as a Preliminary Tool for Process Design". In: *Waste Biomass Valor* 4 (Sept. 2013), pp. 409–420. DOI: 10.1007/s12649-013-9198-y.
- [22] J.S. Tumuluru et al. "GC Analysis of Volatiles and Other Products from Biomass Torrefaction Process". In: Mar. 2012. ISBN: 978-953-51-0298-4. DOI: 10.5772/33488.
- [23] S. Rehman et al. "Xylitol: A Review on Bioproduction, Application, Health Benefits, and Related Safety Issues". In: *Critical reviews in food science and nutrition* 55 (Oct. 2013). DOI: 10.1080/10408398.2012.702288.
- [24] H. Liu. "5 - Biomass fuels for small and micro combined heat and power (CHP) systems: resources, conversion and applications". In: *Small and Micro Combined Heat and Power (CHP) Systems*. Ed. by Robert Beith. Woodhead Publishing Series in Energy. Woodhead Publishing, 2011, pp. 88 –122. ISBN: 978-1-84569-795-2. DOI: <https://doi.org/10.1533/9780857092755>.

- 1.88. URL: <http://www.sciencedirect.com/science/article/pii/B9781845697952500052>.
- [25] M.M. Mariano. “Chapter 8 - Biomass”. In: *Industrial Chemical Process Analysis and Design*. Ed. by M.M. Mariano. Boston: Elsevier, 2016, pp. 405–447. ISBN: 978-0-08-101093-8. DOI: <https://doi.org/10.1016/B978-0-08-101093-8.00022-7>. URL: <http://www.sciencedirect.com/science/article/pii/B9780081010938000227>.
- [26] P. Brachi et al. “Valorization of Sugar Beet Pulp via Torrefaction with a Focus on the Effect of the Preliminary Extraction of Pectins”. In: *Energy & Fuels* 31.9 (2017), pp. 9595–9604. DOI: 10.1021/acs.energyfuels.7b01766. eprint: <https://doi.org/10.1021/acs.energyfuels.7b01766>. URL: <https://doi.org/10.1021/acs.energyfuels.7b01766>.
- [27] J. Poudel et al. “Effect of Torrefaction on the Properties of Corn Stalk to Enhance Solid Fuel Qualities”. In: *Energies* 7 (Sept. 2014), pp. 5586–5600. DOI: 10.3390/en7095586.
- [28] M. Kanit. “Inert torrefaction of sugarcane bagasse to improve its fuel properties”. In: *Case Studies in Thermal Engineering* 19 (2020), p. 100623. ISSN: 2214-157X. DOI: <https://doi.org/10.1016/j.csite.2020.100623>. URL: <http://www.sciencedirect.com/science/article/pii/S2214157X19305118>.
- [29] B. Tofanica et al. “Properties of Rapeseed (*Brassica napus*) Stalks Fibers”. In: *Journal of Natural Fibers* 8 (Oct. 2011), pp. 241–262. DOI: 10.1080/15440478.2011.626189.
- [30] E. Bilgic et al. “Limits of variations on the structure and the fuel characteristics of sunflower seed shell through torrefaction”. In: *Fuel Processing Technology* 144 (2016), pp. 197–202. ISSN: 0378-3820. DOI: <https://doi.org/10.1016/j.fuproc.2016.01.006>. URL: <http://www.sciencedirect.com/science/article/pii/S0378382016300066>.
- [31] L.J.R. Nunes et al., eds. *Torrefaction of Biomass for Energy Applications*.
- [32] A. Özyuğuran et al. “Prediction of Calorific Value of Biomass from Proximate Analysis”. In: *Energy Procedia* 107 (Feb. 2017), pp. 130–136. DOI: 10.1016/j.egypro.2016.12.149.
- [33] D. Medic et al. “The Effects of Particle Size, Different Corn Stover Components, and Gas Residence Time on Torrefaction of Corn Stover”. In: *Energies* 5 (Dec. 2012). DOI: 10.3390/en5041199.

- [34] J.S. Tumuluru et al. "Proximate and Ultimate Compositional Changes in Corn Stover during Torrefaction using Thermogravimetric Analyzer and Microwaves". In: *American Society of Agricultural and Biological Engineers Annual International Meeting 2012, ASABE 2012 2* (July 2012). DOI: 10.13031/2013.41777.
- [35] A. Anukam et al. "Blending Influence on the Conversion Efficiency of the Cogasification Process of Corn Stover and Coal". In: *Journal of Chemistry* 2016 (July 2016). DOI: <https://doi.org/10.1155/2016/3910986>.
- [36] A. Demirbaş. "Calculation of higher heating values of biomass fuels". In: *Fuel* 76.5 (1997), pp. 431 –434. ISSN: 0016-2361. DOI: [https://doi.org/10.1016/S0016-2361\(97\)85520-2](https://doi.org/10.1016/S0016-2361(97)85520-2). URL: <http://www.sciencedirect.com/science/article/pii/S0016236197855202>.
- [37] B. Biswas et al. "Pyrolysis of agricultural biomass residues: Comparative study of corn cob, wheat straw, rice straw and rice husk". In: *Bioresource Technology* 237 (Feb. 2017). DOI: 10.1016/j.biortech.2017.02.046.
- [38] Akinwale O.A. et al. "Non-isothermal kinetic analysis of the devolatilization of corn cobs and sugar cane bagasse in an inert atmosphere". In: *Thermochimica Acta* 517.1 (2011), pp. 81 –89. ISSN: 0040-6031. DOI: <https://doi.org/10.1016/j.tca.2011.01.035>. URL: <http://www.sciencedirect.com/science/article/pii/S0040603111000670>.
- [39] J. Rajeev et al. "Sugarcane leaf-bagasse gasifiers for industrial heating applications". In: *Biomass and Bioenergy* 13.3 (1997), pp. 141 –146. ISSN: 0961-9534. DOI: [https://doi.org/10.1016/S0961-9534\(97\)00014-7](https://doi.org/10.1016/S0961-9534(97)00014-7). URL: <http://www.sciencedirect.com/science/article/pii/S0961953497000147>.
- [40] M.G.Pérez et al. "Vacuum pyrolysis of sugarcane bagasse". In: *Journal of Analytical and Applied Pyrolysis* 65.2 (2002), pp. 111 –136. ISSN: 0165-2370. DOI: [https://doi.org/10.1016/S0165-2370\(01\)00184-X](https://doi.org/10.1016/S0165-2370(01)00184-X). URL: <http://www.sciencedirect.com/science/article/pii/S016523700100184X>.
- [41] M Garcia-Pérez et al. "Co-pyrolysis of sugarcane bagasse with petroleum residue. Part I: thermogravimetric analysis". In: *Fuel* 80.9 (2001), pp. 1245 –1258. ISSN: 0016-2361. DOI: [https://doi.org/10.1016/S0016-2361\(00\)00215-5](https://doi.org/10.1016/S0016-2361(00)00215-5). URL: <http://www.sciencedirect.com/science/article/pii/S0016236100002155>.
- [42] L. Cuiping et al. "Chemical elemental characteristics of biomass fuels in China". In: *Biomass Bioenergy - BIOMASS BIOENERG* 27 (Aug. 2004), pp. 119–130. DOI: 10.1016/j.biombioe.2004.01.002.

- [43] E.T. Filiz Karaosmanoglu. “Charcoal from the Pyrolysis of Rapeseed Plant Straw-Stalk”. In: *Energy Sources* 21.6 (1999), pp. 503–510. DOI: 10.1080/00908319950014632. eprint: <https://doi.org/10.1080/0090831995001463>. URL: <https://doi.org/10.1080/0090831995001463>.
- [44] ECN. <https://phyllis.nl/Browse/Standard/ECN-Phyllis#543>.
- [45] P.S. Li et al. “Combustion reaction mechanism of four typical Chinese biomass by TG and DTG”. In: *Asia-Pacific Journal of Chemical Engineering* 7 (July 2012). DOI: 10.1002/apj.616.
- [46] A. Figen et al. “Devolatilization non-isothermal kinetic analysis of agricultural stalks and application of TG-FT/IR analysis”. In: *Journal of Thermal Analysis and Calorimetry* 107 (Mar. 2012). DOI: 10.1007/s10973-011-1959-x.
- [47] T. Rizvi et al. “Prediction of biomass ash fusion behaviour by the use of detailed characterisation methods coupled with thermodynamic analysis”. In: *Fuel* 141 (Oct. 2014). DOI: 10.1016/j.fuel.2014.10.021.
- [48] S. Karnjanakom et al. “Catalytic steam reforming of tar derived from steam gasification of sunflower stalk over ethylene glycol assisting prepared Ni/MCM-41”. In: *Energy Conversion and Management* 98 (July 2015). DOI: 10.1016/j.enconman.2015.04.007.
- [49] K. Sirisomboon et al. “Effects of air staging on emission characteristics in a conical fluidized-bed combustor firing with sunflower shells”. In: *Journal of the Energy Institute* 90 (Dec. 2015). DOI: 10.1016/j.joei.2015.12.001.
- [50] A. Zabaniotou et al. “Sunflower shells utilization for energetic purposes in an integrated approach of energy crops: Laboratory study pyrolysis and kinetics”. In: *Bioresource technology* 99 (June 2008), pp. 3174–81. DOI: 10.1016/j.biortech.2007.05.060.
- [51] ECN. <https://phyllis.nl/Biomass/View/878>. Accessed: 26-05-2020.
- [52] M. Yilgin et al. “Co-pyrolysis of lignite and sugar beet pulp”. In: *Energy Conversion and Management* 51 (May 2010), pp. 1060–1064. DOI: 10.1016/j.enconman.2009.12.010.
- [53] X. Liu et al. “Oxygen enriched co-combustion characteristics of herbaceous biomass and bituminous coal”. In: *Thermochimica Acta* 569 (Oct. 2013), pp. 17–24. DOI: 10.1016/j.tca.2013.06.037.
- [54] M. Akram et al. “Co-firing of pressed sugar beet pulp with coal in a laboratory-scale fluidised bed combustor”. In: *Applied Energy* 139 (Nov. 2014). DOI: 10.1016/j.apenergy.2014.11.008.

- [55] P. Basu. “Chapter 3 - Pyrolysis and Torrefaction”. In: *Biomass Gasification and Pyrolysis*. Ed. by P. Basu. Boston: Academic Press, 2010, pp. 65 –96. ISBN: 978-0-12-374988-8. DOI: <https://doi.org/10.1016/B978-0-12-374988-8.00003-9>. URL: <http://www.sciencedirect.com/science/article/pii/B9780123749888000039>.
- [56] K. Deepchand. “Commercial scale cogeneration of bagasse energy in Mauritius”. In: *Energy for Sustainable Development* 5.1 (2001), pp. 15 –22. ISSN: 0973-0826. DOI: [https://doi.org/10.1016/S0973-0826\(09\)60016-8](https://doi.org/10.1016/S0973-0826(09)60016-8). URL: <http://www.sciencedirect.com/science/article/pii/S0973082609600168>.
- [57] *Fuels - Higher and Lower Calorific Values*. https://www.engineeringtoolbox.com/fuels-higher-calorific-values-d_169.html. Accessed: 17-03-2020.
- [58] A. Visconti et al. “Equilibrium-based simulation of lignocellulosic biomass pyrolysis via Aspen Plus”. In: *Recent Advances in Applied Mathematics, Modelling and Simulation: Proceedings of the 8th International Conference on Applied Mathematics, Simulation, Modelling: November*. 2014, pp. 22–24.
- [59] S. Dhanushkodi et al. “Mathematical modeling of drying behavior of cashew in a solar biomass hybrid dryer”. In: *Resource-Efficient Technologies* 3.4 (2017), pp. 359 –364. ISSN: 2405-6537. DOI: <https://doi.org/10.1016/j.reffit.2016.12.002>. URL: <http://www.sciencedirect.com/science/article/pii/S2405653716302275>.
- [60] M. Hakkı et al. “Liquefaction Processes of Biomass for the Production of Valuable Chemicals and Biofuels: A Review”. In: June 2013.
- [61] JS Tumuluru et al. *A review on biomass torrefaction process and product properties for energy applications. Ind Biotechnol*. 2011.
- [62] W.H. Chen et al. “A state-of-the-art review of biomass torrefaction, densification and applications”. In: *Renewable and Sustainable Energy Reviews* 44 (2015), pp. 847–866.
- [63] M. J. Prins et al. “Torrefaction of wood: Part 1. Weight loss kinetics”. In: *Journal of Analytical and Applied Pyrolysis* 77.1 (2006), pp. 28 –34. ISSN: 0165-2370. DOI: <https://doi.org/10.1016/j.jaap.2006.01.002>. URL: <http://www.sciencedirect.com/science/article/pii/S0165237006000179>.
- [64] P. Basu et al. “Effect of torrefaction on the density and volume changes of coarse biomass particles”. In: *The Canadian Journal of Chemical Engineering* 91 (June 2013). DOI: 10.1002/cjce.21817.

- [65] J. H. Peng et al. “A Study of Particle Size Effect on Biomass Torrefaction and Densification”. In: *Energy & Fuels* 26.6 (2012), pp. 3826–3839. DOI: 10.1021/ef3004027. eprint: <https://doi.org/10.1021/ef3004027>. URL: <https://doi.org/10.1021/ef3004027>.
- [66] P. Basu et al. “An investigation into the effect of biomass particle size on its torrefaction”. In: *The Canadian Journal of Chemical Engineering* 91 (Mar. 2013). DOI: 10.1002/cjce.21710.
- [67] B. Batidzirai et al. “Biomass torrefaction technology: Techno-economic status and future prospects”. In: *Energy* 62 (2013), pp. 196 –214. ISSN: 0360-5442. DOI: <https://doi.org/10.1016/j.energy.2013.09.035>. URL: <http://www.sciencedirect.com/science/article/pii/S036054421300786X>.
- [68] J.S. Tumuluru et al. “Torrefaction Process and Desing of Moving Bed Reactor”. In: May 2011.
- [69] D.A. Granados et al. “Biomass Torrefaction in a Two-Stage Rotary Reactor: Modeling and Experimental Validation”. In: *Energy Fuels* 31 (Apr. 2017). DOI: 10.1021/acs.energyfuels.7b00653.
- [70] J. Koppeman et al. *Status overview of torrefaction technologies*. Tech. rep. IEA Bioenergy, 2015.
- [71] M. Svanberg et al. “Analysing biomass torrefaction supply chain costs”. In: *Bioresource Technology* 142 (2013), pp. 287 –296. ISSN: 0960-8524. DOI: <https://doi.org/10.1016/j.biortech.2013.05.048>. URL: <http://www.sciencedirect.com/science/article/pii/S0960852413008080>.
- [72] M. Mobini et al. “Assessing the integration of torrefaction into wood pellet production”. In: *Journal of Cleaner Production* 78 (2014), pp. 216 –225. ISSN: 0959-6526. DOI: <https://doi.org/10.1016/j.jclepro.2014.04.071>. URL: <http://www.sciencedirect.com/science/article/pii/S095965261400434X>.
- [73] A. Uslu et al. “Pre-treatment technologies, and their effect on international bioenergy supply chain logistics. Techno-economic evaluation of torrefaction, fast pyrolysis and pelletisation”. In: *Energy* 33.8 (2008), pp. 1206 –1223. ISSN: 0360-5442. DOI: <https://doi.org/10.1016/j.energy.2008.03.007>. URL: <http://www.sciencedirect.com/science/article/pii/S0360544208000893>.

- [74] B. Batidzirai et al. "Biomass torrefaction technology: Techno-economic status and future prospects". In: *Energy* 62 (2013), pp. 196 –214. ISSN: 0360-5442. DOI: <https://doi.org/10.1016/j.energy.2013.09.035>. URL: <http://www.sciencedirect.com/science/article/pii/S036054421300786X>.
- [75] C. Di Blasi et al. "Intrinsic kinetics of isothermal xylan degradation in inert atmosphere". In: *Journal of Analytical and Applied Pyrolysis* 40-41 (1997). PYROLYSIS '96, pp. 287 –303. ISSN: 0165-2370. DOI: [https://doi.org/10.1016/S0165-2370\(97\)00028-4](https://doi.org/10.1016/S0165-2370(97)00028-4). URL: <http://www.sciencedirect.com/science/article/pii/S0165237097000284>.
- [76] Q.V. Bach et al. "Process modeling and optimization for torrefaction of forest residues". In: *Energy* 138 (2017), pp. 348 –354. ISSN: 0360-5442. DOI: <https://doi.org/10.1016/j.energy.2017.07.040>. URL: <http://www.sciencedirect.com/science/article/pii/S036054421731215X>.
- [77] D. Neves et al. "Characterization and prediction of biomass pyrolysis products". In: *Progress in Energy and Combustion Science* 37.5 (2011), pp. 611 –630. ISSN: 0360-1285. DOI: <https://doi.org/10.1016/j.pecs.2011.01.001>. URL: <http://www.sciencedirect.com/science/article/pii/S0360128511000025>.
- [78] E. Ranzi et al. "Chemical Kinetics of Biomass Pyrolysis". In: *Energy Fuels* 22 (Jan. 2009), pp. 4292–4300. DOI: 10.1021/ef800551t.
- [79] R. Dudgeon. "An aspen plus model of biomass torrefaction". In: *University Turbine Systems Research (UTSR) Fellowship* (2009).
- [80] T Haryadi et al. "The AspenTM Software Simulation of a Peat Torrefaction System Using RYield and SSplit Block as Reactor Model". In: *The international symposium on sustainable energy and environmental protection (ISSEEP), Yogyakarta, Indonesia*. 2009.
- [81] N. Nikolopoulos et al. "Modeling of Wheat Straw Torrefaction as a Preliminary Tool for Process Design". In: *Waste Biomass Valor* 4 (Sept. 2013), pp. 409–420. DOI: 10.1007/s12649-013-9198-y.
- [82] M. M. Hossain et al. "Chemical-looping combustion (CLC) for inherent CO₂ separations—a review". In: *Chemical Engineering Science* 63.18 (2008), pp. 4433 –4451. ISSN: 0009-2509. DOI: <https://doi.org/10.1016/j.ces.2008.05.028>. URL: <http://www.sciencedirect.com/science/article/pii/S0009250908002947>.

- [83] J. Adanez et al. "Progress in Chemical-Looping Combustion and Reforming technologies". In: *Progress in Energy and Combustion Science* 38.2 (2012), pp. 215–282. ISSN: 0360-1285. DOI: <https://doi.org/10.1016/j.pecs.2011.09.001>. URL: <http://www.sciencedirect.com/science/article/pii/S0360128511000505>.
- [84] Z. Sarshar et al. "Novel oxygen carriers for chemical looping combustion: $\text{La}_{1-x}\text{Ce}_x\text{BO}_3$ ($B = \text{Co}, \text{Mn}$) perovskites synthesized by reactive grinding and nanocasting". In: *Energy Environ. Sci.* 4 (Sept. 2011), pp. 4258–4269. DOI: 10.1039/C1EE01716K.
- [85] P. Gupta et al. "Syngas Redox (SGR) Process to Produce Hydrogen from Coal Derived Syngas". In: *Energy & Fuels* 21.5 (2007), pp. 2900–2908. DOI: 10.1021/ef060512k. eprint: <https://doi.org/10.1021/ef060512k>. URL: <https://doi.org/10.1021/ef060512k>.
- [86] F. Li et al. "Syngas Chemical Looping Gasification Process: Oxygen Carrier Particle Selection and Performance". In: *Energy & Fuels* 23.8 (2009), pp. 4182–4189. DOI: 10.1021/ef900236x. eprint: <https://doi.org/10.1021/ef900236x>. URL: <https://doi.org/10.1021/ef900236x>.
- [87] K.S. Kang et al. "Oxygen-carrier selection and thermal analysis of the chemical-looping process for hydrogen production". In: *International Journal of Hydrogen Energy* 35.22 (2010). Bio-Ethanol and Other Renewable Sources and Reforming Process for Sustainable Hydrogen Production, pp. 12246–12254. ISSN: 0360-3199. DOI: <https://doi.org/10.1016/j.ijhydene.2010.08.043>. URL: <http://www.sciencedirect.com/science/article/pii/S0360319910016824>.
- [88] M. Johansson et al. "Comparison of oxygen carriers for chemical-looping combustion". In: *Thermal Science - THERM SCI* 10 (Jan. 2006), pp. 93–107. DOI: 10.2298/TSCI0603093J.
- [89] P. Gayán et al. "Evaluation of the oxygen carrier particle lifetime in a Chemical Looping Combustion process". In: June 2015.
- [90] F. Bimbela et al. "Hydrogen production by catalytic steam reforming of acetic acid, a model compound of biomass pyrolysis liquids". In: *Journal of Analytical and Applied Pyrolysis* 79.1 (2007). PYROLYSIS 2006: Papers presented at the 17th International Symposium on Analytical and Applied Pyrolysis, Budapest, Hungary, 22-26 May 2006, pp. 112–120. ISSN: 0165-2370. DOI: <https://doi.org/10.1016/j.jaap.2006.11.006>. URL: <http://www.sciencedirect.com/science/article/pii/S0165237006001562>.

- [91] L. Heng et al. “Hydrogen production from heavy fraction of bio-oil using iron-based chemical looping process: Thermodynamic simulation and performance analysis”. In: *International Journal of Hydrogen Energy* 41.40 (2016), pp. 17771 –17783. ISSN: 0360-3199. DOI: <https://doi.org/10.1016/j.ijhydene.2016.07.068>. URL: <http://www.sciencedirect.com/science/article/pii/S0360319916320559>.
- [92] K. Deshpande et al. “Process Simulation of Chemical Looping Combustion for a Mixture of Biomass”. In: *Biomass Valorization to Bioenergy* (2019), p. 177.
- [93] *Boudouard reaction*. <http://www.crct.polymtl.ca/reacweb.htm>. Accessed: 16-1-2020.
- [94] C.R. Müller et al. “The production of separate streams of pure hydrogen and carbon dioxide from coal via an iron-oxide redox cycle”. In: *Chemical Engineering Journal* 166.3 (2011), pp. 1052 –1060. ISSN: 1385-8947. DOI: <https://doi.org/10.1016/j.cej.2010.11.067>. URL: <http://www.sciencedirect.com/science/article/pii/S1385894710011630>.
- [95] P.C. Kuo et al. “Hydrogen production from biomass using iron-based chemical looping technology: Validation, optimization, and efficiency”. In: *Chemical Engineering Journal* 337 (2018), pp. 405 –415. ISSN: 1385-8947. DOI: <https://doi.org/10.1016/j.cej.2017.12.121>. URL: <http://www.sciencedirect.com/science/article/pii/S1385894717322441>.
- [96] R. Zacharias et al. “High-pressure hydrogen production with inherent sequestration of a pure carbon dioxide stream via fixed bed chemical looping”. In: *International Journal of Hydrogen Energy* 44.16 (2019), pp. 7943 –7957. ISSN: 0360-3199. DOI: <https://doi.org/10.1016/j.ijhydene.2019.01.257>. URL: <http://www.sciencedirect.com/science/article/pii/S0360319919304410>.
- [97] *Write-up Brazil for GYGA*. <http://www.yieldgap.org/brazil>. Accessed: 17-03-2020.
- [98] E.M.W. Smeets et al. “Sustainability of Brazilian Bioethanol”. In: (Jan. 2006).
- [99] *Curitiba Climate*. <https://en.climate-data.org/south-america/brazil/parana/curitiba-2010/>. Accessed: 17-03-2020.
- [100] *Average Humidity In Curitiba (Parana)*. <https://weather-and-climate.com/average-monthly-Humidity-perc,curitiba,Brazil>. Accessed: 17-03-2020.

- [101] I. Bonner et al. "Impact of Sequential Ammonia Fiber Expansion (AFEX) Pretreatment and Pelletization on the Moisture Sorption Properties of Corn Stover". In: *Drying Technology* 33 (Sept. 2015), pp. 1768–1778. DOI: 10.1080/07373937.2015.1039127.
- [102] K.G. Ewsuk. "Powder Granulation and Compaction". In: *Encyclopedia of Materials: Science and Technology*. Ed. by K.H. Jürgen Buschow et al. Oxford: Elsevier, 2001, pp. 7788 –7800. ISBN: 978-0-08-043152-9. DOI: <https://doi.org/10.1016/B0-08-043152-6/01401-7>. URL: <http://www.sciencedirect.com/science/article/pii/B0080431526014017>.
- [103] Z. Berk. "Chapter 22 - Dehydration". In: *Food Process Engineering and Technology*. Ed. by Z.Berk. Food Science and Technology. San Diego: Academic Press, 2009, pp. 459 –510. ISBN: 978-0-12-373660-4. DOI: <https://doi.org/10.1016/B978-0-12-373660-4.00022-3>. URL: <http://www.sciencedirect.com/science/article/pii/B9780123736604000223>.
- [104] A. Lakshmanan et al. *Modeling Solids Dryers and Granulators with Aspen Plus V8*. https://www.aspentech.com/email/email_archive/modeling_solids_dryers_granulators.pdf. Apr. 2013.
- [105] F. Scheufele et al. "Assessment of drying temperature of sugarcane bagasse on sorption of reactive blue 5G dye". In: *Fibers and Polymers* 16 (Aug. 2015), pp. 1646–1656. DOI: 10.1007/s12221-015-5087-2.
- [106] S. Sokhansanj et al. "Techno-economic analysis of using corn stover to supply heat and power to a corn ethanol plant – Part 1: Cost of feedstock supply logistics". In: *Biomass and Bioenergy* 34.1 (2010), pp. 75 –81. ISSN: 0961-9534. DOI: <https://doi.org/10.1016/j.biombioe.2009.10.001>. URL: <http://www.sciencedirect.com/science/article/pii/S0961953409002049>.
- [107] J. Costa et al. "Drying and Isotherms of Sugar Cane Bagasse". In: *Revista Engenharia na Agricultura - REVENG* 23 (Apr. 2015), pp. 128–142. DOI: 10.13083/1414-3984/reveng.v23n2p128-142.
- [108] C. Dupont et al. "Heat capacity measurements of various biomass types and pyrolysis residues". In: *Fuel* 1 (Jan. 2013). DOI: 10.1016/j.fuel.2013.07.086.
- [109] W.M. Deen. *Analysis of Transport Phenomena*. Topics in Chemical Engineering. OUP USA, 2012. ISBN: 9780199740253.
- [110] DW Green et al. *Perry's Chemical Engineers' Handbook*. Blacklick, USA: McGraw-Hill Professional Publishing, 2007.

- [111] X. Ren et al. "Evolution of Chlorine-Bearing Gases During Corn Straw Torrefaction at Different Temperatures". In: *Energy Fuels* 31 (Nov. 2017). DOI: 10.1021/acs.energyfuels.7b02540.
- [112] J.S. Tumuhuru. "Comparison of Chemical Composition and Energy Property of Torrefied Switchgrass and Corn Stover". In: *Frontiers in Energy Research* 3 (Nov. 2015). DOI: 10.3389/fenrg.2015.00046.
- [113] F. Marias et al. "Torrefaction of Corn Stover in a Macro- thermobalance: Influence of Operating Conditions". In: *Waste and Biomass Valorization* (Mar. 2013). DOI: 10.1007/s12649-013-9235-x.
- [114] S. Ren et al. "The integrated process of microwave torrefaction and pyrolysis of corn stover for biofuel production". In: *Journal of Analytical and Applied Pyrolysis* 108 (2014), pp. 248 –253. ISSN: 0165-2370. DOI: <https://doi.org/10.1016/j.jaap.2014.04.008>. URL: <http://www.sciencedirect.com/science/article/pii/S0165237014000849>.
- [115] A. Toptas et al. "Combustion behavior of different kinds of torrefied biomass and their blends with lignite". In: *Bioresource Technology* 177 (Dec. 2014), pp. 328–336. DOI: 10.1016/j.biortech.2014.11.072.
- [116] X. Wang et al. "Comparative study of wet and dry torrefaction of corn stalk and the effect on biomass pyrolysis polygeneration". In: *Bioresource Technology* 258 (Feb. 2018). DOI: 10.1016/j.biortech.2018.02.114.
- [117] D. Chen et al. "Restudy on torrefaction of corn stalk from the point of view of deoxygenation and decarbonization". In: *Journal of Analytical and Applied Pyrolysis* 135 (Sept. 2018). DOI: 10.1016/j.jaap.2018.09.015.
- [118] A. Conag et al. "Energy densification of sugarcane bagasse through torrefaction under minimized oxidative atmosphere". In: *Journal of Environmental Chemical Engineering* 5 (Oct. 2017). DOI: 10.1016/j.jece.2017.10.032.
- [119] D.A. Granados et al. "Study of Reactivity Reduction in Sugarcane Bagasse as consequence of a Torrefaction Process". In: *Energy* 139 (Aug. 2017). DOI: 10.1016/j.energy.2017.08.013.
- [120] D.A. Granados et al. "Energetic and exergetic evaluation of residual biomass in a torrefaction process". In: *Energy* 74 (Sept. 2014). DOI: 10.1016/j.energy.2014.05.046.
- [121] S. Kanwal et al. "Effect of torrefaction conditions on the physicochemical characterization of agricultural waste (sugarcane bagasse)". In: *Waste Management* 88 (Mar. 2019), pp. 280–290. DOI: 10.1016/j.wasman.2019.03.053.

- [122] S. Chaluvadi et al. “Effect of Torrefaction Prior to Biomass Size Reduction on Ethanol Production”. In: *Waste and Biomass Valorization* (June 2018). DOI: 10.1007/s12649-018-0389-4.
- [123] D.A. Iryani et al. “characterization and Production of Solid Biofuel from Sugarcane Bagasse by Hydrothermal Carbonization”. In: *Waste Biomass Valor* 8 (Mar. 2017). DOI: <https://doi.org/10.1007/s12649-017-9898-9>.
- [124] Y. Joshi et al. “Torrefaction: Mechanistic study of constituent transformations in herbaceous biomass”. In: *Journal of Analytical and Applied Pyrolysis* 115 (Sept. 2015), pp. 353–361. DOI: 10.1016/j.jaap.2015.08.014.
- [125] S. Diamond et al. “CVXPY: A Python-embedded modeling language for convex optimization”. In: *Journal of Machine Learning Research* 17.83 (2016), pp. 1–5.
- [126] A. Agrawal et al. “A rewriting system for convex optimization problems”. In: *Journal of Control and Decision* 5.1 (2018), pp. 42–60.
- [127] M. Valix et al. “Combustion of thermochemically torrefied sugar cane bagasse”. In: *Bioresource Technology* 223 (2017), pp. 202–209. ISSN: 0960-8524. DOI: <https://doi.org/10.1016/j.biortech.2016.10.053>. URL: <http://www.sciencedirect.com/science/article/pii/S0960852416314596>.
- [128] S. Rösnsch et al. “Calculation of heating values for the simulation of thermochemical conversion plants with Aspen”. In: 2012.
- [129] E. Peduzzi et al. “Biomass modelling: Estimating thermodynamic properties from the elemental composition”. In: *Fuel* 181 (Oct. 2016), pp. 207–217. DOI: 10.1016/j.fuel.2016.04.111.
- [130] M. Kumar. “An experimental study to evaluate the calorific values of bagasse after open sun drying”. In: *International Journal of Science, Engineering and Technology Research* 5 (6 2016).
- [131] D.R. Nhuchhen et al. “Investigation into overall heat transfer coefficient in indirectly heated rotary torrefier”. In: *International Journal of Heat and Mass Transfer* 102 (2016), pp. 64–76. ISSN: 0017-9310. DOI: <https://doi.org/10.1016/j.ijheatmasstransfer.2016.06.011>. URL: <http://www.sciencedirect.com/science/article/pii/S0017931016300357>.
- [132] D. Price et al. “1 - Introduction: polymer combustion, condensed phase pyrolysis and smoke formation”. In: *Fire Retardant Materials*. Ed. by A.R. Horrocks et al. Woodhead Publishing, 2001, pp. 1–30. ISBN: 978-1-85573-419-7. DOI: <https://doi.org/10.1533/9781855737464.1>. URL: <http://www.sciencedirect.com/science/article/pii/B9781855734197500056>.

- [133] C. Mashuga et al. "Derivation of Le Chatelier's mixing rule for flammable limits". In: *Process Safety Progress* 19 (Apr. 2004), pp. 112 –117. DOI: 10.1002/prs.680190212.
- [134] A. Nandy et al. "Present status and overview of Chemical Looping Combustion technology". In: *Renewable and Sustainable Energy Reviews* 59 (2016), pp. 597 –619. ISSN: 1364-0321. DOI: <https://doi.org/10.1016/j.rser.2016.01.003>. URL: <http://www.sciencedirect.com/science/article/pii/S1364032116000319>.
- [135] *Brazil's center-south ending sugar season earlier due to dry weather*. <https://www.nasdaq.com/articles/brazils-center-south-ending-sugar-season-earlier-due-to-dry-weather-2019-11-11>. Accessed: 17-03-2020.
- [136] *Brazil Month-By-Month Crop Cycle*. <http://soybeansandcorn.com/Brazil-Crop-Cycles>. Accessed: 17-03-2020.
- [137] S. Jenkins. *2019 chemical engineering plant costs index annual average*. <https://www.chemengonline.com/2019-chemical-engineering-plant-cost-index-annual-average>.
- [138] M. Worley. *Biomass drying technology update*. <http://www.tappi.org/content/events/11biopro/19.2worley.pdf>. 2011.
- [139] T.X. Do et al. "Techno-economic analysis of fry-drying and torrefaction plant for bio-solid fuel production". In: *Renewable Energy* 119 (2018), pp. 45 –53. ISSN: 0960-1481. DOI: <https://doi.org/10.1016/j.renene.2017.11.085>. URL: <http://www.sciencedirect.com/science/article/pii/S0960148117311862>.
- [140] O.V. Ogidiama et al. "Techno-economic evaluation of a chemical looping combustion plant with waste heat utilization". In: *Energy Procedia* 142 (2017). Proceedings of the 9th International Conference on Applied Energy, pp. 2990 –2995. ISSN: 1876-6102. DOI: <https://doi.org/10.1016/j.egypro.2017.12.371>. URL: <http://www.sciencedirect.com/science/article/pii/S1876610217361192>.
- [141] G. Thek et al. "Wood pellet production costs under Austrian and in comparison to Swedish framework conditions". In: *Biomass and Bioenergy* 27.6 (2004). Pellets 2002. The first world conference on pellets, pp. 671 –693. ISSN: 0961-9534. DOI: <https://doi.org/10.1016/j.biombioe.2003.07.007>. URL: <http://www.sciencedirect.com/science/article/pii/S0961953404001084>.

- [142] S. Mani et al. “Economics of producing fuel pellets from biomass”. In: *Applied engineering in agriculture* 22 (Aug. 2006), pp. 1–6. DOI: 10.13031/2013.20447.
- [143] J. R. Cooper. *Process Engineering Economics*. New York: Marcel Dekker, Inc, 2003.
- [144] W. Pippo et al. “Sugarcane energy use: Accounting of feedstock energy considering current agro-industrial trends and their feasibility”. In: *International Journal of Energy and Environmental Engineering* 4 (Jan. 2013). DOI: 10.1186/2251-6832-4-10.
- [145] CBS. *Aardgas en elektriciteit, gemiddelde prijzen van eindverbruikers*. <https://opendata.cbs.nl/statline/#/CBS/nl/dataset/81309NED/table?fromstatweb>. Accessed: 26-05-2020.
- [146] A.K. Olaleye et al. “Techno-economic analysis of chemical looping combustion with humid air turbine power cycle”. In: *Fuel* 124 (2014), pp. 221–231.
- [147] L.G. Velazquet-Vargas et al. “Techno-economic analysis of a 550 MWe atmospheric iron-based coal-direct chemical looping process”. In: *Proceeding of 3rd International Conference on Chemical Looping, Goteborg, Sweden*. 2014, pp. 9–11.
- [148] J. Jagerson. *What Is the Formula for Calculating Net Present Value (NPV)?* <https://www.investopedia.com/ask/answers/032615/what-formula-calculating-net-present-value-npv.asp>.
- [149] *Total energy consumption*. <https://yearbook.enerdata.net/total-energy/world-consumption-statistics.html>. Accessed: 26-05-2020.
- [150] *Mapped: The world’s coal power plants*. <https://www.carbonbrief.org/mapped-worlds-coal-power-plants>. Accessed: 26-05-2020.
- [151] A. Uslu et al. “Pre-treatment technologies, and their effect on international bioenergy supply chain logistics. Techno-economic evaluation of torrefaction, fast pyrolysis and pelletisation”. In: *Energy* 33.8 (2008), pp. 1206 – 1223. ISSN: 0360-5442. DOI: <https://doi.org/10.1016/j.energy.2008.03.007>. URL: <http://www.sciencedirect.com/science/article/pii/S0360544208000893>.
- [152] M. Beets. “A Torrefied Wood Pellet Supply Chain”. MA thesis. the Netherlands: Utrecht University, 2017.
- [153] P. Hitchin. *High-Efficiency, Low-Emissions Coal Plants: Come HELE or High Water*. <https://www.ge.com/power/transform/article.transform.articles.2018.mar.come-hele-or-high-water#>.

- [154] <https://www.inflationtool.com/euro>. Accessed: 26-05-2020.
- [155] .I. Radics et al. “Systematic review of torrefied wood economics”. In: *BioResources* 12.3 (2017), pp. 6868–6884.
- [156] F. Rosillo-Calle et al. *Industrial Uses of Biomass Energy: The Example of Brazil*. Taylor & Francis, 2000. ISBN: 9780203194034. URL: https://books.google.nl/books?id=Jc50_Guxk_AC.
- [157] P.H. May. *Natural Resource Valuation and Policy in Brazil*. Issues, Cases, and Methods in Biodiversity Conservation. Columbia University Press, 2000. ISBN: 9780231504669. URL: <https://books.google.nl/books?id=QuZ0HW1iojEC>.
- [158] *Residential wood pellets futures*. <https://live.euronext.com/en/product/commodities-futures/RWP-DPAR/contract-specification>. Accessed: 16-05-2020.
- [159] BEI. *Electricity generation costs*. 2016.
- [160] DOE. *Annual energy outlook 2015*. 2015.

Appendices

1.1 Coefficients V1 and V2

Table 1: Coefficients V1 SCB

Compound	a	b
CO2	0.00290682	0.32803559
CO	0.00047541	0.1392614
CH4	0.00055408	-0.00553267
H2	0.00055408	-0.00553266
Water	-0.00398395	0.35437072
Acetic acid	-0.00241662	0.20847517
Furane	0.00060896	-0.00608146
Phenol	0.00060216	-0.00601344
HMF	0.00069908	-0.00698266

Table 2: Coefficients V2 SCB

Compound	a	b
CO2	0.0135665	0.186011
CO	-0.00251369	0.150822
CH4	-4.6671e-09	2.80026e-07
H2	-4.66738e-09	2.80043e-07
Water	-0.00632358	0.379415
Acetic acid	-0.00472919	0.283752
Furane	-4.67634e-09	2.80581e-07
Phenol	-4.66765e-09	2.80059e-07
HMF	-4.6672e-09	2.80032e-07

Table 3: Coefficients V1 CS

Compound	a	b
CO_2	0.002949	0.07157
CO	0.000890	0.0588
CH_4	-0.000593	0.0619
C_2H_4	-0.000595	0.0620
C_2H_6	-0.000593	0.0619
Water	0.001246	0.298
Acetic Acid	-0.00132	0.128
Acetol	-0.000569	0.0680
Methanol	-0.000713	0.0680
Formaldehyde	-0.000119	0.0595
Formic Acid	-0.000587	0.0622

Table 4: Coefficients V2 CS

Compound	a	b
CO_2	-0.0101	0.586
CO	-0.001311	0.0596
CH_4	0.000108	0.0318
C_2H_4	0.00177	0.0170
$\%C_2H_6$	0.000108	0.0318
Water	-0.000109	0.0494
Acetic Acid	-0.00244	0.251
Acetol	-0.00133	0.0604
Methanol	0.00257	0.000257
Formaldehyde	-0.00135	0.0622
Formic Acid	0.0111	-0.150

1.2 PFD configurations

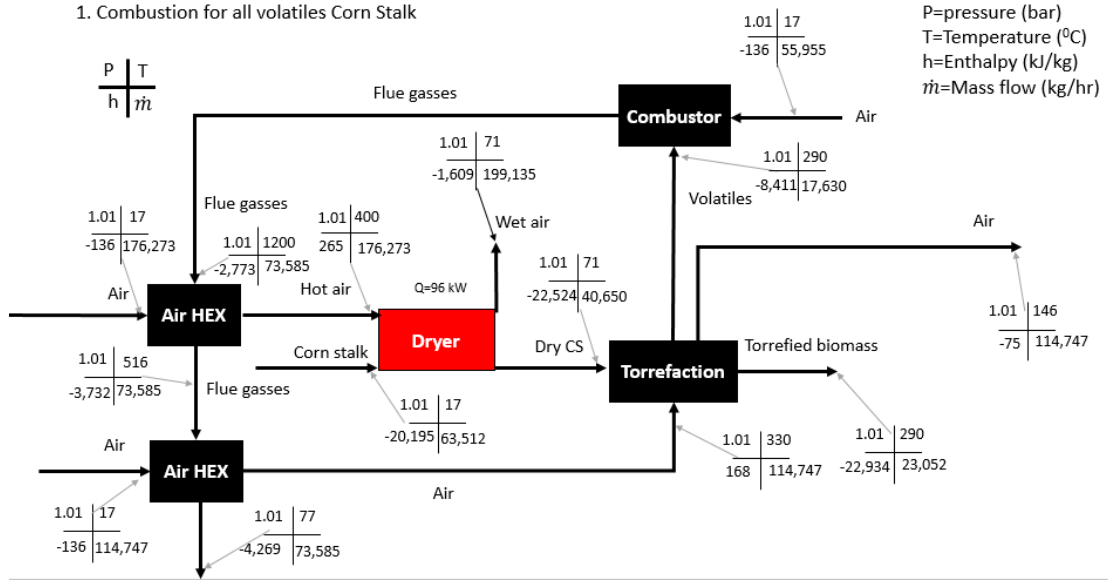


Figure 1: PFD configuration 1

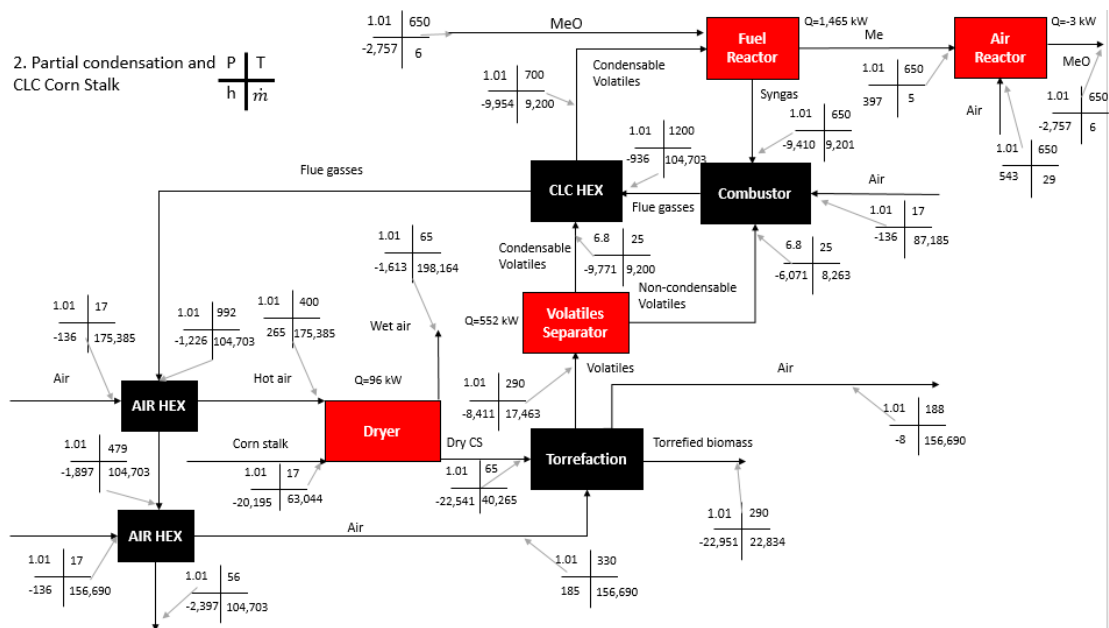


Figure 2: PFD configuration 2

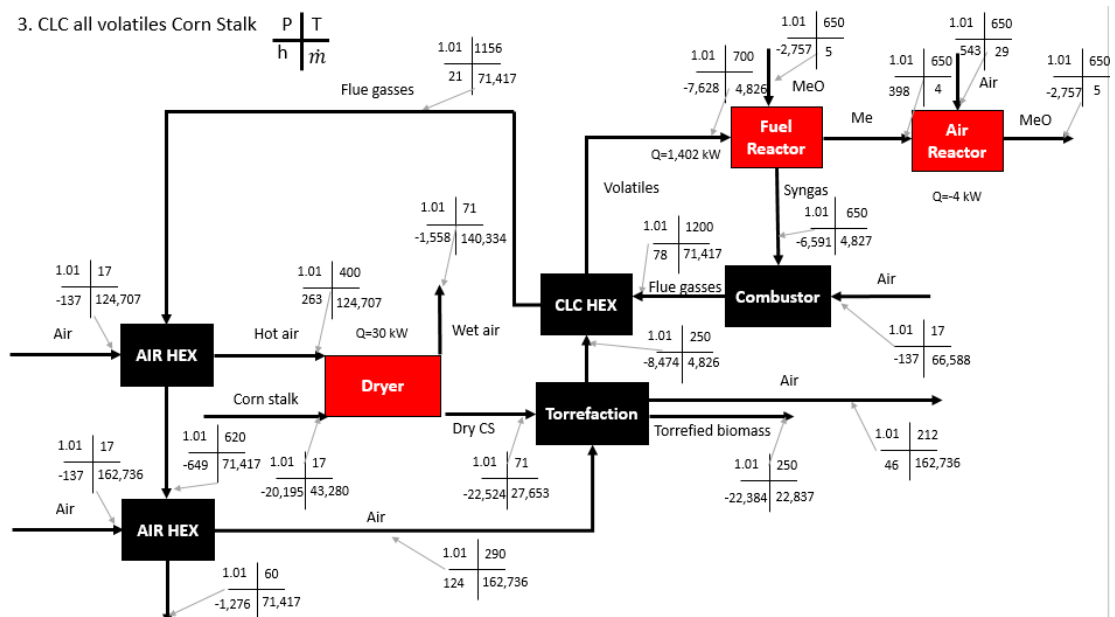


Figure 3: PFD configuration 3

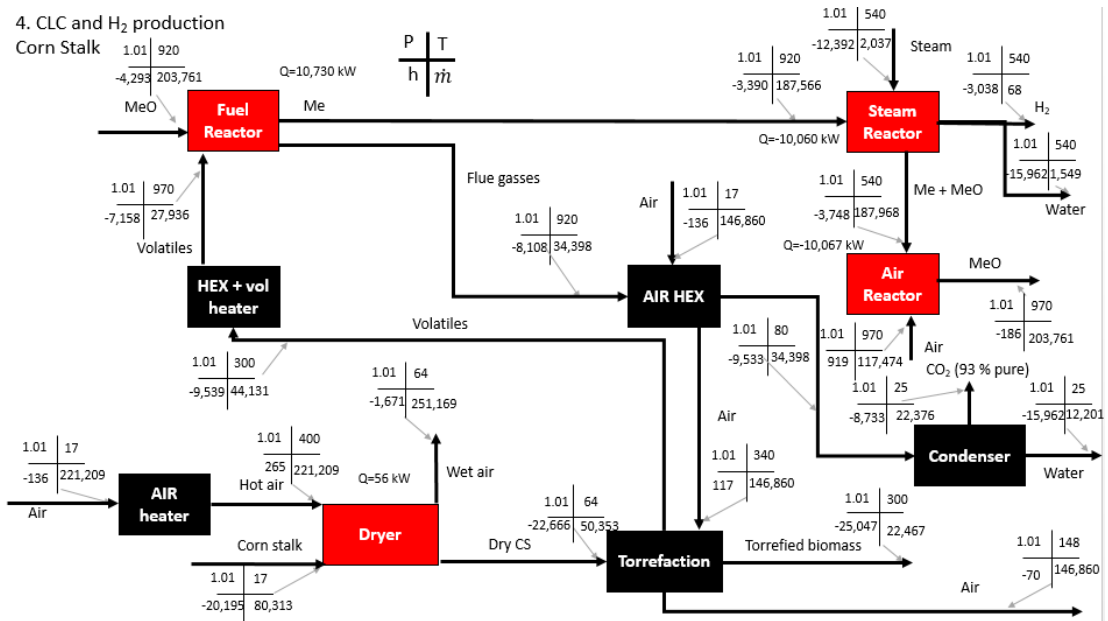


Figure 4: PFD configuration 4

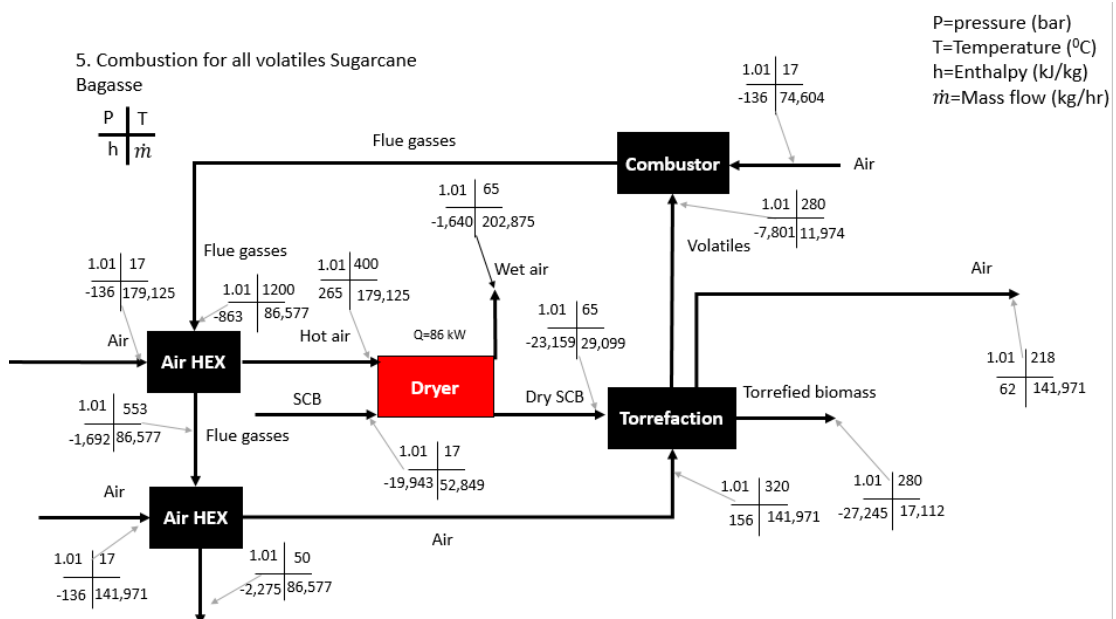


Figure 5: PFD configuration 5

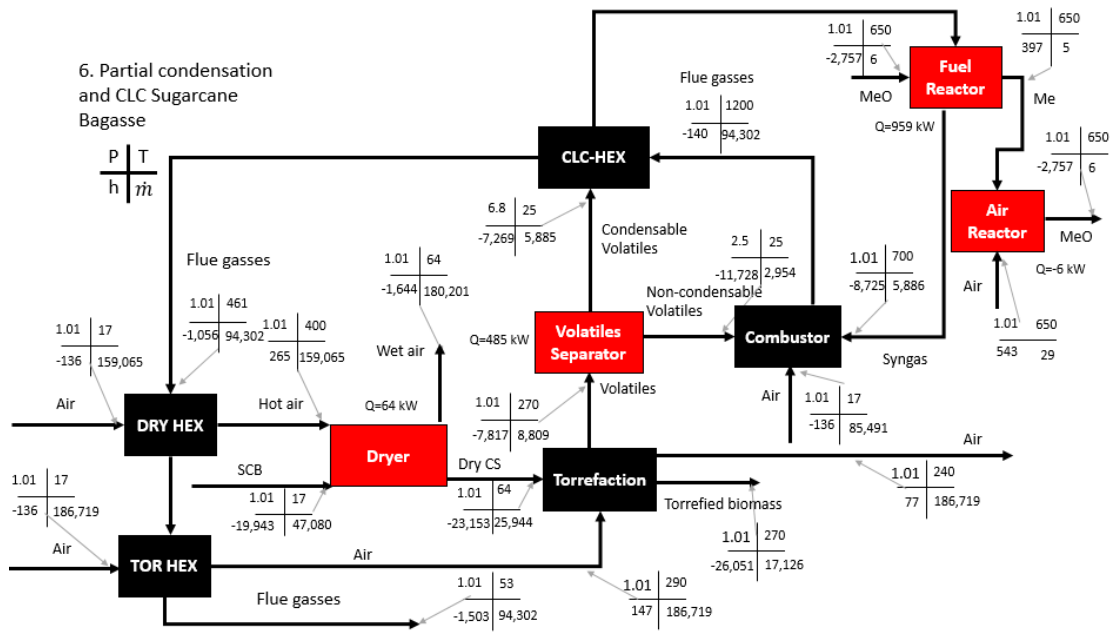


Figure 6: PFD configuration 6

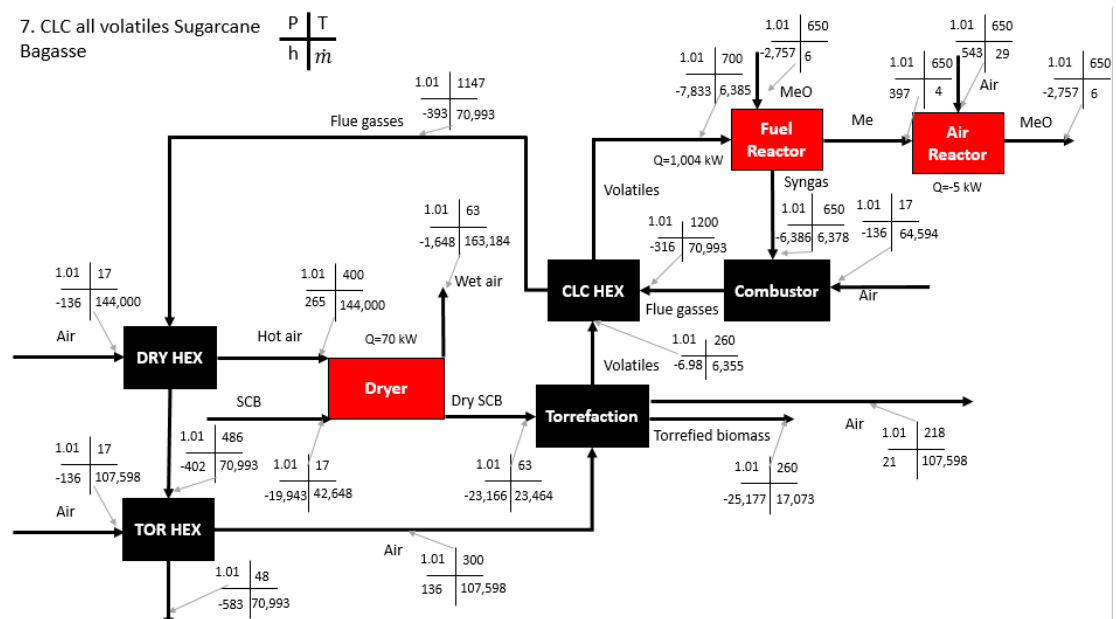


Figure 7: PFD configuration 7

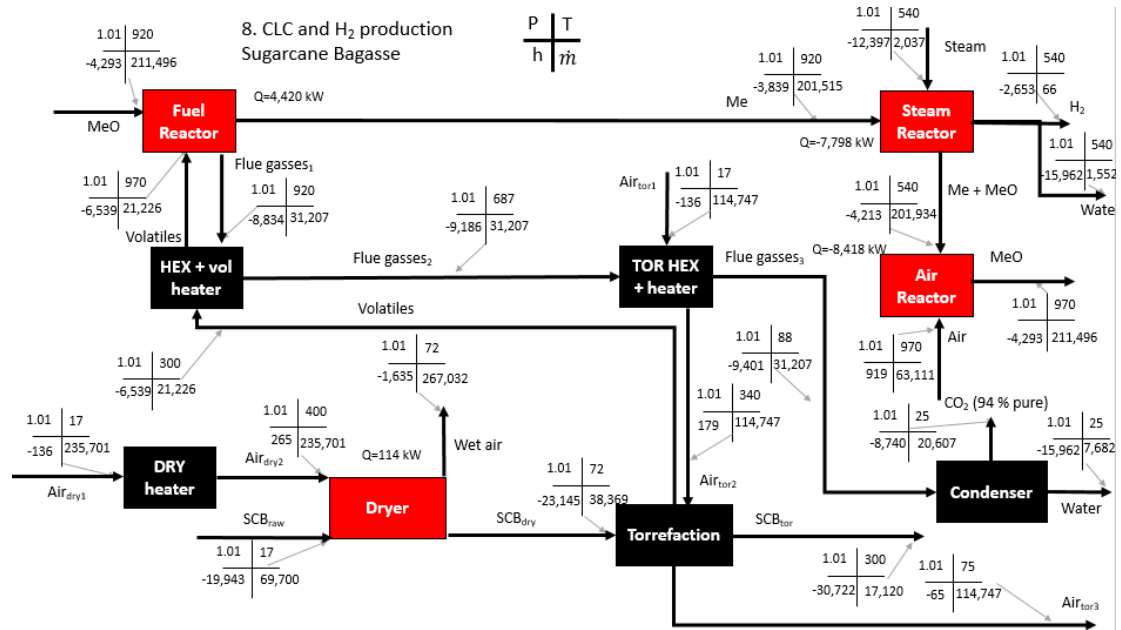


Figure 8: PFD configuration 8

1.3 Economics

Table 5: Equipment costs

Configuration	Dryer (M€)	Torrefaction reactor (M€)	CLC reactor (M€)	Pelletizer (M€)	Other (M€)
Total (M€)					
CS_{comb}	4.6	5.6	-	2.6	0.6
$CS_{comb+clc}$	4.6	5.5	0.7	2.6	1.9
CS_{clc}	3.4	4.3	0.4	2.6	0.9
CS_{H_2}	5.4	6.5	3.8	2.6	1.7
SCB_{comb}	4	4.4	-	2.1	0.7
$SCB_{comb+clc}$	3.7	4.1	0.2	2.1	1.8
SCB_{clc}	3.5	3.8	0.6	2.1	1.2
SCB_{H_2}	4.8	5.3	2.9	2.1	1.7

Table 6: CAPEX

Configuration	Equipment (M€)	Installed (M€)	I&C (M€)	Piping (M€)	B&S (M€)	Total physical (M€)	E&C (M€)	Contingencies (M€)	Total CAPEX (M€)
CS_{comb}	13.4	19.2	4.8	11.5	3.8	39.3	13.7	5.9	58.9
$CS_{comb+clc}$	15.3	21.9	5.5	13.1	4.4	44.9	15.7	6.7	67.4
CS_{clc}	11.7	16.7	4.2	10.0	3.3	34.2	12.0	5.1	51.3
CS_{H_2}	20.0	28.6	7.1	17.1	5.7	58.6	20.5	8.8	87.9
SCB_{comb}	11.2	16.1	4.0	9.6	3.2	32.9	11.5	4.9	49.4
$SCB_{comb+clc}$	11.9	17.0	4.3	10.2	3.4	34.9	12.2	5.2	52.4
SCB_{clc}	11.2	16.0	4.0	9.6	3.2	32.7	11.5	4.9	49.1
SCB_{H_2}	16.8	24.1	6.0	14.4	4.8	49.3	17.3	7.4	74.0

Table 7: OPEX

Configuration	Raw material (M€/yr)	Utilities (M€/yr)	Maintenance (M€/yr)	Labor (M€/yr)	Supervision (M€/yr)	Operational supplies (M€/yr)	Indirect expenses (M€/yr)	Overhead (M€/yr)	Depreciation (M€/yr)	Total OPEX (M€/yr)
CS_{comb}	11.9	1.2	4.7	0.6	0.2	0.0	2.4	1.1	3.9	26.1
$CS_{comb+elc}$	11.8	1.5	5.4	0.9	0.2	0.1	2.7	1.2	4.5	28.3
CS_{elc}	8.1	1.2	4.1	0.8	0.2	0.1	2.1	0.9	3.4	20.8
CS_{H_2}	19.3	2.9	7.0	1.2	0.3	0.1	3.5	1.9	5.9	42.1
SCB_{comb}	7.6	0.9	4.0	0.6	0.2	0.0	2.0	0.8	3.3	19.3
$SCB_{comb+elc}$	6.7	1.1	4.2	0.9	0.2	0.1	2.1	0.8	3.5	19.6
SCB_{elc}	6.1	0.9	3.9	0.8	0.2	0.1	2.0	0.7	3.3	17.9
SCB_{H_2}	10.0	3.4	5.9	1.2	0.3	0.1	3.0	1.3	4.9	30.0

Table 8: NPV

Year	Annual change NPV CS	Combined NPV CS	Annual change NPV SCB	Combined NPV SCB
0	-51,264,581	-51,264,581	-49,083,032	-49,083,032
1	6,127,226	-45,137,356	5,866,483	-43,216,549
2	5,570,205	-39,567,151	5,333,167	-37,883,382
3	5,063,823	-34,503,328	4,848,333	-33,035,049
4	4,603,475	-29,899,853	4,407,576	-28,627,473
5	4,184,978	-25,714,875	4,006,887	-24,620,586
6	3,804,525	-21,910,350	3,642,625	-20,977,962
7	3,458,659	-18,451,691	3,311,477	-17,666,485
8	3,144,236	-15,307,455	3,010,434	-14,656,051
9	2,858,396	-12,449,060	2,736,758	-11,919,293
10	2,598,542	-9,850,518	2,487,962	-9,431,332
11	2,362,311	-7,488,207	2,261,783	-7,169,549
12	2,147,555	-5,340,652	2,056,167	-5,113,382
13	1,952,323	-3,388,329	1,869,242	-3,244,140
14	1,774,839	-1,613,490	1,699,311	-1,544,828
15	1,613,490	-	1,544,828	-0

1.4 Python code

1.4.1 Drying functions

```
# -*- coding: utf-8 -*-
"""
Created on Mon Oct 7 15:14:51 2019

@author: Jan de Koning
"""

import pandas as pd
import math as m
import numpy as np
from matplotlib import pyplot as plt
from scipy.interpolate import *
from scipy.stats import *

def torgascomp(x,a,b,c):
    return a*x**2+b*x+c
def dryingmassloss(t,a,k):
    return a*np.exp(-k*t)
def torrmasloss(t,a,k,b):
    return a*np.exp(-k*t)+b
```

```

def linrel(x,a,b):
    return a*x+b
def shapefactor(X,F):
    return 2*F*X-(2*F-1)*X**2

def shapecurve(M,Me,Mc,t,w,MaxMoisture): #Drying kinetics data for
    ↪ Aspen
    M = M[~np.isnan(M)] #filtering out NaN's if they are present
    X=np.zeros(len(M)) #moisture content
    DR=np.zeros(len(M)-1) #drying rate
    NMR=np.zeros(len(M)) #normalized moisture content
    F=np.zeros(len(M)-1) #drying curve shape factor
    XX=np.zeros(len(M))
    for i in range(len(M)): #converting Moisture ratio to moisture
        ↪ content (kg/kg dry matter)
        X[i]=M[i]*(MaxMoisture-Me)+Me
        XX[i]=X[i]/Mc
        NMR[i]=round((X[i]-Me)/(Mc-Me),5) #normalized drying rate
        ↪ for different Mc
    DR[0]=-(X[2]-X[0])/(t[2]-t[0]) #First drying rate
    DR[-1]=0
    for i in range(len(NMR)-2): #drying rate by using transformed
        ↪ Euler
        DR[i+1]=-(X[i+2]-X[i])/(t[i+2]-t[i])
    NMR=NMR[:-1]
    for i in range(len(NMR)):
        if NMR[i]<1:
            NMR[i]=NMR[i]
        else:
            NMR[i]=0
    NMR=NMR[NMR !=0]
    DR=DR[-len(NMR):]
    X=X[-len(NMR):]
    XX=XX[-len(NMR):]
    NDR=np.zeros(len(NMR))
    CDR=np.nanmax(DR) #Constant drying rate, the max drying rate
    ↪ which is reached in the beginning
    for i in range(len(NMR)):
        NDR[i]=round(DR[i]/CDR,9) #normalized drying rate
    a=np.zeros(len(NMR))

```

```

# for i in range(len(NMR)):
# a[i]= round((NMR[i]*(Mc-Me)+Me)/Mc,3) #X/Mc
# F[i]=round((NDR[i]-a[i]**2)/(2*(a[i]-a[i]**2)),2) #shape factor
    ↪ calculation
# F=F[F !=0]
# F=F[~np.isnan(F)]
    return X,DR,NMR,NDR,XX

def moisturecalc(Deff, L, n,w,tfin,MaxMoisture,Me,Mc):
    t=np.linspace(0, tfin, n)
    M=np.zeros((n,w))
    for i in range(len(t)):
        for j in range(w):
            M[i,j]=8/((m.pi**2))*m.exp(m.pi**2*Deff[j]*t[i]/(4*L**2))
            ↪ )
    X=np.zeros(n)
    for i in range(w):
        X=M[:,i]
        X,Dr,NMR,NDR=shapecurve(X,Me,Mc,t,w,MaxMoisture)
        plt.figure(i)
        plt.plot(NMR,NDR,linewidth=3)
        plt.xlabel('Normalized moisture content')
        plt.ylabel('Normalized drying rate')
    return NMR,NDR

def dryingcomparison(poptpopt,T,t,Lfactor): #comparison for
    ↪ different drying times
    popt=np.zeros((2,n))
    MR=np.zeros((len(t),len(T)))
    for i in range(len(T)):
        popt[:,i]=linrel(T[i],*poptpopt)
        popt[1,i]=popt[1,i]/Lfactor #only k is changed due to new L
            ↪ factor, as L is part of k, k=(pi^2*Deff)/(4*L^2)
        for j in range(len(t)):
            MR[j,i]=dryingmassloss(t[j],*popt[:,i])*100
    for i in range(2):
        poptpopt[:,i],pcov=curve_fit(linrel,T,popt[i,:])
    return popt,MR,poptpopt

```



```

def dryingfitting(df,n,w,labels,Tdata):
    guess=[1,0.001]
    t=np.linspace(0,65,n)
    popt=np.zeros((w,2))
    poptpopt=np.zeros((2,2))
    abserror=np.zeros(len(df))
    Rsquared=np.zeros(w)
    X=np.zeros(w)
    for i in range(w):
        ydata=df.iloc[:,2*i+1]
        xdata=df.iloc[:,2*i]
        ydata=ydata[~np.isnan(ydata)]
        xdata=xdata[:len(ydata)]
        popt[i,:],pcov=curve_fit(dryingmassloss,xdata,ydata,p0=guess
            ↪ )
        y=dryingmassloss(xdata,*popt[i,:])
        X[i],p=chisquare(y.iloc[:,-1],ydata.iloc[:,-1])
        slope,intercept,R,p,sterr=linregress(y,ydata)
        Rsquared[i]=R**2
        plt.figure(11)
        plt.scatter(df.iloc[:,2*i],df.iloc[:,1+2*i])
        plt.plot(t,dryingmassloss(t,*popt[i,:]),linewidth=3)
        plt.xlabel('drying time (min)')
        plt.ylabel('Moisture ratio')
    # plt.title('Drying curve fitting Sugarcane Bagasse')
    plt.legend(labels,frameon=False)
    T=np.linspace(np.min(Tdata),np.max(Tdata),n)
    labels1=['A sugarcane bagasse', 'k sugarcane bagasse']
    for i in range(2):
        poptpopt[:,i],pcov=curve_fit(linrel,Tdata,popt[:,i])
        plt.figure(19)
        plt.scatter(Tdata,popt[:,i])
        plt.plot(T,linrel(T,*poptpopt[:,i]))
        plt.xlabel('Temperature ( $^{\circ}$ C)')
        plt.ylabel('Coefficients')
        #plt.title('Coefficients versus temperature')
        plt.legend(labels1)
    return popt,Rsquared,X,poptpopt

```

```

def finaldryingtime(Mfinal,popt,T,Tsens,tsens):
    tfinal=np.zeros(n)
    for i in range(n):
        tfinal[i]=-np.log(Mfinal/popt[0,i])/popt[1,i]
    plt.figure()
    plt.plot(T,tfinal,linewidth=3,label='Calculated by author')
    #plt.scatter(Tsens,tsens,linewidth=3, label='Calculated by Aspen
    ↪ ')
    plt.xlabel('Temperature ( $^{\circ}\text{C}$ )')
    plt.ylabel('drying time (min)')
    plt.title('Drying time until final moisture is reached')
    plt.legend()
    return tfinal

def fitDeff(x,y): #Deff fit
    z=np.polyfit(x,y,1)
    p=np.poly1d(z)
    ymodel=p(x)
    yaver=np.average(y)
    SStot=np.sum((y-yaver)**2)
    SSreg=np.sum((ymodel-yaver)**2)
    SSres=np.sum((y-ymodel)**2)
    R=1-SSres/SStot
    plt.figure()
    plt.scatter(x,y,linewidth=5)
    plt.plot(x,p(x), "r--",label='Sugarcane bagasse')
    plt.xlim(0.99*np.min(x), 1.01*np.max(x))
    #plt.title('Effective Diffusion Coefficient')
    plt.xlabel('1/T (1/K)')
    plt.ylabel('Ln D (Ln(m $\text{m}^2/\text{s}$ ))')
    return z,R,p

def energybalancecocurrent(MaxMoisture,Mfinal,Ws,DT,n,Tair):
    Cpbio=np.zeros(n)
    Qbio=np.zeros(n)
    Q=np.zeros(n)
    Wair=np.zeros((n,n))
    Cpwater=4.184 #heat capacity water (kJ/kg)
    Wbio=(1-MaxMoisture)*Ws
    LH=2260 #Latent heat of water, kJ/kg

```

```

Tbegin=298 #beginning temperature of the biomass
T=np.linspace(313,333,n)
Cpbio=(5.340*T-299)/1000 #heat capacity biomass (kJ/mol) for
    ↪ different temperatures
for i in range(n):
    Qbio[i]=(T[i]-Tbegin)*np.average(Cpbio)*Wbio+Mfinal*Cpwater
        ↪ *(T[i]-Tbegin)*Wbio#Heat needed for biomass heating
        ↪ and water remaining
    Qwater=(Ws-Wbio*1.1)*LH #heat needed for evaporation of
        ↪ water
    Q[i]=Qbio[i]+Qwater
    Cpair=1
    for j in range(n):
        Wair[j,i]=(Q[i]-(Ws-Wbio*1.1)*Cpwater*(T[i]-Tbegin))/((
            ↪ Tair[j]-T[i])*Cpair)
plt.figure()
ax=plt.axes(projection='3d')
Td=np.linspace(40,60,n)
Tair=np.linspace(100,400,n)
TD,TAIR=np.meshgrid(Td,Tair)
ax.plot_surface(TD,TAIR,Wair*3600)
ax.set_title('Dryer requirements')
ax.set_xlabel('Temperature dryer ($^0$C)')
ax.set_ylabel('Temperature air ($^0$C)')
ax.set_zlabel('Air required (kg/hr)')
return Wair,Q,Tair

```

1.4.2 Torrefaction functions

```

# -*- coding: utf-8 -*-
"""
Created on Wed Nov 13 12:36:51 2019

@author: Jan de Koning
"""

import pandas as pd
import math as m
import numpy as np
from matplotlib import pyplot as plt

```

```

from scipy.interpolate import *
from scipy.stats import *
from scipy.integrate import odeint
from scipy.optimize import curve_fit

def torgascomp(x,a,b,c):
    return a*x**2+b*x+c
def dryingmassloss(t,a,k):
    return a*np.exp(-k*t)
def torrmassloss(t,a,k,b):
    return a*np.exp(-k*t)+b
def linrel(x,a,b):
    return a*x+b
def fourthpoly(x,a,b,c,d,e):
    return a*x**4+b*x**3+c*x**2+d*x+e
def torrmasslosskinetics(t,k1,k2,kv1,kv2): #mass los kinetics
    ↪ during torrefaction
    kk1=k1+kv1
    kk2=k2+kv2
    return (1+((k1*kk1-k1*k2)/(kk1*(kk2-kk1))))*np.exp(-kk1*t)+((-k1
        ↪ *kk2+k1*k2)/(kk2*(kk2-kk1)))*np.exp(-kk2*t)+k1*k2/(kk1*
        ↪ kk2)
def krel(T,a,b): #k relation with temperature
    return a*np.exp(-b/(8.314*T))
def kcalc(T,poptpopt): #k relation with temperature
    return poptpopt[0]*np.exp(-poptpopt[1]/(8.314*(T+273)))
def volatilescalc(T,poptpopt,time,df): #volatiles size calculation
    ↪ using k's
    V1=np.zeros(np.size(T))
    V2=np.zeros(np.size(T))
    V=np.zeros((np.size(T),2))
    for i in range(np.size(T)):
        k=np.zeros(4)
        for j in range(4):
            popt=poptpopt[j,:]
            k[j]=kcalc(T[i],popt)
            kk1=k[0]+k[2]
            kk2=k[1]+k[3]
        V1[i]=k[2]/kk1*(1-np.exp(-kk1*time))

```

```

        V2[i]=k[3]*k[0]/((kk1-kk2)*kk1*kk2)*(kk1-kk2-kk1*np.exp(-kk2
        ↪ *time)+kk1*np.exp(-kk1*time))
V[:,0]=V1
V[:,1]=V2
return V
def volatilescalc2(T,poptpopt,time,df):
    V1=np.zeros(np.size(T))
    V2=np.zeros(np.size(T))
    V=np.zeros((np.size(T),2))
    for i in range(np.size(T)):
        k=np.zeros(4)
        for j in range(4):
            popt=poptpopt[j,:]
            k[j]=kcalc(T,popt)
            kk1=k[0]+k[2]
            kk2=k[1]+k[3]
        V1[i]=k[2]/kk1*(1-np.exp(-kk1*time))
        V2[i]=k[3]*k[0]/((kk1-kk2)*kk1*kk2)*(kk1-kk2-kk1*np.exp(-kk2
        ↪ *time)+kk1*np.exp(-kk1*time))
    V[:,0]=V1
    V[:,1]=V2
    return V

def torgascompositioncurve(df,n): #not used
    guess=[0.01,0.01,1]
    labels=['CO2', 'CO', 'CH4', 'H2']
    xdata=df.iloc[:,0]
    a=int(np.size(df)/len(df))
    x=np.linspace(np.min(xdata),np.max(xdata),n)
    popt=np.zeros((a-1,3))
    for i in range(a-1):
        ydata=df.iloc[:,i+1]
        xdata=df.iloc[:,0]
        xdata=xdata*ydata
        xdata=xdata[~np.isnan(xdata)]
        ydata=ydata[~np.isnan(ydata)]
        xdata=xdata/(ydata)
        x=np.linspace(np.min(xdata),np.max(xdata),n)
        popt[i,:],pcov=curve_fit(torgascomp,xdata,ydata,guess)
    plt.figure(10)

```

```

        plt.scatter(xdata,ydata)
        plt.plot(x,torgascomp(x,*popt[i,:]))
        plt.xlabel('Temperature ($^0$C)')
        plt.ylabel('Fraction in torgas')
        plt.legend(labels,bbox_to_anchor=(1, 1))
    return popt

def torgascompositioncurve2(df,n,xdata,T): #not used
    guess=[0.01,0.01,1]
    labels=['CO2', 'CO', 'CH4', 'H2']
    a=int(np.size(df)/len(df))*2
    x=np.linspace(np.min(xdata),np.max(xdata),n)
    popt=np.zeros((a-1,3))
    poptmean=np.zeros((a,3))
    ydatamean=np.zeros(len(T))
    xdatamean=np.zeros(len(T))
    for i in range(a):
        ydata=df.iloc[:,i]
        ydata=ydata[~np.isnan(ydata)]
        for j in range(len(T)):
            xdatamean[j]=T[j]
            ydatamean[j]=np.mean(ydata.loc[T[j]])
        x=np.linspace(np.min(xdata),np.max(xdata),n)
        poptmean[i,:],pcov=curve_fit(torgascomp,xdatamean,ydatamean)
        plt.figure(100)
        plt.scatter(xdatamean,ydatamean)
        plt.plot(x,torgascomp(x,*poptmean[i,:]))
        plt.xlabel('Temperature ($^0$C)')
        plt.ylabel('Fraction torgas products')
        plt.title('Torgas composition Sugarcane Bagasse')
        plt.legend(labels,bbox_to_anchor=(1, 1))
    return popt

def Torliquidgasdistribution(df,n,xdata,T): #not used
    guess=[0.000001,0.001,1]
    labels=['Gas', 'Liquid']
    a=int(np.size(df)/len(df))
    x=np.linspace(np.min(xdata),np.max(xdata),n)
    popt=np.zeros((a,3))
    poptmean=np.zeros((a,3))

```

```

ydatamean=np.zeros(len(T))
xdatamean=np.zeros(len(T))
for i in range(a):
    ydata=df.iloc[:,i]
    ydata=ydata[~np.isnan(ydata)]
    for j in range(len(T)):
        xdatamean[j]=T[j]
        ydatamean[j]=np.mean(ydata.loc[T[j]])
    x=np.linspace(np.min(xdata),np.max(xdata),n)
    popt[i,:],pcov=curve_fit(torgascomp,xdata,ydata,p0=guess)
    poptmean[i,:],pcov=curve_fit(torgascomp,xdatamean,ydatamean)
    plt.figure(11)
    plt.scatter(xdatamean,ydatamean)
    plt.plot(x,torgascomp(x,*poptmean[i,:]))
    plt.xlabel('Temperature ($^0C$)')
    plt.ylabel('Fraction of torrefaction products')
    plt.title('Torrefaction products distribution Sugarcane
    ↪ Bagasse')
    plt.legend(labels,bbox_to_anchor=(1, 1))
return popt

def Torliquidgasdistribution2(df,n): #not used
    guess=[0.000001,0.001,1]
    labels=['Gas', 'Liquid']
    a=int(np.size(df)/len(df))
    xdata=df.iloc[:,0]
    x=np.linspace(np.min(xdata),np.max(xdata),n)
    popt=np.zeros((a,3))
    for i in range(a-1):
        ydata=df.iloc[:,i+1]
        xdata=df.iloc[:,0]
        xdata=xdata*ydata
        xdata=xdata[~np.isnan(xdata)]
        ydata=ydata[~np.isnan(ydata)]
        xdata=xdata/(ydata)
        x=np.linspace(np.min(xdata),np.max(xdata),n)
        popt[i,:],pcov=curve_fit(torgascomp,xdata,ydata,p0=guess)
        plt.figure(155)
        plt.scatter(xdata,ydata)
        plt.plot(x,torgascomp(x,*popt[i,:]))

```

```

        plt.xlabel('Temperature ($^0$C)')
        plt.ylabel('Fraction')
        plt.title('Torproducts distribution Corn Stalk')
        plt.legend(labels,bbox_to_anchor=(1, 1))
    return popt

def torliquidimprovedcurve(df,n,labels): #not used
    guess=[0.01, 0.1, 0.3]
    xdata=df.iloc[:,0]
    a=int(np.size(df)/len(df))
    x=np.linspace(np.min(xdata),np.max(xdata),n)
    popt=np.zeros((a-1,3))
    for i in range(a-1):
        ydata=df.iloc[:,i+1]
        xdata=df.iloc[:,0]
        xdata=xdata*ydata
        xdata=xdata[~np.isnan(xdata)]
        ydata=ydata[~np.isnan(ydata)]/100
        xdata=xdata/(ydata*100)
        x=np.linspace(np.min(xdata),np.max(xdata),n)
        popt[i,:],pcov=curve_fit(torgascomp,xdata,ydata,p0=guess)
    plt.figure(15)
    plt.scatter(xdata,ydata)
    plt.plot(x,torgascomp(x,*popt[i,:]))
    plt.xlabel('Temperature (C)')
    plt.ylabel('Fraction in torliquid')
    plt.title('Torliquid composition')
    plt.legend(labels,bbox_to_anchor=(1, 1))
    return popt

def Torbiocomposition(df,n): #not used
    guess=[0.01, 0.1, 0.3]
    labels=['Moisture', 'FC', 'VM', 'Ash']
    a=int(np.size(df)/len(df))
    poptprox=np.zeros((4,3))
    poptult=np.zeros((4,3))
    for i in range(4):
        ydata=df.iloc[:,i+1]
        xdata=df.iloc[:,0]
        xdata=xdata*ydata

```



```

        xdata=xdata[~np.isnan(xdata)]
        ydata=ydata[~np.isnan(ydata)]/100
        xdata=xdata/(ydata*100)
        x=np.linspace(np.min(xdata),np.max(xdata),n)
        poptprox[i,:],pcov=curve_fit(torgascomp,xdata,ydata,p0=guess
        ↪ )
        plt.figure(13)
        plt.scatter(xdata,ydata)
        plt.plot(x,torgascomp(x,*poptprox[i,:]))
        plt.xlabel('Temperature (C)')
        plt.ylabel('Fraction')
        plt.title('Proximate analysis Sugarcane Bagasse')
        plt.legend(labels,bbox_to_anchor=(1, 1))
    labels=['C', 'H', 'N', 'O']
    for i in range(4):
        ydata=df.iloc[:,i+5]
        xdata=df.iloc[:,0]
        xdata=xdata*ydata
        xdata=xdata[~np.isnan(xdata)]
        ydata=ydata[~np.isnan(ydata)]/100
        xdata=xdata/(ydata*100)
        x=np.linspace(np.min(xdata),np.max(xdata),n)
        poptult[i,:],pcov=curve_fit(torgascomp,xdata,ydata,p0=guess)
        plt.figure(14)
        plt.scatter(xdata,ydata)
        plt.plot(x,torgascomp(x,*poptult[i,:]))
        plt.xlabel('Temperature ($^0$C)')
        plt.ylabel('Fraction')
        plt.title('Ultimate analysis Sugarcane Bagasse')
        plt.legend(labels,bbox_to_anchor=(1, 1))
    return poptprox,poptult

def weightlosskinetics(df,n,labels,Tdata,guess,factor,boundslow,
    ↪ boundsup): #weight loss kinetics function in Python
    guess1=[0.2, 0.02, 0.9]
    xdata=df.iloc[:,0]
    a=int(np.size(df)/len(df))
    poptkin=np.zeros((a-1,4))
    poptnum=np.zeros((a-1,3))
    poptpopt=np.zeros((4,2))

```

```

t=np.linspace(0,120,n)
x=np.linspace(523,573,n)
for i in range(a-1):
    ydata=df.iloc[:,i+1]
    xdata=df.iloc[:,0]
    xdata=xdata*ydata
    xdata=xdata[~np.isnan(xdata)]
    ydata=ydata[~np.isnan(ydata)]/100
    xdata=xdata/(ydata*100)
    poptkin[i,:],pcov=curve_fit(torrmasslosskinetics,xdata,ydata
        ↪ ,p0=guess,bounds=(boundslow,boundsup)) #weight loss
        ↪ kinetics based on 2-step mechanism
    poptnum[i,:],pcov=curve_fit(torrmassloss,xdata,ydata,p0=
        ↪ guess1) #weight loss kinetics based on general decay
        ↪ formula (torrmassloss above)
    boundslow=np.array(poptkin[i,:])*factor*0.6 #set bounds to
        ↪ not let a k value decrease as temperature increases
    boundsup=np.array(poptkin[i,:])*factor*1
    print(boundsup)
    guess=poptkin[i,:]*factor
    plt.figure(21)
    plt.scatter(xdata,ydata)
    #plt.plot(t,torrmasslosskinetics(t,*poptkin[i,:]))
# plt.plot(t,torrmassloss(t,*poptnum[i,:]),"--")
    plt.xlim(-1,65,n)
    plt.ylim(0.4,1.2)
    plt.xlabel('Time (min)')
    plt.ylabel('Weight fraction')
    #plt.title('Weight loss solids torrefaction sugarcane
        ↪ bagasse')
    plt.legend(labels,frameon=False)
    guess=[10000,50000]
    labels=['kb','kc','kv1','kv2']
    x=1000/x
    Tdata=1000/Tdata
    for i in range(4):
        poptpopt[i,:],pcov=curve_fit(krel,1000/Tdata,poptkin[:,i],p0
            ↪ =guess,bounds=(0,1000000))
        ln=np.log(poptkin[:,i])
        b,pcov=curve_fit(linrel,Tdata,ln)

```

```

    print(ln)
    plt.figure(222)
    plt.scatter(Tdata,ln)
    plt.plot(x,linrel(x,*b))
    plt.xlabel('1000/T (1/K)')
    plt.ylabel('LN of coefficient')
    plt.ylim(-8,2)
    #plt.title('Coefficients corn stalks relationship with
    ↪ temperature')
    plt.legend(labels,frameon=False,loc='center right')
    plt.figure(44)
    plt.scatter(1000/Tdata-273,poptkin[:,i])
    plt.plot(1000/x-273,krel(1000/x,*poptpopt[i,:]))
    plt.ylim(0,0.1)
    plt.xlabel('Temperature ( $^{\circ}$ C)')
    plt.ylabel('Value of coefficient')
    plt.legend(labels,bbox_to_anchor=(1,0.5),loc='center left',
    ↪ frameon=False)
    return poptkin,poptpopt

def Volatiles(df,time): #volatiles composition calculation
    a=0
    df=df.loc[df['time (min)']==time,:] #selecting certain time from
    ↪ experimental data
    T=np.array(df.iloc[:,0])
    Tuniq=np.unique(T) #removing duplicate T values
    V=volatilescalc(T,poptpopt,time,df) #calculate volatiles size
    y=df.iloc[:,2:]
    x=cp.Variable((2,len(df.iloc[0])-2))
    objective=cp.Minimize(cp.sum_squares(V*x-y)) #determine x: the
    ↪ composition
    constraints=[x>=0,sum(x[0,:])==1,sum(x[1,:])==1] #constraints on
    ↪ V1 and V2
    prob=cp.Problem(objective,constraints)
    prob.solve()
    labels=['Kinetically', 'Numerical linear fit']
    y=df.iloc[:,a+2]
    guess=[0.01,0.01]
    Tlin=np.linspace(np.min(T),np.max(T),n)
    V=np.zeros((len(Tlin),2))

```

```

V=volatilesalc(Tlin,poptpopt,time,df)
popt,pcov=curve_fit(linrel,T,y,guess)
V=volatilesalc(Tuniq,poptpopt,time,df)
y=np.dot(V,x.value)
return x.value,y, Tuniq

def Flammability(x,a,LFLx,HFLx): #flammability limiets
    T=np.linspace(250,300,n)
    V=volatilesalc(T,poptpopt,time,df)
    y=np.dot(V,x)
    c=np.zeros(n)
    b=int(np.size(y)/len(y))
    for i in range(n):
        c[i]=np.sum(y[i,:])
    for i in range(n):
        for j in range(b):
            y[i,j]=y[i,j]/c[i]
    y=y[:,a]
    LFL=np.zeros(n)
    HFL=np.zeros(n)
    nomL=np.zeros(len(LFLx))
    nomH=np.zeros(len(HFLx))
    for i in range(n):
        for j in range(len(LFLx)):
            nomL[j]=y[i,j]/LFLx[j]
            nomH[j]=y[i,j]/HFLx[j]
        LFL[i]=1/np.sum(nomL)
        HFL[i]=1/np.sum(nomH)
    plt.figure()
    plt.plot(T,LFL,label='LFL SCB', linewidth=3)
    plt.plot(T,HFL,label='HFL SCB', linewidth=3)
    plt.xlabel('Temperature (C)')
    plt.ylabel('Flammability limit (/%)')
    plt.title('LFL and HLF CS')
    return LFL,HFL

def TorrefactionplotsCS(df,time,T,HHVRAW,poptult,coeff): #
    → Torrefaction results plots
    Solids=np.zeros((len(time),len(T)))

```

```

Condensables=np.zeros((len(time),len(T)))
Noncondensables=np.zeros((len(time),len(T)))
Efficiency=np.zeros((len(time),len(T)))
V1=np.zeros((len(time),len(T)))
V2=np.zeros((len(time),len(T)))
k=np.zeros(4)
for i in range(len(time)):
    V=volatilescale(T,poptpopt,time[i],df)
    V1[i,:]=V[:,0]
    V2[i,:]=V[:,1]
    for j in range(len(T)):
        A=np.zeros(5)
        for z in range(4):
            popt=poptpopt[z,:]
            k[z]=kcalc(T[j],popt)
        A[0]=torgascomp(T[j],*poptult[0,:])
        A[1]=torgascomp(T[j],*poptult[1,:])
        A[2]=torgascomp(T[j],*poptult[2,:])
        A[3]=torgascomp(T[j],*poptult[3,:])
        A[4]=torgascomp(T[j],*poptult[4,:])
        HHVT=100*(A[0]*coeff[0]+A[1]*coeff[1]+A[2]*coeff[2]+A
            ↳ [3]*coeff[3]+A[4]*coeff[4])+coeff[5]
        Solids[i,j]=torrmasslosskinetics(time[i],*k)
        Noncondensables[i,j]=V1[i,j]*(fourthpoly(time[i],*popt1
            ↳ [0,:])+fourthpoly(time[i],*popt1[1,:])+fourthpoly(
            ↳ time[i],*popt1[2,:])+fourthpoly(time[i],*popt1
            ↳ [3,:])+fourthpoly(time[i],*popt1[4,:]))+V2[i,j]*(
            ↳ fourthpoly(time[i],*popt2[0,:])+fourthpoly(time[i]
            ↳ ],*popt2[1,:])+fourthpoly(time[i],*popt2[2,:])+
            ↳ fourthpoly(time[i],*popt2[3,:])+fourthpoly(time[i]
            ↳ ],*popt2[4,:]))
        Condensables[i,j]=V1[i,j]*(fourthpoly(time[i],*popt1
            ↳ [5,:])+fourthpoly(time[i],*popt1[6,:])+fourthpoly(
            ↳ time[i],*popt1[7,:])+fourthpoly(time[i],*popt1
            ↳ [8,:])+fourthpoly(time[i],*popt1[9,:])+fourthpoly(
            ↳ time[i],*popt1[10,:]))+V2[i,j]*(fourthpoly(time[i]
            ↳ ],*popt2[5,:])+fourthpoly(time[i],*popt2[6,:])+
            ↳ fourthpoly(time[i],*popt2[7,:])+fourthpoly(time[i]
            ↳ ],*popt2[8,:])+fourthpoly(time[i],*popt2[9,:])+
            ↳ fourthpoly(time[i],*popt2[10,:]))

```

```

Efficiency[i,j]=Solids[i,j]*HHVT/HHVCSRAW*100

r1=np.arange(len(time))*4
r2=np.arange(len(time))*4+1
r3=np.arange(len(time))*4+2
plt.figure(1)
plt.bar(r1,Solids[:,0],color='b',edgecolor='white',width=
    ↪ Barwidth,label='Solids')
plt.bar(r1,Condensables[:,0],bottom=Solids[:,0],color='r',
    ↪ edgecolor='white',width=Barwidth,label='Condensables')
plt.bar(r1,Noncondensables[:,0],bottom=Condensables[:,0]+Solids
    ↪[:,0],color='g',edgecolor='white',width=Barwidth,label='
    ↪ Non-condensables')
plt.bar(r2,Solids[:,1],color='b',edgecolor='white',width=
    ↪ Barwidth)
plt.bar(r2,Condensables[:,1],bottom=Solids[:,1],color='r',
    ↪ edgecolor='white',width=Barwidth)
plt.bar(r2,Noncondensables[:,1],bottom=Condensables[:,1]+Solids
    ↪[:,1],color='g',edgecolor='white',width=Barwidth)
plt.bar(r3,Solids[:,2],color='b',edgecolor='white',width=
    ↪ Barwidth)
plt.bar(r3,Condensables[:,2],bottom=Solids[:,2],color='r',
    ↪ edgecolor='white',width=Barwidth)
plt.bar(r3,Noncondensables[:,2],bottom=Condensables[:,2]+Solids
    ↪[:,2],color='g',edgecolor='white',width=Barwidth)
plt.plot(r1[:-1],df.iloc[[0,2,4,6],2],c='k',marker="X",linestyle
    ↪=" ",label='Exp solids')
plt.plot(r3[:-2],df.iloc[[1,3,5],2],c='k',marker="X",linestyle
    ↪=" ")
# plt.plot(r1[:-1],df.iloc[[0,2,4,6],3]+Condensables[:-1,0]+Solids
    ↪[:-1,0],c='k',marker="P",linestyle=" ")
# plt.plot(r3[:-2],df.iloc[[1,3,5],3]+Condensables[:-2,2]+Solids
    ↪[:-2,2],c='k',marker="P",linestyle=" ")
# plt.plot(r1[:-1],df.iloc[[0,2,4,6],4]+Solids[:-1,1],c='k',marker
    ↪="*",linestyle=" ")
# plt.plot(r3[:-2],df.iloc[[1,3,5],4]+Solids[:-2,2],c='k',marker
    ↪="*",linestyle=" ")
plt.xticks(r2, time)
plt.legend(bbox_to_anchor=(1, 1),frameon=False)
plt.ylim([0,1])

```

```

plt.xlabel('Torrefaction time (min)')
plt.ylabel('Fraction of dry weight')
# plt.title('Distribution of products CS torrefaction')

plt.figure(4)
plt.bar(r1, Efficiency[:,0], edgecolor='white', width=Barwidth,
        ↪ label='250 $^0$C')
plt.bar(r2, Efficiency[:,1], edgecolor='white', width=Barwidth,
        ↪ label='275 $^0$C')
plt.bar(r3, Efficiency[:,2], edgecolor='white', width=Barwidth,
        ↪ label='300 $^0$C')
plt.xticks(r2, time)
plt.legend(frameon=False)
plt.ylim([0,110])
plt.xlabel('Torrefaction time (min)')
plt.ylabel('Thermal efficiency (%)')
# plt.title('Thermal efficiency of torrefaction unit')

return Solids, Noncondensables, Condensables, Efficiency

def TorrefactionplotsSCB(df, time, T, HHVRAW, poptult, coeff): #
    ↪ Torrefaction results plots
    Solids=np.zeros((len(time),len(T)))
    Condensables=np.zeros((len(time),len(T)))
    Noncondensables=np.zeros((len(time),len(T)))
    Efficiency=np.zeros((len(time),len(T)))
    V1=np.zeros((len(time),len(T)))
    V2=np.zeros((len(time),len(T)))
    k=np.zeros(4)
    for i in range(len(time)):
        V=volatilesalc(T, poptpopt, time[i], df)
        V1[i,:]=V[:,0]
        V2[i,:]=V[:,1]
        for j in range(len(T)):
            A=np.zeros(5)
            for z in range(4):
                popt=poptpopt[z,:]
                k[z]=kcalc(T[j], popt)
            A[0]=torgascomp(T[j], *poptult[0,:])
            A[1]=torgascomp(T[j], *poptult[1,:])

```

```

A[2]=torgascomp(T[j],*poptult[2,:])
A[3]=torgascomp(T[j],*poptult[3,:])
A[4]=torgascomp(T[j],*poptult[4,:])
HHVT=100*(A[0]*coeff[0]+A[1]*coeff[1]+A[2]*coeff[2]+A
    ↪ [3]*coeff[3]+A[4]*coeff[4])+coeff[5]
Solids[i,j]=torrmasslosskinetics(time[i],*k)
Noncondensables[i,j]=V1[i,j]*(linrel(time[i],*popt1
    ↪ [0,:])+linrel(time[i],*popt1[1,:])+linrel(time[i]
    ↪ ],*popt1[2,:])+linrel(time[i],*popt1[3,:]))+V2[i,j
    ↪ ]*(linrel(time[i],*popt2[0,:])+linrel(time[i],*
    ↪ popt2[1,:])+linrel(time[i],*popt2[2,:])+linrel(
    ↪ time[i],*popt2[3,:]))
Condensables[i,j]=V1[i,j]*(linrel(time[i],*popt1[4,:])+
    ↪ linrel(time[i],*popt1[5,:])+linrel(time[i],*popt1
    ↪ [6,:])+linrel(time[i],*popt1[7,:])+linrel(time[i]
    ↪ ],*popt1[8,:])+linrel(time[i],*popt1[9,:])+linrel(
    ↪ time[i],*popt1[10,:]))+V2[i,j]*(linrel(linrel(time
    ↪ [i],*popt2[4,:])+time[i],*popt2[5,:])+linrel(time[
    ↪ i],*popt2[6,:])+linrel(time[i],*popt2[7,:])+linrel
    ↪ (time[i],*popt2[8,:])+linrel(time[i],*popt2[9,:])+
    ↪ linrel(time[i],*popt2[10,:]))
Efficiency[i,j]=Solids[i,j]*HHVT/HHVCSRAW*100
print(popt1)
r1=np.arange(len(time))*4
r2=np.arange(len(time))*4+1
r3=np.arange(len(time))*4+2
plt.figure(1)
plt.bar(r1,Solids[:,0],color='b',edgecolor='white',width=
    ↪ Barwidth,label='Solids')
plt.bar(r1,Condensables[:,0],bottom=Solids[:,0],color='r',
    ↪ edgecolor='white',width=Barwidth,label='Condensables')
plt.bar(r1,Noncondensables[:,0],bottom=Condensables[:,0]+Solids
    ↪[:,0],color='g',edgecolor='white',width=Barwidth,label='
    ↪ Non-condensables')
plt.bar(r2,Solids[:,1],color='b',edgecolor='white',width=
    ↪ Barwidth)
plt.bar(r2,Condensables[:,1],bottom=Solids[:,1],color='r',
    ↪ edgecolor='white',width=Barwidth)
plt.bar(r2,Noncondensables[:,1],bottom=Condensables[:,1]+Solids
    ↪[:,1],color='g',edgecolor='white',width=Barwidth)

```



```

plt.bar(r3,Solids[:,2],color='b',edgecolor='white',width=
    ↪ Barwidth)
plt.bar(r3,Condensables[:,2],bottom=Solids[:,2],color='r',
    ↪ edgecolor='white',width=Barwidth)
plt.bar(r3,Noncondensables[:,2],bottom=Condensables[:,2]+Solids
    ↪[:,2],color='g',edgecolor='white',width=Barwidth)
plt.plot(r1,df.iloc[[0,2,4,6],2],c='k',marker="X",linestyle="",
    ↪ label='Exp solids')
plt.plot(r3,df.iloc[[1,3,5,7],2],c='k',marker="X",linestyle="")
# plt.plot(r1[:-1],df.iloc[[0,2,4,6],3]+Condensables[:-1,0]+Solids
    ↪[:-1,0],c='k',marker="P",linestyle="")
# plt.plot(r3[:-2],df.iloc[[1,3,5],3]+Condensables[:-2,2]+Solids
    ↪[:-2,2],c='k',marker="P",linestyle="")
# plt.plot(r1[:-1],df.iloc[[0,2,4,6],4]+Solids[:-1,1],c='k',marker
    ↪="*",linestyle="")
# plt.plot(r3[:-2],df.iloc[[1,3,5],4]+Solids[:-2,2],c='k',marker
    ↪="*",linestyle="")
plt.xticks(r2, time)
plt.legend(bbox_to_anchor=(1, 1),frameon=False)
plt.ylim([0,1])
plt.xlabel('Torrefaction time (min)')
plt.ylabel('Fraction of dry weight')
#plt.title('Distribution of products SCB torrefaction')

plt.figure(4)
plt.bar(r1,Efficiency[:,0],edgecolor='white',width=Barwidth,
    ↪ label='250 $^0$C')
plt.bar(r2,Efficiency[:,1],edgecolor='white',width=Barwidth,
    ↪ label='275 $^0$C')
plt.bar(r3,Efficiency[:,2],edgecolor='white',width=Barwidth,
    ↪ label='300 $^0$C')
plt.xticks(r2, time)
plt.legend(frameon=False)
plt.ylim([0,115])
plt.xlabel('Torrefaction time (min)')
plt.ylabel('Thermal efficiency (%)')
#plt.title('Thermal efficiency of torrefaction unit')

return Solids, Noncondensables,Condensables, Efficiency

```

```

def Comput(df):
    poptult=np.zeros((5,3))
    labels=['C', 'H','S', 'O', 'N']
    guess=[0.01, 0.1, 0.3]
    for i in range(5):
        ydata=df.iloc[:,i+1]
        xdata=df.iloc[:,0]
        x=np.linspace(np.min(xdata),np.max(xdata),n)
        poptult[i,:],pcov=curve_fit(torgascomp,xdata,ydata,p0=guess)
        plt.figure(14)
        plt.scatter(xdata,ydata)
        plt.plot(x,torgascomp(x,*poptult[i,:]))
        plt.xlabel('Temperature ( $^{\circ}$ C)')
        plt.ylabel('Fraction')
        plt.title('Ultimate analysis Sugarcane Bagasse')
        plt.legend(labels,bbox_to_anchor=(1, 1))
    return poptult
def HHVcalc(df): #hhv using Boie
    coeff=cp.Variable((6,1))
    A=np.array(df.iloc[:,1:-1])
    b=np.array(df.iloc[:,-1]).T
    b=np.reshape(b, (b.shape[0], 1))
    objective=cp.Minimize(cp.sum_squares((A*coeff[0:-1])*100+coeff
        ↪ [-1]-b))
    prob=cp.Problem(objective)
    prob.solve()
    HHV=np.dot(A,coeff.value[0:-1])*100+coeff.value[-1]
    return coeff.value, HHV

```

1.4.3 Corn Stalk code

```

# -*- coding: utf-8 -*-
"""
Created on Tue Oct 1 14:51:01 2019

@author: Jan de Koning
"""

import pandas as pd
import math as m

```

```

import numpy as np
import sympy as sp
from matplotlib import pyplot as plt
from mpl_toolkits import mplot3d
font={'family' : 'normal',
      'weight' : 'bold',
      'size': 12}
plt.rc('font',**font)
from scipy.stats import chisquare
import cvxpy as cp
Mfinal=0.06 #final moisture content needed
Ws=1 #kg/s of solid
n=100 #numer of elements
DT=5 # degrees difference between air and solid at the end of the
    ↪ dryer
MaxMoisture=0.4
Me=0.03
L=0.0125
Loriginal=L
#%%
#begin
df=pd.read_csv (r'C:\Users\Jan de Koning\Documents\Studie\Master
    ↪ scheikunde\MEP\Drying Data\CS.csv', float_precision = 'high')
w=int(np.size(df)/(2*len(df))) #amount of different T's
Mdata=df.iloc[:,1::2] #all moisture ratio's
tdata=df.iloc[:,::2] #all times
plt.figure()
plt.scatter(tdata.iloc[:,0],Mdata.iloc[:,0])
plt.scatter(tdata.iloc[:,1],Mdata.iloc[:,1])
plt.scatter(tdata.iloc[:,2],Mdata.iloc[:,2])
plt.xlabel('Time (min)')
plt.ylabel('Moisture Ratio')
#plt.title('Drying data Corn stalks')
plt.legend(['T= 40 $^{\circ}$C', 'T= 50 $^{\circ}$C', 'T= 60 $^{\circ}$C'],frameon=
    ↪ False)
Mc=[0.26, 0.25, 0.36]
Tdata=np.array([40,50,60])
a,pcov=curve_fit(torgascomp,Tdata,Mc)
F=np.zeros(3)
b=np.linspace(0,1,n)

```

```

for i in range(w):
    X=Mdata.iloc[:,i]
    y=tdata.iloc[:,i]
    MC=Mc[i]
    X,DR,NMR,NDR,XX= shapecurve(X,Me,MC,y,w,MaxMoisture)
    F[i],pcov=curve_fit(shapefactor,NMR,NDR,bounds=(-1,1))
    plt.figure()
    plt.scatter(NMR,NDR,linewidth=2)
    plt.plot(b,shapefactor(b,F[i]))
    plt.title('Normalized drying curve')
    plt.xlabel('Normalized moisture content')
    plt.ylabel('Normalized drying rate')
plt.figure()
plt.scatter(Tdata,F)
print(F)
print(NMR)
print(NDR)
#%%
#Deff
MaxMoisture=0.4
Me=0.03
L=0.0125
n=100
df=pd.read_csv (r'C:\Users\Jan de Koning\Documents\Studie\Master
    ↪ scheikunde\MEP\Drying Data\CS.csv', float_precision = 'high')
w=int(np.size(df)/(2*len(df)))
Deff=np.zeros(w)
M=np.zeros(len(df))
t=np.zeros(len(df))
labels=['T= 40 $^0$C', 'T= 50 $^0$C', 'T= 60 $^0$C']
plt.figure()
for i in range(w):
    plt.scatter(df.iloc[:,2*i],np.log(df.iloc[:,1+2*i])) #plot ln
    ↪ values
plt.xlabel('drying time (min)')
plt.ylabel('Moisture ratio (Ln)')
plt.title('Ln moisture ratio versus drying time Corn stalks')
plt.legend(labels)

```

```

t=df.iloc[5:9,0] #calculate effective diffusion coefficient (Deff)
    → for each drying temperature
M=np.log(df.iloc[5:9,1])
z=np.polyfit(t,M,1)
p=np.poly1d(z)
Deff[0]=z[0]*4*L**2/(m.pi**2)

t=df.iloc[4:9,2]
M=np.log(df.iloc[4:9,3])
z=np.polyfit(t,M,1)
p=np.poly1d(z)
Deff[1]=z[0]*4*L**2/(m.pi**2)

t=df.iloc[3:7,4]
M=np.log(df.iloc[3:7,5])
z=np.polyfit(t,M,1)
p=np.poly1d(z)
Deff[2]=z[0]*4*L**2/(m.pi**2)

Deffcs=Deff
T=np.array([313, 323, 333]) #making ln(Deff) vs 1/T graph
ycs=np.log(-Deff)
xcs=1/T
z,R,pcs=fitDeff(xcs,ycs)
plt.title('Effective Diffusion Coefficient Corn Stalks')
Ea=-z[0]*8.314

#Deff is in m2/min

#%% Drying curve fitting
labels=['T= 40 °C', 'T= 50 °C', 'T= 60 °C']
Tdatacs=[40, 50, 60]
poptcs1,R,X,poptpoptcs1=dryingfitting(df,n,w,labels,Tdatacs) #
    → Fitting to Henderson-Pabis
print("Rsquared:",R)
print("X squared:",X)
Lnew=0.006
Lfactor=(Lnew/Loriginal)**2 #Lfactor for different particle sizes
print(Lfactor)
print(Lnew)

```

```

# Comparison of drying times
t=[20,40,80,160]
Tcs=np.linspace(40,70,n)
poptcs2,MR,poptpoptcs2=dryingcomparison(poptpoptcs1,Tcs,t,Lfactor)
    → # see influence drying time/temperature
print(poptpoptcs2)
plt.figure(8)
plt.plot(Tcs,MR[0,:], label="20 min",linewidth=5)
plt.plot(Tcs,MR[1,:], label="40 min",linewidth=5)
plt.plot(Tcs,MR[2,:], label="80 min",linewidth=5)
plt.plot(Tcs,MR[3,:], label="160 min",linewidth=5)
#plt.title('Moisture content for T and drying times corn stalk')
plt.xlabel('Temperature ($^{\circ}$C)')
plt.ylabel('Moisture ratio (%)')
plt.legend(frameon=False)

sensdryer=pd.read_csv (r'C:\Users\Jan de Koning\Documents\Studie\
    → Master scheikunde\MEP\Sensitivity\CSdryer.csv',
    → float_precision = 'high')
Tsens=sensdryer.iloc[:,1]
tsens=sensdryer.iloc[:,5]
Wairsenscs=sensdryer.iloc[:,2]/3600
tfinalcs=finaldryingtime(Mfinal,poptcs2,Tcs,Tsens,tsens) #final
    → drying time calculation for certain final moisture content
    → desired
print(tfinalcs[-1])

###
#Energy balance
Tair=np.linspace(150,400,n)+273 #temperature of air at entrance of
    → dryer
Waircs,Qcs,Tair=energybalancecocurrent(MaxMoisture,Mfinal,Ws,DT,n,
    → Tair)
plt.figure()
plt.plot(Tcs,Waircs[:,0],linewidth=3,label='Calculated by author')
plt.plot(Tsens,sensdryer.iloc[:,2]/3600,linewidth=3,label='
    → Calculated by Aspen')
plt.title('Air required for drying')
plt.xlabel('Temperature of dryer ($^{\circ}$C)')
plt.ylabel('Air required (kg/s)')

```

```

plt.legend()

Edryeracs=sensdryer.iloc[:,3]*1000
plt.figure()
plt.plot(Tcs,Qcs,linewidth=3,label='Calculated by author')
plt.plot(Tsens,Edryer,linewidth=3,label='Calculated by Aspen')
plt.xlabel('Temperature of dryer ($^0C$)')
plt.ylabel('Heat required for heating air (kW)')
plt.ylim([0,1100])
plt.title('Heat required for drying')
plt.legend()

###
#Torrefaction
df=pd.read_csv (r'C:\Users\Jan de Koning\Documents\Studie\Master
    ↳ scheikunde\MEP\Torrefaction\Mass yield limited.csv',
    ↳ float_precision = 'high')
Tdata=np.array([250,270,300])+273
labels=['250 $^0C$', '270 $^0C$', '300 $^0C$']
guess=np.array([0.015, 0.5, 0.002,0.007]) #initial guesses to fit
    ↳ torrefaction curves properly.
factor=np.array([1.5,1.5,3,3])
boundslow=np.array([0.0001,0.1,0.002,0.001]) #boundaries such that
    ↳ all k's increases with temperature
boundsup=np.array([0.015,1.5,0.01,0.01])
popt,poptpopt=weightlosskinetics(df,n,labels,Tdata,guess,factor,
    ↳ boundslow,boundsup)
plt.title('Coefficients corn stalk relationship versus temperature
    ↳ ')
print(poptpopt)
print(popt)

### not used
df=pd.read_csv (r'C:\Users\Jan de Koning\Documents\Studie\Master
    ↳ scheikunde\MEP\Torrefaction\Tor liquid gas distribution.csv',
    ↳ float_precision= 'high')
xdata=df.iloc[:,0]
df=pd.read_csv (r'C:\Users\Jan de Koning\Documents\Studie\Master
    ↳ scheikunde\MEP\Torrefaction\Tor liquid gas distribution.csv',
    ↳ index_col=0)

```

```

T=[200, 220,230, 250, 260, 280, 290, 300]
poptprodfrac=Torliquidgasdistribution(df,n,xdata,T)
plt.title('Tor products distribution Corn Stalk')
#%% not used
df=pd.read_csv (r'C:\Users\Jan de Koning\Documents\Studie\Master
    ↳ scheikunde\MEP\Torrefaction\Torgas composition.csv',
    ↳ float_precision = 'high')
popt=torgascompositioncurve(df,n)
plt.title('Composition torgas Corn Stalk')
#%% not used
df=pd.read_csv (r'C:\Users\Jan de Koning\Documents\Studie\Master
    ↳ scheikunde\MEP\Torrefaction\products lumped.csv',
    ↳ float_precision = 'high')
time=np.unique(np.array(df.iloc[:,1]))
Barwidth=1
for i in range(len(time)):
    t=time[i]
    x,y,Tuniq=Volatiles(df,t)
    r1=np.arange(len(y))*4
    r2=np.arange(len(y))*4+1
    r3=np.arange(len(y))*4+2
    plt.figure()
    plt.bar(r1,y[:,0],width=Barwidth,label='Water')
    plt.bar(r2,y[:,1],width=Barwidth,label='CO2')
    plt.bar(r3,y[:,2],width=Barwidth,label='C_2 Compound')
    plt.xticks(r2, Tuniq)
    plt.legend()
    plt.xlabel('Temperature ($^0$C)')
    plt.ylabel('Fraction of dry weight')
    plt.title('Distribution of products after torrefaction')

#%% not used
df=pd.read_csv (r'C:\Users\Jan de Koning\Documents\Studie\Master
    ↳ scheikunde\MEP\Torrefaction\Torliquid improved composition.
    ↳ csv', float_precision = 'high')
labels=['Acetic Acid', 'Propionic Acid', 'Palmitic Acid', 'Stearic
    ↳ Acid', 'Glyoxal', 'Acetone', 'Hydroxyacetone','1-hydroxybutan
    ↳ -2-one', 'Ethanol', 'Vinylphenol', 'Levoglucon', 'Furans','
    ↳ Methanol']

```



```

popt=torliquidimprovedcurve(df,n,labels)
print(popt)
plt.title('Torliquid composition Corn Stalk')

df=pd.read_csv (r'C:\Users\Jan de Koning\Documents\Studie\Master
    ↳ scheikunde\MEP\Torrefaction\Tor liquid gas distribution.csv',
    ↳ float_precision= 'high')
popt=Torliquidgasdistribution2(df,n)
#%% Volatiles with time
df=pd.read_csv(r'C:\Users\Jan de Koning\Documents\Studie\Master
    ↳ scheikunde\MEP\Torrefaction\Products.csv', float_precision='
    ↳ high')
Syngas=pd.read_csv (r'C:\Users\Jan de Koning\Documents\Studie\
    ↳ Master scheikunde\MEP\Sensitivity\CSsyngas.csv',
    ↳ float_precision = 'high')
uniquetime=np.unique(df.iloc[:,1]) #all unique times from
    ↳ experiments
V1=np.zeros((11,len(uniquetime)))
V2=np.zeros((11,len(uniquetime)))
popt1=np.zeros((11,5))
popt2=np.zeros((11,5))
labels=['$CO_{2,nc}$ ', '$CO_{nc}$ ', '$CH_{4,nc}$ ', '$C_2H_{4,nc}$ ',
    ↳ '$C_2H_{6,nc}$ ', '$Acetic Acid_{c}$ ', '$Water_{c}$ ', '$Acetol_
    ↳ {c}$ ', '$Formaldehyde_{c}$ ', '$Formic Acid_{c}$ ']
for i in range(len(uniquetime)): #volatiles composition for every
    ↳ time available
    time=uniquetime[i]
    x,y,T=Volatiles(df,time)
    V1[:,i]=x[0,:]
    V2[:,i]=x[1,:]
for i in range(len(V1)):
    popt1[i,:],pcov=curve_fit(linrel,uniquetime,V1[i,:]) #fit to 4th
        ↳ polynomial
    popt2[i,:],pcov=curve_fit(linrel,uniquetime,V2[i,:])
    plt.figure(1)
    plt.scatter(uniquetime,V1[i,:])
    plt.plot(uniquetime,linrel(uniquetime,*popt1[i,:]),"--")
    plt.xlabel('Torrefaction time (min)')
    plt.ylabel('Fraction in V1')
    #plt.title('V1 composition versus time')

```

```

plt.legend(labels,bbox_to_anchor=(1,0.5),loc='center left',
    ↪ frameon=False)
plt.figure(2)
plt.scatter(uniquetime,V2[i,:])
plt.plot(uniquetime,linrel(uniquetime,*popt2[i,:]),"--")
plt.xlabel('Torrefaction time (min)')
plt.ylabel('Fraction in V2')
#plt.title('V2 composition versus time')
plt.legend(labels,bbox_to_anchor=(1,0.5),loc='center left',
    ↪ frameon=False)
time=np.linspace(10,60,n)
c1=np.zeros(n)
c2=np.zeros(n)
V1=np.zeros((11,n))
V2=np.zeros((11,n))
for i in range(11):
    V1[i,:]=fourthpoly(time,*popt1[i,:])
    V2[i,:]=fourthpoly(time,*popt2[i,:])

r=[44,28,16,28,30,18,60,74,32,30,46]
b=np.zeros(n)
for i in range(11):
    V1[i,:]=V1[i,:]/r[i]
for i in range(100):
    b[i]=np.sum(V1[:,i])
for i in range(100):
    for j in range(11):
        V1[j,i]=V1[j,i]/b[i]

time=30
x,y,Tuniq=Volatiles(df,time)
for i in range(int(np.size(y)/len(y))):
    plt.figure(3)
    plt.plot(Tuniq,y[:,i])
plt.ylabel('Fraction of original solids')
plt.xlabel('Temperature ( $^{\circ}$ C)')
plt.title('Composition volatiles')
LFL,HFL=Flammability(x,a,LFLx,HFLx)
print(LFL)
print(HFL)

```

```

time=np.linspace(10,60,n)
a=np.array([1,2,3,4,5,7,8,9]) #for selecting the correct rows with
    ↳ combustable compounds
LFLx=np.array([12,5,2.7,3,4,6.3,7,18]) #LFL for compounds from a
HFLx=np.array([75,14.3,36,12.2,20,36,73,57]) #HFL for compounds
    ↳ from a
V1=V1[a,:]

nomL=np.zeros(len(V1))
nomH=np.zeros(len(V1))
LFLCS=np.zeros(n)
HFLCS=np.zeros(n)
FLCS=np.zeros(n)
for i in range(len(time)):
    for j in range(len(nomH)):
        nomL[j]=V1[j,i]/LFLx[j]
        nomH[j]=V1[j,i]/HFLx[j]
    LFLCS[i]=1/np.sum(nomL)
    HFLCS[i]=1/np.sum(nomH)
    FLCS[i]=LFLCS[i]/((100-LFLCS[i])/1.3+LFLCS[i])*100
plt.figure()
plt.plot(time,LFLCS,label='LFL-CS')
plt.plot(time,HFLCS,label='HFL-CS')
plt.plot(time,FLCS,label='FL-CS Aspen')
plt.xlabel('time (min)')
plt.ylabel('Flammability limit (%)')
plt.xlim(10,40)
plt.ylim(0,100)
plt.legend(frameon=False)
#%%

for i in range(len(time)):
    t=time[i]
    V1=V1[:,a]
plt.figure()
plt.plot(time,LFLCS)
plt.plot(time,HFLCS)
labels=[('CO','CH4','C2H4','C2H6','Acetic Acid','Methanol','
    ↳ Formaldehyde','Formic Acid')]

```

```

LFLCS,HFLCS=Flammability(x,a,LFLx,HFLx)
#%% HHV
df=pd.read_csv (r'C:\Users\Jan de Koning\Documents\Studie\Master
    ↳ scheikunde\MEP\Torrefaction\Torbio composition.csv',
    ↳ float_precision = 'high')
poptprox,poptult=Torbiocomposition(df,n)
df=pd.read_csv(r'C:\Users\Jan de Koning\Documents\Studie\Master
    ↳ scheikunde\MEP\Torrefaction\HHVCS.csv', float_precision='high
    ↳ ')
HHVexpcsT=df.iloc[:,0]
HHVexpcs=df.iloc[:,-1]
poptult=Compult(df)
print(poptult)
coeff,HHV=HHVcalc(df)
T=250
print(coeff)
A=np.zeros(5)
for i in range(len(A)):
    A[i]=torgascomp(T,*poptult[i,:])
print(A)
HHVT=100*(A[0]*coeff[0]+A[1]*coeff[1]+A[2]*coeff[2]+A[3]*coeff[3]+A
    ↳ [4]*coeff[4])+coeff[5]
print(HHVT)
bcs=np.linspace(200,400,n)
HHVTCS=np.linspace(200,400,n)
for i in range(len(b)):
    for j in range(len(A)):
        A[j]=torgascomp(bcs[i],*poptult[j,:])
        HHVTCS[i]=100*(A[0]*coeff[0]+A[1]*coeff[1]+A[2]*coeff[2]+A[3]*
            ↳ coeff[3]+A[4]*coeff[4])+coeff[5]
plt.figure()
plt.xlabel('Temperature ($^{\circ}$C)')
plt.ylabel('HHV (MJ/kg)')
#plt.title('HHV with temperature CS')
plt.plot(bcs,HHVTCS)
plt.scatter(df.iloc[:,0],df.iloc[:,-1])

#%%
HHVCSRAW=17.98

```

```

time=np.array([10,20,30,40,50])
T=np.array([250,275,300])
Barwidth=1
df=pd.read_csv (r'C:\Users\Jan de Koning\Documents\Studie\Master
    ↳ scheikunde\MEP\Torrefaction\Yields.csv', float_precision = '
    ↳ high')
Solids,Noncondensables,Condensables,Efficiency=TorrefactionplotsCS(
    ↳ df,time,T,HHVCSRAW,poptult,coeff)

```

1.5 Aspen calculator blocks

1.5.1 Dryer

```

CPA=1.00 c heat capacity air
CPB=1.423 c heat capacity biomass
CPW=4.188 c heat capacity water
MBIOONLY=MBIO*(1-M/100)*(1+MFINAL) c mass biomass (M is
    ↳ moisture content)
MWATER=MBIO-MBIOONLY c mass water in biomass
LH=2270 c latent heat water
T=(-TBIO*CPB*MBIOONLY-TAIR*CPA*MAIR+LH*MWATER-TBIO*MWATER*CPW)
    ↳ c energy balance
T=T/(-CPB*MBIOONLY-CPA*MAIR-MWATER*CPW) c energy balance
MFINAL=0.06 c final moisture content
A=1.1556-0.002194*T c Drying variables with T
k=0.00340*T-0.1038 c Drying variables with T
RESTIME=-LOG(MFINAL/A)/k c Drying time calculation
DENSITY=500 c density biomass
Vs=RESTIME/60*MBIO/DENSITY c volume biomass in dryer
FILL=0.15 c filling grade
Vd=Vs/((1-POROSITY)*FILL) c Volume dryer
L=Vd/AREA c length dryer
RESTIME=L/(RESTIME*60) c solid velocity dryer
R=SQRT(AREA/3.1415) c r dryer
HLOSS=1.32*((T-17)/(R*2))**0.25*(3.1415*2*R*L*(T-17))/1000 c
    ↳ heatloss dryer
VGAS=MAIR/N2DENS/(3600*AREA) c volume gas/s dryer
Diff = 0.0000282 c diffusion coefficient water
RE = VGAS*SQRT(AREA/3.1415)*2/Diff c Reynolds number

```

```

Sc = 0.704 c Schmidt number
Pr = 0.71 c Prandtl number
SH1 = 0.664*RE**(1/2)*Sc**(1/3) c sherwood laminar
SH2 = 0.037*RE**(0.8)*Pr/(1+2.433*RE**(-1/10)*(Pr**(2/3)-1)) c
    ↪ sherwood turbulent
SH = SQRT(SH1**2+SH2**2) c combined sherwood

```

1.5.2 Torrefaction reactor

```

t=30 c torrefaction time
XC02=(0.002949*t+0.07157)/44.01 c CO2 yield divided by Mw
XC0=(0.000890*t+0.0588)/28.01 c CO yield divided by Mw etc
XCH4=(0.0619-0.000593*t)/16.04
XC2H4=(0.0620-0.000595*t)/28.05
XC2H6=(0.0619-0.000593*t)/30.07
XACETIC=(0.128-0.00132*t)/60.052
XWATER=(0.001246*t+0.298)/18.02
XHYDROXY=(0.0680-0.000569*t)/74.08
XMETH=(0.0680-0.000713*t)/32.04
XFORMAL=(0.0595-0.000119*t)/30.03
XFORMIC=(0.0622-0.000587*t)/46.03
R=8.314 c Gas constant
k1=12.116*2.781**(-29320.7/(R*(TEMP+273))) c k1
kv1=342204*2.781**(-74943/(R*(TEMP+273))) c kv1 calc
kk1=k1+kv1 c kk1 calc
CONV=kv1/kk1*(1-2.781**(-kk1*t)) c solid loss A

Cout=CONV*M*(XC02+XC0+XCH4+2*XC2H4+2*XC2H6)*12 c Carbon in
    ↪ volatiles
Cout=Cout+CONV*M*(2*XACETIC+3*XHYDROXY+XMETH+XFORMAL+XFORMIC)
    ↪ *12
Hout=CONV*M*(4*XCH4+4*XC2H4+6*XC2H6+6*XHYDROXY+4*XMETH)*1 c
    ↪ Hydrogen in volatiles
Hout=Hout+CONV*M*(4*XACETIC+2*XWATER+2*XFORMAL+2*XFORMIC)*1
Oout=CONV*M*(2*XC02+XC0+2*XACETIC+XWATER+2*XHYDROXY)*16 c
    ↪ Oxygen in volatiles
Oout=Oout+CONV*M*(XMETH+2*XFORMIC+XFORMAL)*16

C=(CI*M/100-Cout)/((1-CONV)*M)*100 c Carbon left in solids
O=(OI*M/100-Oout)/((1-CONV)*M)*100 c Hydrogen left in solids

```

$H = (HI * M / 100 - H_{out}) / ((1 - CONV) * M) * 100$ <p>c Oxygen left in solids</p> $S = SI * M / 100 / ((1 - CONV) * M) * 100$ <p>c Sulfur left in solids</p> $N = NI * M / 100 / ((1 - CONV) * M) * 100$ <p>c Nitrogen left in solids</p>
--